Preparation and Characterization of SiO_2-CaO-MgO-K_2O Glasses as Biomaterials

A

Thesis

Submitted for the partial fulfillment

of the requirements for the award of degree of

Doctor of Philosophy

By

Praveen Jha
(Registration No. 950912011)

Under the supervision of

Dr. Kulvir Singh
(Professor & Associate Dean Strategy)

School of Physics and Materials Science

Thapar University, Patiala-147004 (Punjab), India

June-2017

Certificate

I hereby certify that the work which is presented in thesis entitled **"Preparation and Characterization of SiO_2-CaO-MgO-K_2O Glasses as Biomaterials"** in the partial fulfillment of requirements for the award of the degree of DOCTOR OF PHILOSOPHY in School of Physics and Materials Science, Thapar University, Patiala (Punjab), India is an authentic record of my own research work carried out under the supervision of Dr. Kulvir Singh. The matter embodied in this thesis has not been submitted in part or full to any other university or institute for the award of any degree.

(Praveen Jha)
Registration No. 950912011

Dated: 21.06.17

It is certified that the above statement made by the student is correct to the best of my knowledge and belief.

21/6/17

(Dr. Kulvir Singh)
Professor, School of Physics and Materials Science
Thapar University, Patiala-147004 (Punjab), India.

Acknowledgement

The PhD period is not just a degree begging course but a short journey of learning. On the completion of this beautiful period of time, I would like to express my feelings for all the people, who made this journey easy and ever memorable for me. Words are not enough to express my heartfelt gratitude towards my research supervisor, Dr. Kulvir Singh, Professor and Associate Dean Strategy, Thapar University Patiala. He has been with me, along the way, with esteemed guidance, parental care and immeasurable patience and forgiveness of towards my guilt. He not only guided me for research, but socially and spiritually too. I expect that his love will keep showering to my life throughout.

I express my gratitude to Professor Prakash Gopalan, honorable director, Thapar University, Patiala, for providing me the necessary infrastructure and lab facilities without which this work could not have been possible. I am also thankful to Dr. N.S. Parmar, Director State Forensic science Laboratory, Sagar for his support to complete my ongoing research work. The same level of thanks to my ex- Director Sh. A.K. Ganjoo, Central Forensic Science Laboratory, Chandigarh for his support to continue my research work on weekend days and holidays.

I am deeply thankful to Dr. O.P. Pandey, Senior Professor and Dean (R&SP) for his continuous attention and hard concern about my research work. His timely suggestions and admonishment polished my research skills. I am deeply obliged to Dr. B. N. Chudasama, Dr. Puneet Sharma and Dr. Amjad Ali, who resolved any technical or practical problems that I faced. They monitored my ongoing work very keenly and suggested pinned solutions to my research queries during the progress reports. My special thanks to Head SPMS, Dr, Manoj Kumar Sharma and all the fantastic faculty members of School of Physics and Materials Science for their continuous moral support and motivation. A special word of thanks goes to Ms. Parveen, Mr. P.K. Singh, Mr. Jant Singh, Mr. Indermani Mishra, Mr. S.P. Verma, Mr. Lalji Verma and Ms. Neelam Sadana for their valuable official and technical support. All the staff members and operators of SAI Labs (Thapar University, Patiala), SAIF (Panjab University, Chandigarh), other instrumentation laboratories and centers and the research scholars of various departments and schools of Thapar University are also acknowledged, who always offered their precious time and services for any characterization or related help. Colleagues have a special place of respect in my heart; they helped me understanding research terminology and introduced me to the data analysis techniques. I must acknowledge Dr. Samita Thakur, Dr. Bhupinder Kaur, Dr. Kapil Sood, Dr. Harjinder Singh, Dr. Chandni,

Dr. Jagdeep Kaur, Dr. Ranvir Panwar, Dr. Paramjyot Jha, Dr. Gaurav Singla, Dr. Suresh Kumar, Dr. Mani Mahajan for their extensive scientific discussions time to time.

I am thankful to my lab mates Dr. Sakshi Gupta, Ms. Pooja Singla, Ms. Neetu Bansal, Paramvir Kaur, and Shivani Punj for providing me a very constructive and conducive environment in the lab. Mr. Gaurav Sharma Mr. Savidh Khan, Mr. Devender Kumar, and have always acted like my brothers to help me thoroughly during experimental work. Dr. S.K. Arya and Dr. Gurbinder Kaur always motivated me and suggested the best methods to tackle any research problem and to represent it among the research community. Dr. Satwinder Singh stood like a mentor for Ph.D during hard days of my research. He always acted as a bridge between me and my supervisor. I cannot forget the extreme love and help that I got from my contemporary research fellows, Ms. Parveer Kaur, Ms. Kamaldeep Kaur, Ms. Suninder jeet Kaur, Ms. Purnima Sharma, Ms. Navjot Kaur Dhindsa, Ms. Manpreet Kaur, Mr. Ayush Gupta, Mr. Santosh Mahadevan, Mr. Rameez Mir, Mr. Piyush Sharma and many others.

I dedicate this thesis to my loving family. My grandparents Sh. Satya Narain Jha and Smt Bangla Mukhi Devi, parents Sh. Sudhir Kumar Jha and Smt. Tara Jha, who dreamt of highest degree of education in the family. Because of their blessings, I could complete this piece of work. My brother Prashant Jha and sister-in-law Nidhi Roy, always prayed for this day to come true. My partner Swati Jha and daughters Nandini and Rihanshi, who sacrificed their most valuable time for completion of my work. They all were always there to support every way, every day throughout the work.

During my research work, I shared enjoyable time with hundreds of friends. However, it's impossible to name every person in the limited words. I humbly apologize for the same. I heartedly thank every person, which is not listed above, but contributed to this thesis in one or another way.

Above all my beloved Sadguru Sant Shree Asaram ji Bapu always motivated me through his inner voice to do deeds for the God. All that I prey to get from him are strength, patience, encouragement, help, love, care etc. always.

(Praveen Jha)

Dated: 21.06.17

List of Publications

1. **Praveen Jha**, S.S. Danewalia, K. Singh, *Influence of thermal stability on dielectric properties of SiO_2-K_2O-CaO-MgO glasses,* J. Therm. Anal. Calorim. (2017) DOI: 10.1007/s10973-016-6013-6.

2. **Praveen Jha**, K. Singh, *Effect of MgO on bioactivity, hardness, structural and optical properties of SiO_2-K_2O-CaO-MgO glasses*, Ceram. Int. 42(1) (2016) 436-444.

3. **Praveen Jha**, K. Singh, *Effect of field strength and electronegativity of CaO and MgO on structural and optical properties of SiO_2-K_2O-CaO-MgO glasses*, Silicon 8 (2015) 437-442.

4. **Praveen Jha,** S.S. Danewalia, G. Sharma, K. Singh, *Antimicrobial and bioactive phosphate-free glass-ceramics for bone tissue engineering applications,* J. Mater. Sci. & Eng. C (**Under Revision**).

Conference

1. **Praveen Jha,** K.Singh**,** *Structural and thermal properties of 55 SiO_2-10 K_2O-(35-x) CaO-xMgO glasses*, MR-13 IIT Bombay, 2013.

2. **Praveen Jha,** Gaurav Sharma and K. Singh **"***Thermal stability and crystallization kinetics of SiO_2-K_2O-CaO-MgO glasses*" in national conference on Emerging Trends in Physics and Materials Science (ETPMS) in CDLU (Haryana) 19-20th March 2016.

Index

List of Figures

List of Tables

Abstract

Glass and glass-ceramics are very important class of materials. These materials have wide range of applications in nonlinear optical devices, sealants, bioactive materials etc. Bioactivity basically refers to the bone binding capacity of the materials characterized by *in-vitro* formation of interfacial layer of hydroxyapatite (HAp) or carbonated hydroxyl apatite (HCA) when soaked in stimulated body fluids (SBF). Bioactivity is directly dependent on structural linkage of elements with each other in multi-component system. Glasses convert to glass-ceramics on controlled heat-treatment due to growth of some crystalline phases within the glassy matrix. The volume fraction of the crystalline phase(s) should be limited when better bioactivity along with reasonable mechanical strength and chemical durability is sought. The crystallization kinetics of the glasses using different mathematical models also gives insight of the structure of the glasses.

Present thesis describes the preparation of glasses in the system SiO_2-K_2O-CaO-MgO with variable amount of MgO/CaO. As-quenched glasses have been characterized for their physical, thermal, structural and optical properties. The as-prepared and heat-treated glasses/glass-ceramics were soaked in SBF to check their *in-vitro* bioactivity. The prominent surface modification/formation could be better observed in pellets than powder form and it also leads to better mechanical compliance. The surface modifications of the samples can also be checked by UV-Visible spectroscopy due to change in absorption of light. However, this technique only gives some qualitative results in terms of disorder induced during surface reactions. Local change in the structure can most suitably be seen by FTIR spectroscopy. The soaked samples have been characterized using various techniques with respect to (w.r.t.) to the unsoaked samples to observe any the formation of HCA layer. The thesis is divided into five chapters with a list of cited references at the end of each chapter.

- **Chapter 1** introduces glasses and glass-ceramics as biomaterials with a brief account of history and development of biomaterials. The biomaterials have been classified according to their response towards living tissues in physiological environments. The requirement of bioactivity followed by mechanism of formation of apatite layer on the sample surface in SBF has been dealt in detail. This chapter also describes the inspiration in choosing the glass compositions. The merits and demerits of using glass-ceramics in place of glasses have been highlighted. A brief account of the thermal stability conditions to optimize the heat-treatment parameters has been elaborated. The justification and theoretical outcome of characterization techniques has also been provided. The interaction of the implants with the body parts along with possible threat of failure of implant is discussed along with some notes on possible remedy.
- **Chapter 2** reviews the literature related to the bioactive silicate glasses progressed since the development of 45S5 Bioglass ®. The bioactive properties which are directly linked directly to structural properties further depend on compositions of the glasses. The known properties of various oxides and their role in glass formation provide the basis of selection of present compositions. MgO behaves differently at different concentrations in the glass network. It mainly modifies the glass network. However, sometimes MgO can act as glass former by forming tetrahedron units $(MgO_4)^{2-}$. Glass properties can also be tailored by controlled heat-treatment to make the glass suitable for applications where better mechanical properties are required. The thermal stability of the glasses can be checked by various mathematical models, which are used to obtain various parameters, such as activation energy for glass transition, crystallization, inflection point, type of crystallization etc. These parameters are further used to study the crystallization kinetics of the glasses and their effect on the bioactivity.

❖ **Chapter 3** provides the information on the raw materials used, methods of sample preparation and their processing along with the basics of each technique used to characterize these samples. Glasses were prepared by melting the hand milled mixture of raw chemicals by subsequent quenching in air between thick copper plates. Density of as-prepared samples was measured by Archimedes principle. The physical parameters such as molar volume, excess volume, oxygen packing density etc. were derived theoretically using the measured values of density. The structural properties of the as-prepared glasses were analyzed by the X-rays diffraction (XRD), Fourier transform infrared spectroscopy (FTIR) and Raman spectroscopy. Optical properties of the samples were investigated using UV-visible spectroscopic data. The micro hardness of the samples was measured using micro hardness tester. Thermal parameters have been calculated by differential thermal analyser (DTA). Dielectric measurements were carried out on Solartron Impedance Analyzer (SI 1260) within temperature and frequency ranges 100-400°C and 100-1MHz, respectively. The glass pellets were given controlled heat-treatment to make glass or glass-ceramics. The bioactivity of these samples was checked through *in-vitro* tests by soaking the samples into SBF for different time durations. During soaking, the pH and weight of the samples were measured. The samples after soaking in SBF were characterized by XRD, FTIR, UV-Visible spectroscopy, scanning electron microscopy (SEM) with energy dispersive spectroscopy (EDS) and microwave plasma atomic emission spectroscopy (MP-AES).The implant materials are often prone to infection. Therefore, microbial limit test (MLT) has been done. Additionally, the viable microbial count under favorable conditions of microbial growth has been done to check the antimicrobial effect of the glasses.

❖ **Chapter 4** is the interpretation of the data obtained from the various characterization techniques discussed in the previous chapter. Density being an additive property decreased on replacing CaO by MgO. XRD patterns confirmed the amorphous nature of the synthesized glasses. The major silica bands along with contributions from other oxide were identified and labeled with FTIR and Raman spectroscopy. The ratio of areas under the Raman bands within 950-1000 cm^{-1} and 1050-1100 cm^{-1} gives the approximate ratio of NBO/BO for a glass and is proportional to the degree of polymerization (Q3/Q2 ratio). This ratio is highest for glass containing 25 mol% MgO and 10 mol% CaO. The optical band gap of glasses gradually increased from 3.42 eV to 3.65 eV with an increase of MgO content and Urbach energy lies between 0.11 eV to 0.18 eV. The microhardness is in the range of 464-502 HV. The thermal analysis yields two major T_c and T_g corresponding to separated phases which followed the usual behavior with respect to heating rate. However, non-linearity in the properties arises due to the concentration dependent role of MgO. This type of behavior could be related to the mixed alkaline earth metal oxides effect. Crystallization kinetics analysis indicates that glass having CaO/MgO ratio ~1.33 has better polymerization among the present glasses. The highest dielectric permittivity is observed ~22 at room temperature and 100 Hz for the same glass. Higher MgO containing glasses showed reluctant behavior towards crystallization. The crystalline peaks become more prominent after soaking in SBF due to preferential loss of amorphous phase over the crystalline phase in the SBF. After soaking, the pH change of the SBF and leaching of ions as measured through MP-AES were consistent with the sequential series of changes occurring on the surface of glasses as explained in literature. Moreover, many weak bands/shoulders appeared in the FTIR spectra. An extra band at ~876 appears in most bioactive glass originating from v2 frequency of carbonate ions formed on the glass. FTIR bands due

to NBOs are lost after the glass pellets were soaked. IR spectra of the soaked samples similar to that of as-quenched glasses. The optical band gap of the glasses increased after soaking which is an indicative of the reduction in NBOs caused by leaching of alkali and alkaline earth metal ions from glass without formation of any significant crystalline layer on the surface. Heterogeneous distribution of flakes has adhered to the glass surface. The MP-AES data also supported the EDS data since the percentage of these elements increased in SBF after glass soaking. The powder glasses exhibited antimicrobial effect.

- **Chapter 5** presents the major conclusions drawn from the results discussed in Chapter 4. The higher MgO contained glasses show better polymerization (cross-linking) and have compact glass network as compared to higher CaO contained glasses. The CaO/MgO ratio influences the thermal stability, which leads to affect the dielectric properties. At CaO/MgO~1.33 most polymerized structure and thermally most stable glass is achieved. The microhardness the glass pellets were found closer to the human bone i.e. 45-60 HV after reaction with SBF. The crystalline peaks are absent in all the glasses even after soaking in SBF solution. However, XRD halo of the samples becomes broader after soaking in SBF. The SEM micrographs clearly showed the adherence of new entities on the glass/glass-ceramic surfaces in both powder form as well as pellet form. The EDS data also suggests increase in elemental composition of Ca, P, O etc. which are suggestive of formation of bioactive layers at the surface. The present glasses/glass-ceramics with good mechanical, bioactive and antimicrobial properties are promising candidates for bone engineering applications. These samples must be tested via more realistic *in-vivo* experiments to explore their candidature as biomaterials.

Chapter 1 Introduction

1.1 Evolution of Biomaterials

Biomaterials are the substance which can be used for treating, augmenting or replacing any tissue, organ and part of the human body for any duration. Alternatively, bio-materials can also be defined as substances that are capable of withstanding and performing their task effectively inside the living body without any detrimental effects on surroundings parts of the body [1]. Efforts have been put in large number to find replacement for parts of human body. The advent in processing and sophisticated techniques leads to the day by day better performance of the artificial parts of the human body. In the pre-Christian era to nineteenth century, the metals, copper and bronze were extensively used for implantation but they created various harms in the body due to their toxic and adverse effect. In 1860, the studies on applications of bio-materials to surgery and medicine were enhanced drastically. For instance, ivory was utilized for developing bio-materials in 1902, for manufacturing of femur head gold. Since then, researchers started using various metallic and alloys implants showing inert nature and durable behavior [2].

Archeological evidences have proven the usage of glasses by human beings in the earliest times [3]. Initially, they had been used for decorative purposes [3]. Later, they found domestic uses such as windows, vehicles glasses, crockery, and laboratory equipment. Modern day's technological and communication devices cannot be imagined without glasses. The era of 1960 is characterized as the golden period for glass science. During this period, the basic properties of glass were understood as a function of their structure. Subsequently, in 1969, Hench *et al.* invented the popular Bioglass® ($45SiO_2$-$24.5CaO$-$24.5Na_2O$-$6P_2O_5$) that could adhere to the natural bone [4]. Bioglass®, readily forms hydroxyl apatite (HAp) layer on the surface, which acts as intermediate interfacial layer to bind glass with the human

tissues. Afterwards, many materials like alumina, zirconia, calcium phosphate, hydroxyapatite glass and glass-ceramics have been tried with better biocompatibility with human body [5].

Before bioglass inventions, alumina and zirconia were also incorporated for inside the body. Such materials offered good mechanical response but faced reduction in their strength after years of implantation. Presently, with the advent in population the thrust for bioactive materials that can withstand the living body has increased many folds due to which, research on these materials has been highly demanding and progressive [6]. Based on materials requirements, nature and role in human body, they can be classified in the following categories.

1.2 Types of biomaterials

1.2.1 Bioinert

The implants, showing high chemical durability and no significant interaction with the implanted site tissues are called bioinert implants. Such materials are surrounded by non-adherent tissues around the implant. Al_2O_3, ZrO_2, zirconia toughened alumina and Y_2O_3 are most common bio-inert ceramics. Theses ceramics are extensively used in orthopedic applications due their good mechanical properties [7]. Additionally, these materials find wide uses in dentistry due to high chemical durability towards both acidic and basic environments as offered by the oral cavity.

1.2.2 Biodegradable

Biodegradable materials are the one that degrade after implantation inside the body in the course of time. When such materials are implanted inside the body, the bone grows at the cost of implanted material and eventually replaces it. This is quite prevailing if the number of osteoclasts (the cells in the body those absorb the implants) are comparable to the number of osteoblasts (the cells in the body those have ability to generate new cells). Tricalcium

phosphate (TCP), calcium phosphate (Ca-P) and its salts, porous hydroxyapatite etc. fall into this category. These are extensively used to cure the bone defects. These materials fill the cracks with time when used as filler in the cracks by being replaced by the human bone [8].

1.2.3 Bioactive

This type of grafts possesses the middle path behavior rather being bioinert and biodegradable. Such materials, called bioactive material can easily form interfacial bond with the human tissues such as bones. The glass- bone bond is mainly formed via an intermediate HAp layer. Further, the ability of the implant to get bonded with the bone depends variedly upon the nature of the implant and their surface phenomenon [9]. The bone binding mechanism of the bio active glasses is elaborated in the following section.

1.3 Glasses and glass-ceramics as bioactive materials

Glasses and Glass-ceramics have been in use in human body parts which is represented in the following table.

Table 1.1 Compositions of different bioglasses and glass-ceramics.

Chemical Composition	45S5 (Glass)	45S5.4F (Glass)	52S4.6 (Glass)	KGC Ceravital® (Glass-ceramics)	A/W-GC (Glass-ceramics)
SiO_2	45	45	52	46.2	34.2
CaO	24.5	14.7	21	20.2	44.9
MgO	-	-	-	2.9	4.6
K_2O	-	-	-	0.4	-
Na_2O	24.5	25.5	21	4.8	-
P_2O_5	6	6	6	-	16.3
$Ca(PO_3)_2$	-	-	-	25.5	-
CaF_2	-	9.8	-	-	0.5

These glasses and glass-ceramics are called bioglass and glass-ceramics. Various kinds of biomaterials include many of the bioglasses that are already being used in various parts of

human body are shown in Figure 1.1. [10]. Most common bioglass is like 45S5 Bioglass® [10]. Some typical bioglasses related to present work is given in Table 1.1.

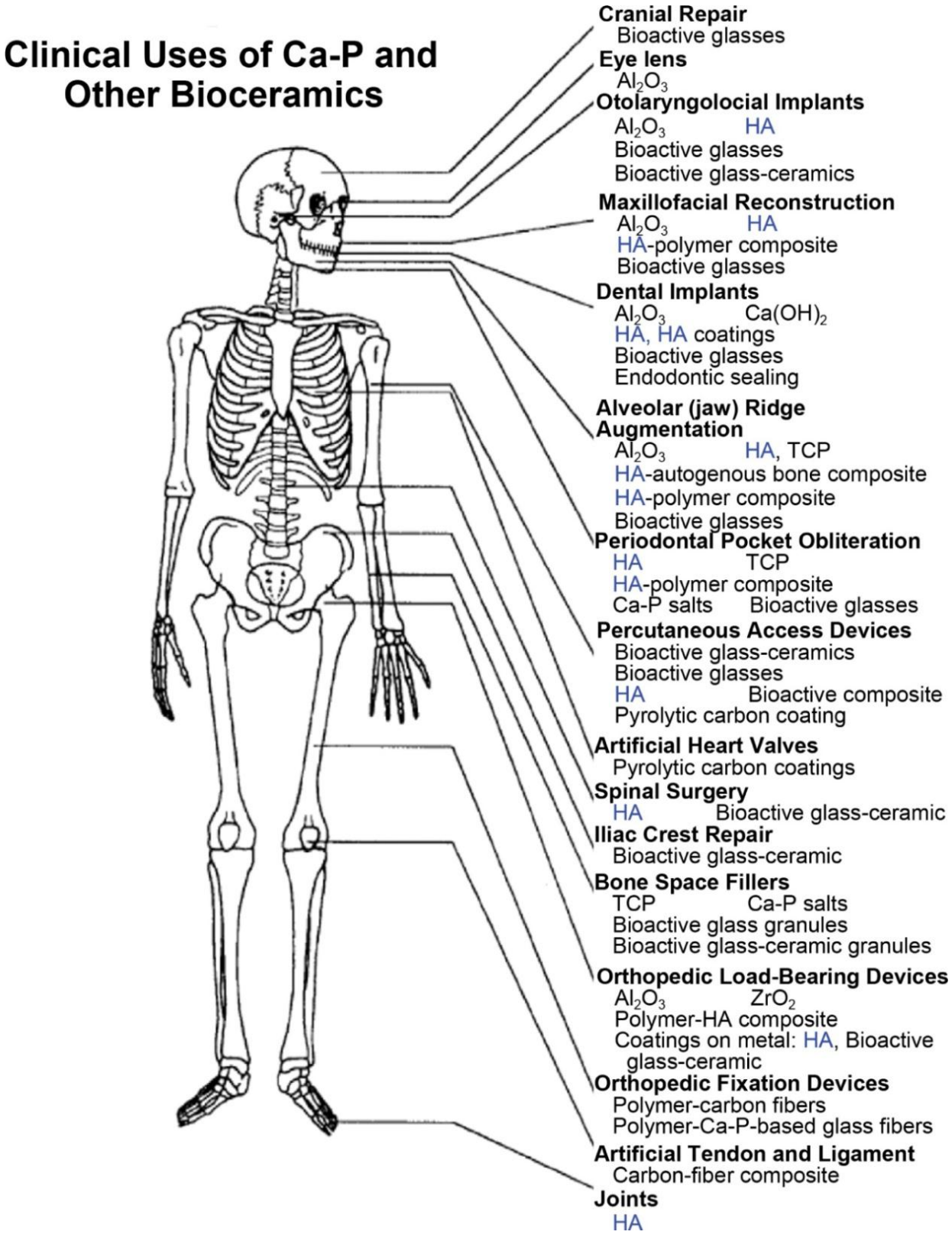

Figure 1.1 Clinical use of biomaterials in human body [10].

1.3.1 Bioglasses and glass-ceramics

Bioglass is an amorphous solid of very short range order. For instance, the silicon atoms in a silica glass are on ~3.4 Å apart. Maximum ordering in glasses has been reported up to ~10 Å. Therefore, it is also called short range order (SRO) materials. Glass is a material which exhibit a characteristic temperature called glass transition temperature *(Tg)* and crystallization temperature (T_c) on heating [11].

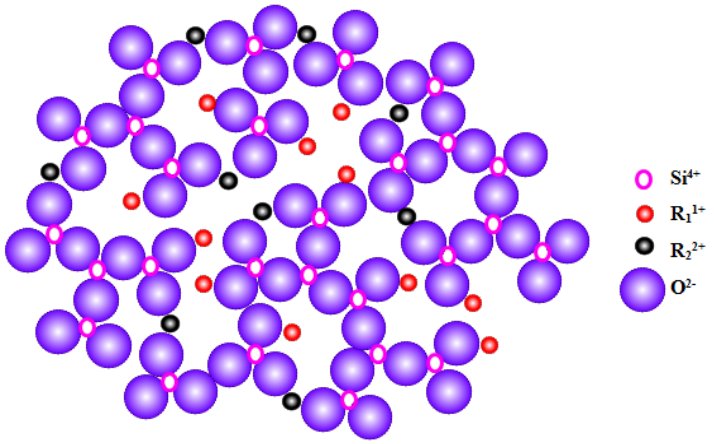

Figure 1.2 Glass structure and its modification by various modifiers ions (R1and R2 are alkali and alkaline ion respectively) [12].

Glasses usually consists of three major constituents namely network formers, modifiers and intermediates. Network former or glass former is the base constituent that forms a 3D network. Some of the oxides such as SiO_2, B_2O_3, and P_2O_5 are extensively used and well known glass formers because they form a continuous 3D network on their own; on the other hand, oxides like CaO, MgO and K_2O etc. ac as network modifiers due to their capability to disrupt the glass network. The additions of network modifier are responsible to tailor the properties of glass and form non-bridging oxygen (NBOs) as shown in Figure 1.2. The NBO/BO ratio has significant effect on the local structural units and modifies the related properties of the glass [13]. Intermediates such as Al_2O_3, V_2O_5, TiO_2 do not form glasses by their selves, but are conditional network formers when some other oxides are present. In addition to this, intermediate oxides act as glass network modifier depending on their amount

in glass compositions as reported by Bahadur *et al.* [14]. Besides above mentioned constituents, some additives can be supplemented to glass batch in minor concentration for example colorants and fining agents which imparts color to the glass and makes the melt bubble free, respectively. These compounds has negligible role in the basic properties of glass [15]. The behavior of the additives primarily depends upon its field strength i.e., $Z/(r_c + r_a)^2$, where letters have usual meanings. As per Dietzel's model, the compounds with field strength >1.3 act as glass formers, while the compounds with field strength <0.4 are network modifiers. Whereas, the conditional formers are having field strength values lied between former and modifiers. Replacement of elements with varying cation charge and ionic radii affects the adjoining local structural units. This can cause increase in defects or conversely may induce ordering of the glass network. In both the conditions, the glass properties will be modified [15]. Glass-ceramic is the materials with crystalline phase(s) embedded within the glass network [16]. These crystalline phase leads to enhance the mechanical strength, chemical and thermal stability [17]. Generally, glass-ceramics are formed by the controlled heat-treatment of the glasses at suitable temperatures for adequate time periods. This heat-treatment favors the formation of nuclei at different sites in glass matrix which develops later to impart devitrification of the glass constituents. Sometimes *in-situ* crystallization is observed during synthesis of melt-derived glass compositions containing transition metal oxides which do not form miscible mixture with each other. As a result, phase separated glasses having matrix within glass matrix are obtained [18]. Additionally, some oxides such as, TiO_2, Fe_2O_3 act as nucleating agents and fasten the nucleation phenomena [19-21]. The quantity of crystallized phases has significant effect on the properties of obtained glass-ceramics. It increases the chemical inertness of the glass-ceramics. In spite of this, crystalline phases within the network may show detrimental influence on glass properties. Many times, it imparts undesirable deviations in functionality

during its usage. For example, glass sealants may suffer drastic failure during operation due to any shift in coefficient of thermal expansion (CTE) [22]. The transparency of the glass is affected by formation of micro crystallite, nano-crystallite phases. As for as biomaterials are concerned, glass-ceramics have low rate of formation of HAp as compared to glasses [23]. One should have smart balance between degree of crystallization and glassy phase meet specific between the glass required properties. Due to superior mechanical and thermal properties, many glass-ceramics compositions have been developed to be used as biomaterials in dentistry, knee replacement, orthopedics etc. Yet, the glass-ceramics experienced a rather slow development before they can be confidently tried in the clinics due to their brittle nature. Their suspicious breakage during operation was expected and the debris could travel within the human body damaging normal tissues. Moreover, particles released as a result of glass dissolution in the physiological environments may be cytotoxic for normal cells. Luckily, bioactive glasses exhibited safer response towards the normal tissues. The major ingredient of bioactive glasses i.e. Si, Ca, Na, O and P already exist in our body. Moreover, the ion release profile is useful for growing the interfacial HAp layer between implant and the bones. Additionally, special cells in human body called phagocytic cells take care of any unusual particles entered in the body. These cells digest all the alien particles [24]. These cells belong to family of white blood corpuscles, which travel from blood to digest the foreign particles and guard the living cells from any damage. After passing initial clinical trials successfully, the glasses and glass-ceramics are revolutionalized the biomedical research and industry.

1.3.2 Glassy structure and mechanism of bioactivity

Bioactivity of a material can be investigated by adopting either of the two commonly modes or both, *in-vitro* and *in-vivo*. *In-vivo* tests consist of checking the tissue-implant interaction by actual implantation in humans or animals. On the other hand, *in-vitro* methods refer to the

research conducted on appropriate tissue or cell cultures, or components of the living organism separated from its biological context, or chemically prepared solutions mimicking body fluids. Rather than using a whole organism, this practice enables more convenient investigation of the specimen. The root of the bone bonding properties of a bioactive glass is its chemical reactivity in body fluids. Subsequently these surface chemical reactions result in the formation of a hydroxycarbonate apatite (HCA) layer to which bone can bond [25]. Hench and Anderson described the three general processes (leaching, dissolution and precipitation) that occur on immersing a bioactive glass in an aqueous solution. Leaching is characterized by release, i.e. the exchange of alkali and alkaline earth ions in the glasses with H^+ and H_3O^+ ions in the solution. This process is comparatively easy because these cations act as network modifiers and thus only weakly bonded to the glass network. Network dissolution occurs simultaneously by the breakdown of -Si-O-Si-O-Si- bonds through the action of hydroxyl (OH^-) ions. Breakdown of the network occurs locally followed by release of silica into the solution in the form of silicic acid ($Si(OH)_4$). Then, poly condensation of silanols occurs, resulting in a silica rich gel on the surface. In the process of precipitation, calcium and phosphate ions released from the glass together with those from solution form a calcium phosphate-rich (CaP rich) layer on top of the Si-rich layer. Finally, due to crystallization, the CaP-rich layer forms the HCA layer. More elaborated reaction processes have been described extensively by Hench and others [10, 26, 27]. The chemical reactions are summarized as follows:

(1) Quick exchange of Na^+ or K^+ with H^+ or H_3O^+ from solution:

$$Si - O - Na^+ + H^+ + OH^- \rightarrow Si - OH + Na^+(aq) + OH^- \quad (1.1)$$

(2) Loss of soluble silica in form of $Si(OH)_4$ to the solution resulting from breakage of Si-O-Si bonds and formation of Si-OH (silanols) at the glass solution interface:

$$Si{-}O{-}Si + H_2O \longrightarrow Si{-}OH + OH{-}Si \quad (1.2)$$

(3) Condensation and re-polymerization of a SiO_2-rich layer on the surface depleted in alkalis and alkaline earth cations:

$$Si - OH + OH - Si \rightarrow Si - O - Si + H_2O \quad (1.3)$$

(4) Movement of Ca^{2+} and PO_4^{3-} groups to the surface through the SiO_2-rich layer forming a Ca-P- rich film on top of the SiO_2-rich layer, followed by growth of the amorphous CaO-P_2O_5- rich film by incorporation of soluble calcium ions and phosphates from solution.

(5) Crystallization of the amorphous CaO-P_2O_5 film by incorporation of OH^-, CO_3^{2-}, or F^- from the solution to form a mixed hydroxyl, carbonate, fluorapatite layer.

1.4. Biocompatibility of the glass

A proper application of the glass for biomedical applications requires satisfying some of the condition. These requirements are discussed in the following section.

1.4.1 Cell culture and cytotoxicity

Cell culture test is mainly done to have further insight into the reactivity of the glass. Cell culture mainly refers to attachment and propagation of the osteoblasts like cell on the surface of the biomaterial. Osteoblasts are cells having a single nucleus that forms bone. An ordered group of osteoblasts produce hydroxyapatite which is deposited into the organic matrix forming a strong and dense mineralized tissue known as bone matrix. The bone matrix comprises of protein and mineral. The protein forms the organic matrix. The vast majority of the organic matrix is collagen, which provides tensile strength to the bone. After the formation of the bone addition of minerals takes place. The matrix is mineralized by deposition of hydroxyapatite. This mineral is rigid, and hence provides better compressive strength to the bone. Thus, the collagen and mineral together forms a composite materials [27], which can bend under a strain and recover its shape without damage, having excellent tensile and compressive strength. This is referred to as elastic deformation. Typically, bone fractures are caused by forces that exceed the capacity of bone to behave elastically. The test

is generally carried out with endothelial cells (EC), because the vascular endothelium interacts with implanted biomaterials in each step of tissue integration [27]. Here, fixed density of cell is planted onto the glass surface and the numbers of cells are measured after some time. Cell spreading and proliferation assays are performed in some cases after seeding, to assess the effect of biomaterials loading in endothelial cells (EC) adhesion. Endothelial cells are known to be very sensitive to pH changes and, for this reason, the rapid increment in pH caused by dissolution of ions could change the cell adhesion and proliferation. Additional release of ions like Zn^{2+} could ultimately lead to decrease in cell count [28-29]. The cytotoxicity of the biomaterials is determined by the ratio of number of viable cells to total number of cells seeded. Hence, cytotoxicity of a material is of major apprehension for materials to be used as biomaterials. Eventually structural dependence of biomaterials on cell attachment, proliferation and growth is evident via release of ions and consequently with pH change.

1.4.2 Mechanical strength of biomaterials

It is a known fact that good bio-materials must show high bio-compatibility along with high strength and sufficient corrosion resistance. Undoubtly, metals, alloys and composites offer good mechanical properties as well as good tissue interaction. However, in some cases, the composites materials release some toxic elements into the human body. While, metals and alloys **are** prone to corrosion inside the body fluid [30-31]. So, bioceramics like Al_2O_3, ZrO_2, hydroxyapatite, bone cement, tricalcium phosphate and bioactive glasses are widely used to restore damaged hard tissues [32-33]. Glass-ceramics materials are being chosen because of comparatively high strengths than glasses. However, glasses have high bio-compatibility than that of glass-ceramics. The mechanical properties of the glass-ceramics depend widely upon microstructure, grain size and volume fraction of the crystalline phases [34-36]. Several glass-ceramics like A-W containing crystalline oxoflouroapatite, wollastonite, hydroxyapatite

and tricalcium phosphate rich phases in glassy matrix have been used as biomaterials for better mechanical properties [37]. However, crystallization may prove detrimental for the bioactive nature of the glasses [38]. Therefore, to achieve optimum mechanical properties without compromising bioactivity, controlled crystallization is needed to the glasses. Apatite-wollastonite containing glass-ceramics (A-W GC) have been reported to be bioactive, having in-vitro and in-vivo stability and are difficult to be resolved in physiological environment [39]. Bioactive glass-ceramics containing apatite and wollastonite phases are having good mechanical properties and can be prepared by the process of sintering and subsequent crystallization of glass powders [40-44].

1.4.3 Thermal stability

Thermal studies play very significant role for tailoring the properties of glasses. In this regard, various mathematical models are available, which helps to obtain various parameters, such as activation energy for glass transition, crystallization, inflection point, type of crystallization etc. [45]. These parameters are further used for studying the crystallization kinetics of the glasses. Like thermal effects, compositional changes vastly affect the local structure of glasses. Addition or replacement of an element with different ionic size, field strength, oxidation state etc. may drive the final properties of the glasses. For instance, Na_2O, CaO, K_2O are well-known network modifiers and weaken the structure of the parent glass. On the other hand, MgO, Al_2O_3, TiO_2 are intermediate oxides, which possess complex concentration dependent role in glasses. Both the thermal and compositional modification affects the stiffness of glasses directly. One of the major usable forms of glass is as a coating material. Generally, for clinical application metallic substrate coated with glass is being used. Although Bioglass® is bioactive; this glass has a high thermal expansion coefficient in comparison to titanium and titanium alloy and tends to crystallize during heat treatment. These drawbacks of Bioglass® reduce its potential usage as coating materials on dental or

orthopedic implants. Attempts have been made to design glasses with high bioactivity that can be sintered without crystallization during the coating process. Elements such as Mg, B and Al have been incorporated into bioactive glasses to fulfill these criteria. Magnesium is of prime interest since it can excite osteoblast expansion [46] and is present in relatively high concentrations in bone [47, 48]. Barrere *et al.* [49] postulated that this element could affect the dissolution and the physical-chemical reaction of glass. Brink [50] incorporated MgO to a series of bioactive glasses to maintain bioactivity and improve their processing ability. As discussed in the previous section thermal study is also important for enhancing the mechanical properties of the glass without compromising bioactivity. Clupper *et al.* [51] studied the function of the heat treatment processing conditions on the strength and toughness of 45S5 Bioglass. They reported that, the strength and toughness of bioactive glass ceramic samples approached that of natural cortical bone. Some authors [52] questioned that the crystallization of 45S5 bioactive glass has a minimal effect on the ability of this bioactive glass to form a tissue bond.

1.4.4 Dielectric behavior of biomaterials

Currently, the dielectric properties of HAp have significant relevance in tissue engineering field. The solubility of the bioactive glass has been directly linked to the ions released from the materials to the host medium. Hence, the understanding of the alkali ion transport mechanism of the bioglass is very significant. Analytical technique of alternating current impedance spectroscopy, which has been considered as the best tool for understanding the dynamics of alkali ions in the bioactive glass, can be used to study the dynamics of charges [53]. Dielectric relaxation and related phenomena are present in this bioactive glass and their investigation is crucial not only from the practical point of view due to the potential application, but also for the insight information that can provide referring to molecular/ions mobility, polarization and conductivity mechanisms [54-56]. Glass-forming materials are

characterized by several unusual properties, which seem to be inherent to the glassy state of matter and which are quite universally found in such different types of materials [57-59]. Furthermore, there are numerous competing theoretical models of the glass transition that can describe the observed performance with various levels of precision. Glass-physics community is still far from reaching any consensus in the settlement of this question. Moreover ferroelectric properties of the glass and glass-ceramics could be used to generate controlled temperature near cancerous cell, so they can be used as a thermo seed for hyperthermia treatment of cancer cell [12].

1.5 Microbial infection susceptibility

Nowadays, there is a widespread concern regarding diseases, infections, corrosion and bio contamination caused by microorganisms. Generally, two main complications that may be faced by the biomaterials are infection and lack of tissue integration. Certain implants such as external fixation pins are susceptible to contamination which leads to failure of the implant. Therefore, the probable threat of microbial contamination and microbial growth on the samples in due course of time after implantation has also been highlighted in the present work. In an aqueous environment, alkaline and alkaline earth ions as well as silicon ions are released from a bioactive glasses (BAG). This raises pH and osmotic pressure near a BAG [60]. The antimicrobial action of a bioactive glass is influenced by its chemical composition and the dissolution conditions in its surroundings. Therefore, the probable mechanisms of the antibacterial effect of 45S5 BAG may include two aspects, one was the higher pH proximal to the 45S5 BAG particles which were closely surrounded by bacteria, and the other was the destruction of the cell walls by 45S5 BAG debris. A schematic illustration of the antimicrobial process of BAG was given in Figure 1.3. Initially, when bioglass particles immerse in solution, alkali ions began to be released. The local pH value on the surface of 45S5 BAG particles was higher than that in the area far from the particles [62]. Secondly,

bacteria were adhered onto the surface of 45S5 BAG particle. The higher local pH value would be beneficial to kill the bacteria around the 45S5 BAG particles. In addition, the 45S5 BAG debris could damage cell walls and can cause bacterial death.

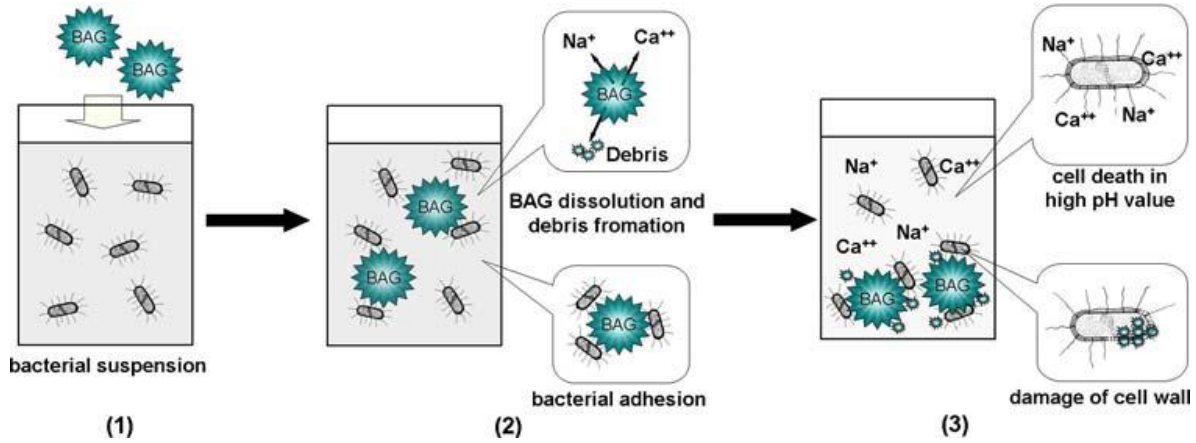

Figure 1.3 Schematic illustration of the bactericidal process of 45S5 BAG [61].

The area of bioglass has many applications, in addition to mentioned and discussed above. The areas is getting much more attention now-a-days. Main work done in the recent few years particularly related to bioceramic glasses and glass-ceramics has been reviewed in the next chapter.

References

[1] L. Nicolodi, E. Sjolander, K. Olsson, Biocompatible Ceramics- An overview of applications and novel materials, KTH (2004) 4.

[2] A. Bardow, D. Moe, B. Nyvad, B. Nauntofte. Arch. Oral. Biol. 45 (2000) 1.

[3] J. Zarzycki (ed.), Glasses and amorphous materials, VCH, The University of California (1991).

[4] L.L. Hench, J. Mater. Sci. Mater. Med. 17 (2006) 967.

[5] V.K.Mishra, B.N. Bhattacharjee, O.Parkash, D.Kumar, S.B.Rai, J.Alloys Compd.614 (2014) 283

[6] M.J. Larsen, E.I.F Peace, Arch. Oral. Biol. 48 (2013) 317.

[7] L.L. Hench, D.E. Day, W. Höland, V.M. Rheinberger, Int. J. Appl. Glass Sci. 1 (2010) 104.

[8] L.L. Hench, J. Am. Ceram. Soc. 74 (1991) 1487.

[9] X. Chen, A. Nouri, Y. Li, J. Lin, P.D. Hodgson, C. Wen, Biotech. Bioeng. 101 (2008) 378.

[10] L.L. Hench, J. Wilson An introduction to bioceramics. World Scientific Publishing CO, London-Singapore, (1993), 2.

[11] J.W.P. Schmelzer, I.S. Gutzow, Glasses and the Glass Transition, Wiley-VCH Verlag GmbH & Co. KGaA, Germany (2011).

[12] S. Singh, Structural and Bioactive Properties of Fe/Mn Oxides substituted Sodium Silicate Glasses, Ph.D Thesis (2017) Thapar University, Patiala

[13] H. Scholze, Glass-Nature, Structure, and Properties, Springer-Verlag, New York (1991).

[14] N. Lahl, K. Singh, L. Singheiser, K. Hilpert, and D. Bahadur, *Crystallization kinetics in AO-Al_2O_3-SiO_2-B_2O_3 glasses (A=Ba, Ca, Mg),* J. Mat. Sci. 35 (2000) 3089-3096.

[15] J.E. Shelby, Introduction to Glass Science and Technology, 2nded. The Royal Society of Chemistry, UK (2005).

[16] J. Hlavac, The technology of glass and ceramics: an introduction, Elsevier scientific publishing company, New York (1993).

[17] P. Jha, M.K. Singh, R.K Gautam, R. Tyagi, D. Kumar, Proceeding of International Conference on Advances in Materials Manufacturing and applications 2015.

[18] O. Bretcanu, E. Verné, M. Cöisson, P. Tiberto, P. Allia, J. Magn. Magn. Mater. 305 (2006) 529.

[19] M.M. Krzmanc, U. Dosler, D. Suvorov, J. Am. Ceram. Soc. 95 (2012) 1920.

[20] H.R. Fernandes, D.U. Tulyaganov, J.M.F. Ferreira, J. Mater. Sci. 48 (2013) 765.

[21] T. Poirier, N. Labrador, M.A. Alvarez, C. Lavelle, N. Enet, J. Lira, Mat. Let. 59 (2005) 308.

[22] G. Kaur, Solid Oxide Fuel Cell Components: Interfacial Compatibility of SOFC Glass Seals, 1st Ed., Springer International Publishing, Switzerland (2016).

[23] P. Ducheyne, A. El-Ghannam, I. Shapiro, Method of forming a porous glass substrate, US patent number 5676 (1997) 720.

[24] F.C. Cabello, C. Pruzzo (eds.), Bacteria, complement and the phagocytic Cell, 1st ed. Springer Berlin Heidelberg, Germany (1988).

[25] T. Nakamura, T. Yamamuro, S. Higashi, T. Kokubo, J. Biomed. Mater. Res. 19 (1985) 685.

[26] D. Zhang, In-vitro characterization of bioactive glass, PhD Thesis, Abo Academi University Finland, (2008) 26.

[27] S. Pezzatini, R. Solito, L. Morbidelli, S. Lamponi, E. Boanini, A. Bigi, J. Biomed Mater Res. A76 (2006) 656.

[28] G. Lusvardi, G. Malavasi, L. Menabue, M.C. Menziani, A. Pedone, U. Segre, J. Biomat. Appl. 22 (2007) 505.

[29] D.A. Wiseman, S.M. Wells, M. Hubbard, J.E. Welker, S.M. Black, Am. J. Phys. Lung. Cell. Mol. Phys. 292 (2007) 165.

[30] T.V. Thamaraiselvi, S. Rajeswari, Trends Biomat. Art. Organ. 18 (2004) 9.

[31] K. Rezwan, Q.Z. Chen, J.J. Blaker, A. R. Boccaccini, Biomaterials. 27 (2006) 3413.

[32] V. Stanic, *et al.* Biomaterials 23 (2002) 3833.

[33] Q.Z. Chen, C.T. Wong, W.W. Lu, K.M.C. Cheung, J.C.Y. Leong, K.D.K Luk, Biomaterials 25 (2004) 4243.

[34] J. Henry, R.G. Hill, J. Non-Cryst. Solids 319 (2003) 13.

[35] W. Holland, H.G. Beall, Glass-ceramic Technology, Am. Ceram. Soc. Inc., New York, 2002.

[36] S.A. Hasan, S.M. Salman, H. Darwish, E.A. Mahdy, Ceramics-Silikaty 53 (2009) 53.

[37] A.K. Srivastav, R. Pyare, J. Mater. Sci. Res. 2 (2012) 207.

[38] O.P. Filho, G.P.L Torre, L.L. Hench, J. Biomed. Mater. Res. Part A. 30 (1996) 509.

[39] H. Teramoto, A. Kawai, S. Sugihara, Acta Medica Okayama. 59 (2005) 201.

[40] B. Yu, K. Liang, S. Gu, Ceram. int. 28 (2002) 695.

[41] T. Kokubo, M. Shigematsu, Y. Nagashisma, Bull. Inst. Chem. Res. Kyoto univ. 60 (1982) 260.
[42] J.J. Shyu, J.M Wu, J. Mater. Sci. Let. 10 (1991) 1056.
[43] J.J. Shyu, J.M Wu, J. Am. Ceram. Soc. 73 (1990) 1062.
[44] D.M. Liu, H.M.Chou, J. Mater. Sci. Mater. Med. (1994) 5.
[45] J. Sesták, P. Simon, Thermal analysis of micro, nano and non-crystalline materials: transformation, crystallization, kinetics and thermodynamics. 1st ed. Springer Netherlands, (2013).
[46] C.C. Liu, J. K. Yeh, J.F. Aloia, J. Bone Miner. Res. 3 (1988) 104.
[47] R.K. Rude, H.E. Gruber, J. Nutr. Biochem. 15 (2004) 710.
[48] T. Okuma, Nutrition 17 (2001) 679.
[49] F. Barrere, C.A.V. Blitterswijk, Biomaterials. 23 (2002) 1921.
[50] M. Brink, J. Biomed. Mater. Res. 36 (1997) 109.
[51] D.C. Clupper, L.L. Hench, J.J. Mecholsky, J. Eur. Ceram. Soc. 24 (2004) 2929.
[52] D.C. Clupper, J.J. Mecholsky Jr., G.P. Latorre, D.C. Greenspan, J. Biomed. Mat. Res. 57 (2001) 532.
[53] A.R. Kulkarni, P. Lunkenheimer, A. Loidl, Solid State Ionics. 112 (1998) 69.
[54] A. Maheswaran, G.H. Kumar, S.K. Prabhu, R.S.D. Bella, J. Alloy Compd. 532 (2012) 86.
[55] A. Maheswaran, G. Hiran Kumar, H. Nithya, S.K. Prabhu, K. J. Appl. Phy. A. 117 (2014) 1323.
[56] M. Hasnaoui, A. Triki, M. Graça, M. Achour, L. Costa, J. Non-Cryst Solids 358 (2012) 2810.
[57] M.D. Ediger, C.A. Angell, S.R. Nagel, J. Phys. Chem. 100 (1996) 13200.
[58] K. Ngai, J. Non-Cryst. Solids 275 (2000) 7
[59] J. Dyre, Rev. Mod. Phys. 78 (2006) 95.
[60] O.H. Andersson, J. Rosenqvist, K.H. Karlsson, J. Biomed. Mater. Res. 27 (1993) 941.
[61] D. Zhang, M. Hupa, L. Hupa, ActaBiomater. 4 (2008) 1498.

Chapter 2 Literature Review

The literature related to the present work has been reviewed and discussed in this chapter. The area of bioglass has got special attention after the publication of the first research paper in 1969. In the recent years only, so the present work comprises of the recent work in the field of bioceramics/bioglasses. Additionally based on the literature the objective of the present work has been also given in this chapter. The work of other researchers and their merits and demerits which led to the methodology adopted by us has also been given. The review of literature has been organized into following.

2.1 Types of biomaterials

Metals and alloys such as titanium, stainless steels and cobalt–chromium-based alloys have been used as biomaterials from very long time [1]. The advantage of the metal lies in their good mechanical strength, fracture toughness and lack of fragility. But only metals are not adequate for use as biomaterials. A major shortcoming of the metallic biomaterials lies in the toxic release of metallic ions through wear processes or corrosion [2–6]. These particles may cause inflammatory cascades [2, 4–7]. Many mechanical parameters of implant materials like elastic moduli are not comparable to bone. It leads to generate the local stress. As a result stimulation of new bones is reduced; this ultimately leads to instability of the implant sites.

Bioceramics have some advantage over the traditional metallic implant materials. These materials have been used as a scaffold material. Generally calcium phosphate ceramics are used in a variety of scaffolds products with variable Ca/P ratio. Many other types of scaffolds have been investigated like hydroxyapatite (HAp), tricalcium phosphate (TCP) as well as composites like biphasic calcium phosphates (BCP). Many ceramics such as HAp 1, 67, TCP 1,5 have structure and Ca/P ratio quite similar to the mineral phase of human the bone . The porosity is also almost comparable to the bone. Therefore, the release of phosphate and calcium ions takes place at the SBF-ceramics interface. Thus, a good connection is formed

between the ceramic and bone [8]. The major drawback of these materials is their less mechanical strength and brittle nature. High porous design of the ceramic materials renders them insufficient as a weight bearing device.

Bioglass is an improved version of the bio ceramic materials in terms bone binding capacity [9]. Bioglass is a special type of phosposilicate glasses which could form intimate bond with the bone instead of being surrounded by fibrous tissue around implant when it used *in-vivo*. Some of the forms of bioglass are already commercialized such as "Stron-Bone" in orthopaedic [10], "NovaBone" in spinal [11]) "BonAlive" in cranio-maxillofacial [12] and "PerioGlas" in periodontal [13] applications. Additionally, some of the bioglasses are being used in personal care products such as NovaMin toothpaste [14]. The bioglass of the trade mark 45S5 Bioglass® by Hench has been used for the last four decades both in the form of bulk as well as particulate [15]. The bulk form of glass cannot be molded into desired shape due to the brittleness and possesses less surface/volume ratio. On the other hand, the powder form has got advantage over bulk for filling bone defects because it may conveniently be filled to the defect [16-17]. Moreover, ion exchange reactions between powder and the surrounding fluids are fast due to high specific surface area and porosity which leads to formation of an apatite-like phase. On the contrary, the particulate form faces the problems in occupying and holding their position in the bone defect. Large particles generally lack cohesiveness with the implant site and mechanical support is also poor [18-19]. So both the powder as well as bulk form of bioglass are in use. Each has some advantage and disadvantage. Additionally bio inert metal coated with bioactive glass is also a choice as implant materials. MgO enameled titanium exhibited better biocompatible environment to fibroblast cells. The material performed remarkably better for osteoblastic growth and proliferation of cell [20].

2.2 Processes and bioactivity

Most commonly, glasses have been synthesized either by melt quench technique or sol-gel method. Sol gel method yields fine glass particle and the method is believed to play better role in bioactivity due to fast dissolution in biological fluid. It is associated with the large surface to volume ratio as compared to melt quench glass. The processing temperature is also low so the technique is ideal for synthesis of glass where low boiling point component are involved and the method also ensures higher purity of glass. However, commercially melt quench method seems advantageous as the yield is more with low preparation time. It is useful where glass is intended to use in bulk (block) form rather than particulate (powder) form. Permissible limit of SiO_2 is 60 mol % of the melt quench glass unlike sol gel prepared glass in which the limit is up to 90 mol % for bioactivity. The coating application of glasses often requires the high temperature sintering of glasses. Hence, it is desirable to have an idea of the structure and crystalline phases that may be available in the glass after heat-treatment. O'Donnell established that accurate estimation of glass transition temperature (Tg) enables to estimate many other temperature parameters, such as annealing temperature, fiber-drawing and sintering temperature of the as prepared glasses [21]. It also helps to correlate to other glass properties like bioactivity and mechanical properties which are directly linked to network connectivity of the glass [22]. Tg of bioactive glasses are influenced by components, local structural effect and the phase separation of bioactive glasses [23]. Crystallization temperature is second characteristic temperature which has its role in influencing the bioactivity and mechanical properties of the glasses. Crystallization of glass is known to have adverse effect on bioactivity; however crystallization enhances the mechanical strength of the materials [24]. Thermal stability of the glass had been checked by employing different mathematical models, which provide in depth analysis of the role of different constituents on the transformation phenomenon in the glass [25]. The properties of the glasses can be

tailored mainly either by compositional changes or by proper heat-treatment of quenched glasses [26-27]. The controlled heat-treatment of the glass devitrifies glass and some crystalline phases are formed. The volume fraction of formed phases changes the properties of the glasses. So, crystallization of the glasses may be favorable or unfavorable depending on the types of formed crystalline phases and their volume fractions. For instance, glass-ceramics have better mechanical strength and chemical durability than counterpart glasses [28]. On the other hand, the crystallization of the glasses becomes unfavorable when undesirable variation in properties occur during its operation; for example, change in coefficient of thermal expansion (CTE) of a glass may leads some stress/ strain in the glasses. The presence of local strain in glasses can affect the bioactivity as well as other properties [29]. Similarly, the mismatch in the CTE of substrate and films may lead to the buckling in both the components. Thus, the thermal behavior and temperature dependence of the properties of glasses are essential to study for knowing their working parameters and for the selection of better glass for specific applications like microelectronic devices. Therefore, thermal studies play very important role for tailoring the properties of glasses. In this regard, various mathematical models are available, which are used to obtain various parameters, such as activation energy for glass transition, crystallization, inflection point, type of crystallization etc. These parameters are further used to study the crystallization kinetics of the glasses. Similar to thermal effects, compositional changes greatly affect the local structure of glasses. Addition or replacement of an element with different ionic size, field strength, oxidation state etc. may drastically drive the final properties of glass. For instance, Na_2O, CaO, K_2O are well-known network modifiers and weaken the structure of the parent glass. On the other hand, MgO, Al_2O_3 and TiO_2 are intermediate oxides, which exhibit complex concentration dependent role in glasses. Both the thermal and compositional alterations affect the rigidity of glasses directly. The network rigidity in turn influences the

ionic motion and leads to change in properties such as dielectric permittivity, electrical conductivity etc. In general, the dielectric permittivity of the glasses varies from 3.7-10 [30]. The low dielectric permittivity independent of temperature and frequency is required for microelectronic applications [31]. Many researchers report the isothermal and non-isothermal properties of glasses using different models to predict their thermal and structural properties [32-35]. The surface of the glass can also be altered by redox reactions. Results of iron based silicate glasses [36-42] established that the modifier ions diffuse from the bulk glass to the surface upon heat-treatment in an oxidizing atmosphere. This happens due to the oxidation of Fe^{2+} ions during heat-treatment. The study proposed that oxidation of the glass is caused by the addition of the oxygen as well as the removal of the cations from the glass surface. Similarly, the surface of sodium deficient glass has been modified to a sodium-rich layer by heat-treatment in an oxidizing environment near the glass transition temperature. This facilitated the easy occurrence of mechanism of bioactivity which is mainly surface dependent mechanism. As a consequence the layer of HCA got enhanced [43].

2.3 Structure/composition and properties correlation

The bioglass is associated with high solubility in physiological media. As a result most of the ions are carried away from the implant sites before formation of new bones. A number of theories have been put forward to predict glass bioactivity such as the established by Strnad *et al.* [44] based on structural parameter. Rawling *et al.* [45] model of bioactivity was based on ionic potential. On the basis of network connectivity, Hill *et al.* [46] suggested an inorganic polymer model for the prediction of bioactivity. Nonetheless, above theories could not explain bioactivity of the glass as structural role of MgO and P_2O_5 have not been taken into account. P_2O_5 is a well-known glass forming oxide but behavior of MgO is debatable. McMillan has recognized the MgO is in dual role [47]. In other words, it can behave like former and modifier at different concentration and different compositions. Magnesium is a

vital element as far as requirement of the body is concerned. Magnesium is naturally found element in bone tissue and is necessary for human action of metabolism [48–53]. It is one of the abundant metals in the human body. Magnesium is a part of many enzymes, and responsible for the structures of DNA and RNA [53]. The range of magnesium level in the extracellular fluid is between 0.7 and 1.05 mMol/L [48]. Barrere *et al*. reported that the relatively high concentration Mg^{2+} at the interface favored the heterogeneous nucleation and growth of small Ca-P specimen onto the Ti_6Al_4V substrate over Ca^{2+} after soaking in 5 SBF solution (ionic solution having concentration 5 times the normal) [54]. The properties of CaO are very similar to MgO but the former always behaves as a glass modifier irrespective to the composition and amount. It occupies the free spaces in the glass network thereby enhances the number of non-bridging oxygen atoms by and thus these NBOs units contributes towards reducing the network connectivity of the glass network. K_2O and other alkali oxides reduce the melting temperature of the mixture of raw material and make the production of the glass more economical. Also it helps in increasing the solubility in aqueous media thereby facilitate the host tissue-material interaction. Similarly, many other bioactive glass compositions also contain significant amounts of K_2O [55–60]. The amount of K_2O used in the glass composition should not be much because it may affect *in-vivo* bioactivity of the glass. High alkali oxide containing glass takes up water from osmosis and results in cracking or swelling of the matrix. These types of bioactive glasses having alkali metals prove inappropriate as coating material for metal substrates due to CTE mismatching. Additionally, the crystallization tendency of glass is increased by high amount of alkali content which reduces the sintering behavior of bioglasses. As already seen such behavior renders them unsuitable as bioactive materials [61]. In addition to various mathematical method and thermal processing technique which has been discussed in section 1.3, the synthesized glass and glass ceramics have been characterized further using various sophisticated instruments

in order to fully understand their properties and structural co-relation. With the help of XRD Adams *et al.* found the mechanically strong crystalline phase $Na_2Ca_2Si_3O_9$ transformed to non-crystalline phase upon soaking in SBF for 14 days. It indicated the biodegradable nature of the material [62]. Modification of the glass due to dopants changes the structure of the glass which could be better understood by the FTIR spectra of the glasses [63–65]. The slight change of bioactivity 45S5in introduction of Li_2O and K_2O in place of Na_2O and introduction of MgO and ZnO in place of CaO, was known by FTIR reflectance spectra. It also revealed that an increase in the number of bonds formed with increasing soaking time in SBF [66]. Optical spectroscopy is an effective method to access any surface modifications occurred on the glass surface due to interaction with SBF [67-68]. Besides these SEM-EDS gives direct insight to the formation or change on surface of the glass soaked in physiological media [69]. Queiroz *et al*. used impedance spectroscopy to observe the non-isothermal crystallization of $0.45SiO_2$-0.36MgO-$0.09K_2O$-$0.1(3CaO{\cdot}P_2O_5)$ glasses to be used as biomaterials [70]. Dielectric study showed that negatively polarized HAp ceramics exhibited the bone formation. Essential biological properties may be attributed to high charge density up to hundreds of mC/cm^2 [71-72].

2.4 *In-Vitro* bioactivity and antimicrobial response

The biological response has been assessed *in-vitro* for various bioglass compositions. The *in-vitro* bioactivity have been evaluated in different media The time required for the formation of the HCA layer depends on various factors, such as composition, structure, geometry of the glass and dipping solution and ratio of surface area to solution volume [73–80]. Jones *et al.* [81] observed that powder to SBF ratio >0.002g/ml retards the *in-vitro* bioactivity of the 45S5 glass. Others than SBF, the *in vitro* bioactivity can also be checked by immersing the glass sample in Dulbecco's modified Eagle's medium (DMEM) buffer solutions. The usage

of this solution helps to monitor interaction of glass in an intricate system very much similar to physiological surrounding [82]

Tris (hydroxymethyl) aminomethane (Tris) is another frequently used media for conducting *in -vitro* bioactivity test. Tris is plain buffering reagent without any ions in it. It has got the benefit of maximum solubility and minimum precipitation. The TRIS buffered base has a CuK_a= 8.1. Therefore, highest buffering capacity of the TRIS is observed at pH=8, although, it can be used for buffer solutions from pH=7.1 to 9.1. However, most of the reports observed decreased pH of the solutions, as the experiments were usually carried out at high pH. Above all Popa *et al*. proposed an improved protocol for assessing the *in vitro* bioactivity[82] Biocompatibility is also concern other than bioactivity. Many other issues like cytotoxicity and antimicrobial effect are also required to meet these requirements. The toxicity activities of the glasses have been verified using endothelial cells (EC). pH change directly affects the growth of EC. The fast increment in pH because of H^+ cation occurs on dissolution of the glass. Li *et al.* performed a basic *in-vitro* examination of the toxic behavior of pristine and surface treated magnesium with bone marrow cells of mice [83]. The activity of alkaline phosphatase, one of a number of well-characterized pointers of an osteoblastic phenotype [84], was investigated as a test for ascorbic acid-induced osteoblast differentiation of MC3T3-E1 cells seeded on 13–93 glass fibers. Earlier reports indicated that MC3T3-E1 cells exhibits many key characteristics of osteoblast differentiation in combination of ascorbic acid like the development of alkaline phoshphate [85-86]. Misra *et al*. studied the cytocompatibility using human MG-63 osteoblast-like cells in osteogenic and non-osteogenic medium and found that the composite substrates are quite preferable for adhesion, proliferation and differentiation of cells [87]. With the increase in glass part, higher weight loss and hydration was witnessed. *In-vitro* study discussed so far is a preliminary method

showing only direction approach but actual behavior of biomaterials in real sense can be judged by *in- vivo* approach.

Many materials have been checked for *in-vivo* bioactivity. For instance a series of 20 cases in which a tricalcium phosphate disc was successfully embedded into the affected surface of tibia bone was reported by Cameron. After six months of the implantation the disc was almost surrounded by tissues and hence was not recognized radio graphically anymore. The disc was almost masked by the bone within 2 years [88]. Polymeric biodegradable synthetic implants are being used clinically for many years. So, biocompatibility nature of these materials has been perceived. Polymers and Ca-P based composite materials have exhibited excellent performance as scaffolds [89-90].

Many others bioglass compositions advanced with time have incorporated different elements in the glass-network [91-95]. The application of bioglasses as implant materials is eye-catching for the specific effect of bioglass on biological response, such as, up regulating the activity of genes that increases release of vascular endothelial growth factor (VEGF) [96-98]. Elements like silver, zinc etc. makes the host glass as antibacterial material [99-101]. In addition to this they also secrete phosphate and sodium silica. These ion released promotes an extra indirect pH-related antibacterial effect [102]. Bioactive glasses act as carrier of ions which governs various cell functions such as drug delivery system and haemostatic agents [103-107]. Now a day, ferromagnetic bioglasses are being synthesized for magnetically induced hyperthermia treatment of cancer [108]. Summary of the key results related along with their reference are given in Table 2.1.

Table 2.1 Overview of the studies carried out on materials for biomedical applications.

Glass Composition	Results	Reference
SiO_2–Na_2O–K_2O–CaO–MgO–P_2O_5	This glass coating was applied on orthopedic metallic implants. The fractional replacement of CaO by MgO and Na_2O by K_2O are done for CTE matching of coatings to the Ti-based alloys. The coating do not show any crack up to 60 wt % SiO_2in glass composition. These glass also show bioactive nature if glass in-*vitro* test.	109
SiO_2-CaO-MgO-ZnO-Na_2O-K_2O-P_2O_5	The bioactivity study was done in SBF and Tris buffer solution. The magnesium did not hampered *in-vitro* bioactivity of the glasses, but slowed down the apatite formation rate. Results indicated that suppression of crystallization and decrease of CTE, T_g and T_s by MgO.	110
SiO_2–P_2O_5-K_2O–CaO-MgO–CuO	It was reported that CuO in place of CaO/MgO enhanced the formation of phosphor oxygen domains comprising of orthophosphate units. The creation bond with high chemical stability at higher CuO concentrations was responsible for slow decrement in the chemical activity of glasses.	111
SiO_2–CaO–Na_2O–P_2O_5	The dissolution test was performed in tris and SBF. The soaked pellet was studied by XRD, SEM and EDS. The cell viability of the glass–ceramics was done via MTT assay using MG-63 cells. The glass composition yield good result in all the tests.	112

SiO_2–CaO–P_2O_5–K_2O–Al_2O_3	Sodium containing glasses were found to be lesser biocompatible as compared to that of potassium containing glasses. The fractional replacement of Al_2O_3 for K_2O increased the mechanical properties, whereas in-vitro bioactivity and cytotoxicity declined. This study concluded that the optimized amount of Al_2O_3 in present glasses would be suitable for biomedical applications.	113
CaO–SiO_2–P_2O_5–B_2O_3	The heat-treatment of the glass formed the calcium borate and wollastonite crystalline phases. The crystallization did not show any adverse effect on the formation of Hap.	114
SiO_2-Na_2O-CaO-B_2O_3	An antimicrobial soda-lime glass was used as a precursor to form bactericidal glass-ceramic with combeite and nepheline phases embedded in the glassy matrix. It inhibited growth of bacterial colony.	115
Na_2O-Ag_2O-SrO-CaO-MgO-ZnO-P_2O_5-SiO_2-Bi_2O_3-CaF_2	The powders derived from glass melts purred in cold water (frits) may completely densify by sintering at temperatures up to 800° C. without devitrification, resulting in bioglass compacts with high flexural strength (˜85 MPa). The bioactive glass powders prepared by sol-gel densify at lower temperatures due to their higher specific surface area and reactivity.	116
SiO_2–CaO–MgO–P_2O_5	The HAp forming ability decreased with MgO, which lowers the degradability rate of glass by improving the network connectivity.	117
K_2O-Na_2O-Fe_2O_3-B_2O_3-P_2O_5,	Substitution of K_2O induced significant decrease of self-connection among different [BO] groups. Thermal stability of the studied glass was enhanced by K_2O's substitution. K_2O's substitution cannot cause basic	118

	changes in structure of borophosphate network.	
SiO_2-B_2O_3-Al_2O_3-CaO-Li_2O-Na_2O-K_2O	This glass possessed low dielectric permittivity and loss along with lower electric conductivity. Whereas, the glasses had a tendency to be phase separated and get eventually crystallized.	119
P_2O_5-Al_2O_3-B_2O_3-PbO-Na_2O-K_2O	Glass transition temperature showed a broad maxima while coefficient of thermal expansion (CTE) a broad minima at ratio Na/(Na+K)=0.54. This behavior was able to explain this on phase separation phenemenon.	120
Na_2O–K_2O–MgO–CaO–B_2O_3–P_2O_5–SiO_2	The NBO/BO ratio for the glasses was accessed using Raman spectroscopy. This ratio varied linearly as a function of the alkali/alkali earth ratio. Amount of ions leached directly depends on the alkali/alkaline ratio.	121
MO–SiO_2 (M = Ca, Mg)	Both CaO and MgO acted as network modifiers. However, CaO seems to be better modifier than MgO as the number of Q^3 was more pronounced in the CaO–SiO_2 glasses. As compared to bulk glass, the porous glasses exhibited better network depolymerization.	122
SiO_2-P_2O_5-CaO-Na_2O-CaF_2	Addition of fluoride results in formation of fluorapatite in SBF, which is more acid resistant than carbonated hydroxyapatite and therefore fluoride-containing bioactive glasses are particularly interesting for applications in dentistry. However the high fluoride-content glasses in this system mainly form fluorite (CaF_2) in SBF and formation of apatite is reduced compared to the fluoride-free composition.	123
Na_2O\K_2O-CaO–P_2O_5-SiO_2	High reaction rate was noticed for potassium substituted 45S5 Bioglass® glass. Every glass of present series formed thick apatite layer on their surfaces in four days. The glasses with lower Na content exhibited delayed ion release during initial stage of bioactivity mechanism. Similarly, Ca deficient glasses underwent lower	124

	nucleation and growth of HCA.	
Na_2O-K_2O-MgO-CaO-B_2O_3-P_2O_5-Al_2O_3-SiO_2	A concentration of 50 mg/mL was effective for antimicrobial effects. Maximum antimicrobial activity and pH change was noticed during first day of cultivation. The release of alkali ions and increase in the pH directly affected the antibacterial effect of these glasses.	125
SiO_2-CaO-P_2O_5	The antibacterial activity was studied using *Escherichia coli, Pseudomonas aeruginosa, Salmonella typhi, and Staphylococcus aureus*. Cytotoxicity of the samples was evaluated using mouse Fibroblast L929 cell line. At broth concentrations below 50 mg/mL, they showed no antibacterial activity	126
Na_2O-K_2O-MgO-CaO-B_2O_3-P_2O_5-Al_2O_3-SiO_2	Flow Cytometric Method (FCM) was able to calculate the viable bacteria in the suspension media tests for antibacterial activity. All the bioactive glasses clearly inhibited the growth of a wide selection of bacterial species causing infection at the body implant surface.	127

The extensive study has been done on glass and glass-ceramics as biomaterials but limited work has been found pertaining to MgO and CaO based glasses particularly in the presence of K_2O as a constituent**.** K_2O is expected to reduce tendency of the glass to crystallize thus better for bioactivity. Magnesium is key element of the bone and it stimulates the osteoblast proliferation. Many researchers have reported the positive influence of MgO on bioactivity. However, some of the researchers have reported either negative or no effect of MgO on bioactivity. The contradictory behavior of magnesium on bioactivity originates due to dual role of MgO in silica network. However, the thermal stability of the glasses and its effect on the dielectric properties of potassium modified silicate glasses is not yet explored extensively Based on above mentioned points the objective of the present research are as follows:

Objectives

- To synthesize $55SiO_2$ +10 K_2O + (35-*x*) CaO + *x* MgO ($0 \leq x \leq 35$) glasses.
- The in-vitro bioactivity and dissolution of these glasses and glass-ceramics will be checked in SBF solutions.
- The un-soaked or soaked glasses and glass-ceramics will be characterized by X-ray diffraction (XRD), Fourier Transform Infrared Spectroscopy (FT-IR), Differential thermal analyzer (DTA)/TG and Scanning Electron Microscopy (SEM) with EDS and Micro-hardness tester.

To meet the above objectives the detailed way out for synthesis of sample and various characterization techniques have been discussed in the next chapter

References

[1] M. Niinomi, Met. Mater. Trans. A. 33 (2002) 477.

[2] D.A. Puleo, W.W. Huh, J. Appl. Biomater. 6 (1995) 109.

[3] J.J. Jacobs, J.L. Gilbert, R.M. Urban. J. Bone Joint Surg. 80 (1998) 268.

[4] C. Lhotka, T. Szekeres, I. Steffan, K. Zhuber, K. Zweymuller. J. Orthop. Res. 21 (2003) 189.

[5] J.J. Jacobs, A.K. Skipor, L.M. Patterson, N.J. Hallab, W.G. Paprosky, J. Black, et al. J. Bone Joint Surg. 80 (1998) 1447.

[6] J.J. Jacobs, N.J. Hallab, A.K. Skipor, R.M. Urban. Clin. Orthop. Rel. Res. 417 (2003) 139.

[7] M.L. Wang, L.J. Nesti, R. Tuli, J. Lazatin, K.G. Danielson, P.F. Sharkey, et al. J. Orthop. Res. 20 (2002) 1175.

[8] P. Lichte, H.C. Pape, T. Pufe, P. Kobbe, H. Fischer, Int. J. Care Injured 42 (2011) 569.

[9] V. Aina, G. Malavasi, A. FiorioPla, L. Munaron, C. Morterra, ActaBiomater. 5 (2009) 1211.

[10] M.D. O'Donnell, P.L. Candarlioglu, C.A. Miller, E. Gentleman, J. Mater. Chem. 20 (2010) 8934.

[11] B. Ilharreborde, E. Morel, F. Fitoussi, A. Presedo, P. Souchet, G. Penneçot, J. Pediatr. Orthop. (2008) 28.

[12] M. Peltola, K. Aitasalo, J. Suonpää, M. Varpula, A. Yli-Urpo. Head Neck, 28 (2006) 834.

[13] S.J. Froum, M.A. Weinberg, D. Tarnow. J. Periodontol. 69 (1998) 698.

[14] B.J. Tai, Z. Bian, H. Jiang, D.C. Greenspan, J. Zhong, A.E. Clark, J Clin. Period. 33 (2006) 86.

[15] L.L. Hench, J. Biomed. Mater. Res. 41 (1998) 511.

[16] E.J.G. Schepers, P. Ducheyne. J. Oral. Rehab. 24 (1997) 171.

[17] H. Oonishi et al. Clin. Orth. Rel. Res. 334 (1997) 316.

[18] C. Chan, I. Thompson, P. Robinson, J. Wilson, L.L. Hench. Int. J. Oral. Maxillofac. Surg. 31 (2002) 73.

[19] A.M. Gonzalez *et al*. J. Craniofac. Surg. 16 (2005) 63.

[20] A.A. Noaman, C.F. Simon, Rawlinson, R.G. Hill, J. Non-Cryst. Solids, 358 (2012) 3019.

[21] D. Matthew. O. Donnell, ActaBiomater. 7 (2011) 2264.

[22] R. Hill. J. Mater. Sci. Letts. 15 (1996) 1122.

[23] G. R. Hill, S. Delia. Brauer, ActaBiomater. 7 (2011) 3601.

[24] P. Li, Q. Yang, F. Zhang, T. Kokubo, J. Mater. Sci. Mater. Med. 3 (1992) 452.

[25] J. Sesták, P. Simon, editors. Thermal analysis of Micro, Nano and Non-Crystalline Materials: Transformation, Crystallization, Kinetics and Thermodynamics. 1st ed. Springer Netherlands. (2013).

[26] J. Hlavac, The Technology of Glass and Ceramics. Elsevier Science Ltd, (1983).

[27] J.E. Shelby. Introduction to Glass Science and Technology. 2nd ed. Cambridge. Roy. Soc. Chem. (2005).

[28] A. Öchsner, L.F.M. Silva, H. Altenbach, editors. Characterization and Development of Biosystems and Biomaterials. 1st ed.: Springer-Verlag Berlin Heidelberg. (2013).

[29] G. Kaur, V. Kumar, O.P. Pandey, K. Singh. J. Electrochem. Soc. 159 (3) (2012) 277.

[30] D.D. Pollock. Physical Properties of Materials for Engineers. 2nd edn. CRC Press, Inc. USA. (1993).

[31] W. Wersing, Solid State Mater. Sci. 1 (1996) 715.

[32] F. Wang, Q. Liao, G. Xiang, S. Pan J. Mol. Struct. 1060 (2014) 176.

[33] K.V. Shah, M. Goswami, D.K. Aswal, V.K. Shrikhande, S.K. Gupta, G.P. Kothiyal, J. Therm. Anal. 89 (2007) 153.

[34] B.K. Money, K. Hariharan, J. Phys. Cond. Matter. 21 (2009) 15102.

[35] J.C. Qiao, J.M. Pelletier, Trans. Nonferrous Met. Soc. China. 22 (2012) 577.

[36] G.B. Cook, R.F. Cooper, T. Wu, J. Non-cryst. Solids. 120 (1990) 207.

[37] R.F. Cooper, J.B. Fanselow, D.B. Poker, Geochim. Cosmochim. Acta. 60 (1996) 3253.

[38] D.R. Smith, R.F. Cooper, J. Non-cryst. Solids, 278 (2000) 145

[39] G.B. Cook, R.F. Cooper, Am. Mineral. 85 (2000) 397.

[40] M.M. Smedskjaer, Y.Z. Yue, Int. J. Appl. Glass Sci. 2 (2011) 117.

[41] V. Magnien, D.R. Neuville, L. Cormier, J. Roux, J.L. Hazemann, D. de Ligny, S. Pascarelli, I. Vickridge, O. Pinet, P. Richet, Geochim. Cosmochim. Acta, 72 (2008) 2157.

[42] D. Wu, D.L. Kohlstedt, J. Am. Ceram. Soc. 71(7) (1988) 540.

[43] E.T. Kang, J. P. Kim, Phys. Procedia. 48 (2013) 46.

[44] Z. Strnad, Biomater. 13 (5) (1992) 317–321.

[45] R.D. Rawlings, Clin. Mater. 14 (2) (1993)155.

[46] R. Hill, J. Mater. Sci. Lett. 15(13) (1996) 1122.

[47] P.W. McMillan, Glass Ceramic, 2nd edition Academic Press, London, 1979.

[48] Water, electrolyte mineral and acid/base metabolism. Section 2.Endocrine & Metabolic Disorders. Merk Manual of Diagnosis and Therapy [Chapter 12].

[49] S. Nel, Clin. Chim. Acta. 294 (2000) 1.

[50] T. Okuma, Nutri.17 (2001) 679.

[51] J. Vormann, Mol. Aspects. Med. 24 (2003) 27.

[52] F.I. Wolf, A. Cittadini, Mol Aspects Med. 24 (2003) 3.

[53] A. Hartwig, Mutat. Res. Fund. Mol. Mech. Mutagen.475 (2001) 113.

[54] F. Barrerea,b, C.A.V. Blitterswijka, K. de Groota, P. Layrolle, Biomater. 23 (2002) 2211.

[55] G. Lusvardi, D. Zaffe, L. Menabue, C. Bertoldi, G. Malavasi, U. Consolo. Acta Biomater. 5 (2009) 419.

[56] G. Lusvardi, G. Malavasi L. Menabue V. Aina, C. Morterra, Acta Biomater. 5 (2009) 3548.

[57] D. Zhang, M. Hupa, L. Hupa, Acta Biomater. 5 (2008) 1498.

[58] Q.Z. Chen, Y. Li, L.Y. Jin, J.M.W. Quinn, P.A. Komesaroff, Acta Biomater. 6 (2010) 4143.

[59] T. Waltimo, T.J. Brunner, M. Vollenweider, W.J. Stark, M. Zehnder, J. Dental Res. 86 (2007) 754.

[60] D.S. Brauer, N. Karpukhina, M.D. O'Donnell, R.V. Law, R.G. Hill, Acta Biomater. 6 (2010) 3275.

[61] A. Goel, S. Kapoor, R.R. Rajagopal, M.J. Pascual, H.W. Kim, M.F.J. Ferreira, Acta Biomater. 8 (2012) 361.

[62] A.L. Adams, R.E. Essien, O. Rafiu, Shaibu, O. Aderemi, New J. Glass & Ceram. 3 (2013) 11.

[63] J. Wong and C.A. Angell, Glass Structure by Spectroscopy (M. Dekker, Inc., New York, 1976), Chapter 7. 409.

[64] E.I. Kamitsos, Phys. Chem. Glasses 44 (2003) 79.

[65] K. El-Egili, Physica B 325 (2003) 340.

[66] M.R. Majhi, R. Pyare S.P. Singh, Int. J. Sci. & Eng. Res. 2 (2011) 9.

[67] K. Singh, I. Bala, V. Kumar, Ceram. Int. 35 (2009) 3401.

[68] D.T. Pierce, W.E. Spicer, Phys. Rev. B 5 (1972) 3017.

[69] G. Kaur, P. Sharma, V. Kumar, K. Singh, Mat. Sci. Eng. C. 32 (2012) 1941.

[70] C.M.Queiroz1, M.H.V. Fernandes, J.R. Frade, Mat. Sci. Forum. 514 (2006) 1078.

[71] S. Bodhak, S. Bose, A. Bandyopadhyay, Acta Biomater. 6 (2010) 641.
[72] D. Kumar, J.P. Gittings, I.G. Turner, et al. Acta Biomater. 6 (2010) 1549.
[73] L.L. Hench, J.K. West. Life Chem. Rep. 13 (1996) 187.
[74] L.L. Hench, Biomater. 19 (1998) 1419.
[75] J.R. Jones, L.L. Hench, Mater. Sci. Technol. 17 (2001) 891.
[76] L.L. Hench, J. Wilson Introduction to bioceramics. Chaps 1.3.4. Singapore, World Scientific, (1993).
[77] L.L. Hench, R.J. Splinter, W.C. Allen, T.K. Greenlee, J. Biomed. Mater. Res. 2 (1971) 117.
[78] M.M. Pereira, A.E. Clark, L.L. Hench, J. Am. Ceram. Soc. 78 (1995) 2463.
[79] M.M. Pereira, A.E. Clark, L.L. Hench, J. Biomed. Mater. Res. 28 (1994) 693.
[80] R.G. Hill, J. Mater. Sci. Letts. 15 (1996) 1122.
[81] J.R. Jones, P. Sepulveda, L.L. Hench, J. Biomed. Mater. Res. 58 (2001) 720.
[82] A.C.Popa, G.E.Stan, M.A.Husanu, I Mercioniu, L.F. Santos, H.R.Fernandes, J.M.F. Ferreira, Int.J. Nanomed. 12 (2017) 683–707.
[83] J. Vormann, Mol. Aspects Med.24 (2003) 2737.
[84] R.T. Franceschi, B.S. Iyer, Y. Cui, J. Bone Miner. Res. 9 (1994) 843.
[85] J. Choi, B. Lee, K. Song, R. Park, I. Kim, K. Sohn, J Cell Biochem. 61 (1996) 609.
[86] D. Wang, K. Christensen, K. Chawla, G. Xiao, P.H. Kresbach, R.T. Franceschi, J. Bone Miner. Res. 14 (1999) 893.
[87] S.K. Misra, T. Ansari, D. Mohn, S.P. Valappil, T.J. Brunner, W.J. Stark, I. Roy, C. Jonathan, J. R. Soc. Interface. 7 (2010) 453.
[88] H.U. Cameron, Contemp. Orthop. 25 (1992) 506.
[89] A. Terella, P. Mariner, N. Brown, K. Anseth, S.O. Streubel. Arch. Facial. Plast. Surg. 12 (2010) 166.
[90] Q. Xu, H. Lu, J. Zhang, Int. J. Nanomed. 5 (2010) 331.
[91] X. Liu, et al. J. Mater. Sci. Mater. Med.20 (2009) 1237.
[92] J. Lao, J. M. Nedelec. E. Jallot, J. Mater. Chem. 19 (2009) 2940.
[93] V.G. Varanasi, Acta Biomater. 5 (2009) 3536.
[94] E. Gentleman, Acta Biomater. 9 (2013) 5771.
[95] M. Diba, F. Tapia, A.R. Boccaccini, L.A. Strobel, Int. J. Appl. Glass. Sci. 3 (2012) 221.
[96] R.M. Day, Biomater. 25 (2004) 5857.
[97] A.A. Gorustovich, J. A. Roether, A.R. Boccaccini, Tissue Eng. Part B. (2010) 199.

[98] A. Leu, J. K. Leach, Pharm. Res., 25 (2008) 1222.

[99] M. Bellantone, H.D. Williams, L.L. Hench, Antimicrob. Agents. Chemother. 46 (2002) 1940.

[100] C.V. Brovarone, M. Miola, C. Balagna, E. Verne, J. Chem. Eng. 137(2008) 129.

[101] S. Haimi, Acta Biomater. 5 (2009) 3122.

[102] M. Gubler, T.J. Brunner, M. Zehnder, T. Waltimo, B. Sener, W.J. Stark, Int. J. End. 4 (2008) 670.

[103] G. Lusvardi, G. Malavasi, L. Menabue, V. Aina, C. Morterra. Acta Biomater. 5 (2009) 3548.

[104] I. Kansal, A. Goel, D.U. Tulyaganov, L.F. Santos, J.M.F. Ferreira. J. Mater. Chem. 21 (2011) 8074.

[105] D.S. Brauer, N. Karpukhina, R.V. Law, R.G. Hill. J. Mater. Chem. 19 (2009) 5629.

[106] M.W.G. Lockyer, D. Holland, R. Dupree. J. Non-Cryst Solids. 188 (1995) 207.

[107] H.A. Abo-Mosallam, R.G. Hill, N. Karpukhina, R.V. Law. J. Mater. Chem. 20 (2010) 790.

[108] A. Tilocca, Phys. Rev. B. 76 (2007) 224202.

[109] S.L. Estebana, E. Saiza, S. Fujinob, T. Okuc, K. Suganumac, A.P. Tomsia, J. Eur. Ceram. Soc. 23 (2003) 2921.

[110] A.A. Noaman, C.F.S. Rawlinson, R.G. Hill, J. Non-Cryst. Solids. 358 (2012) 3019.

[111] J. Sułowska, I. Wacławska, Z. Olejniczak, J. Therm. Anal. Calorim. 116 (2014) 5159.

[112] A. Thomas, Japes Bera, J of Sol-Gel Sci. and Tech.80 (2016) 411.

[113] H. Tripathy, S.K. Hira, A.S. kumar, Uttam Gupta, Parha Pratim Mann, S.P.Singh, 41(2015)11756.

[114] Y. Zhao, X. Zeng, W. Zhang, Y. Zhao, J. Kang, J. Chem. Pharm. Res. 6(7) (2014) 1180.

[115] B. Cabal, L. Alou, F. Cafini, R. Couceiro, D. Sevillano, L.E. Tejeda, F. Guitián, R. Torrecillas, J.S. Moya, Scientific Reports 4 (2014) 5440.

[116] J. Maria, D.F. Ferreira, A. Goel, US Patent No. US20140193499 A1 (2014).

[117] X. Yang, L. Zhang, X. Chen, X. Sun, G. Yang, X. Guo, H. Yang, C. Gao, Z. Gou , J. Non-Cryst. Solids, 358 (2012) 1171.

[118] C. Russel, Chem. Mater. 17 (2005) 5843.

[119] A. Goel. E.R. Shaaban, F.C.L. Melo, M.J. Ribeiro, J.M.F. Ferreira, J. Non-Cryst. Solids. 353 (2007) 2383.

[120] J. Maa, C.Z. Chen, D.G. Wang, Y. Jiao, J.Z. Shi, Biointerfaces. 81 (2010) 87–95.

[121] F. Wanga, Q. Liao, G. Xiang , S. Pan, Journal of Molecular Structure 1060 (2014) 176–181

[122] K.V. Shah, M. Goswami, D.K. Aswal, V.K. Shrikhande, S.K. GuptaG. P. Kothiyal, Journal of Thermal Analysis and Calorimetry, Vol. 89 (2007) 1, 153–157.

[123] D.S. Brauer, N. Karpulthina, M.D. O'Donnell, R.V. Law, R.G. Hill, ActaBiomater. 6 (2010) 3275–3282

[124] L. Marsich, L. Moimas, V. Sergo, C. Schmid , Spectroscopy 23 (2009) 227–232 227.

[125] A.G. Kalampounias, N.K. Nasikas, G.N. Papatheodorou, J. Chem. Phys. 131 (2009) 114513

[126] A. G. Kalampounias, Bull. Mater. Sci. 34 (2011) 299–303.

[127] D. Bellucci, G. Bolelli, V. Cannillo, A. Cattini, A. Sola, Materials Characterization 62 (2011) 1021–1028.

Chapter 3 Materials and Methods

All the samples were synthesized by melt quench technique followed by controlled heat treatments. These samples were characterized by various techniques. The technical details of all the experimental techniques are given in this chapter.

3.1 Sample preparation

3.1.1 Preparation of glasses

Glasses having composition $55SiO_2$-$10K_2O$-(35-*x*)CaO-35MgO (*x*= 0, 5, 10, 15, 20, 25, 30, and 35 mol %) were produced using melt-quench technique. The purity of starting materials was 99 %, and they were used without further purification. All the initial chemicals were taken as oxides. The potassium carbonate (K_2CO_3) was taken according gravimetric factor i.e.1.47. The starting powders were ground and mixed in agate mortar pestle in acetone media for 1 hour (h). The ground powder was melted at 1550 °C in alumina crucibles using a high temperature programmed electric furnace with a heating rate of ~5 °C /min.

Table 3.1 Sample labels along with their composition.

Sample Label	SiO_2	K_2O	CaO	MgO
G1	55	10	35	0
G2	55	10	30	5
G3	55	10	25	10
G4	55	10	20	15
G5	55	10	15	20
G6	55	10	10	25
G7	55	10	5	30
G8	55	10	0	35

To enhancing the fusibility of the chemicals with each other, the furnace was held for 0.5 h at intermediate temperatures (300, 600, 900, 1200° C). The melt was also held at 1550 °C for 1 h to homogenize the melt. To obtain the flakes of samples, the melt was put on a base of thick

copper plate and quenched by another copper plate in air. Some of the part of the melt was put in cuboidal graphite mold to obtain cuboidal glass specimen. The sample labels and their compositions are given in Table 3.1.

3.1.2 Preparation of glass-ceramic pellets

Pellets of diameter 5 mm and thickness ~2-3 mm were obtained by pressing the fine and ground powders of as-quenched samples using a hydraulic press at a pressure 1.25 kN/m^2 for 10 s. Based on thermal analysis, as discussed in later section, nucleation/growth temperature of 850 °C was chosen for controlled heat treatment of all the glasses. The samples were kept in furnace for 0.5 h followed furnace cooling to the ambient temperature. The controlled heat-treatment tends to crystallize some crystalline phase embedded in the glass matrix.

3.2 Characterizations of as quenched/heat-treated samples

All the glass samples have characterized using various techniques as discussed in this section and later section. Physical parameters of all the as quenched samples have been measured for practical applications. The synthesized glass/glass-ceramic pellets were examined for suitable mechanical compliance. Further, the glasses have been examined to check their biocompatibility as an implant material and other related applications. As-quenched samples are characterized to assess the thermal properties. The transport phenomenon and dielectric behavior in these glasses have also been studied. Lastly, the complications of infection faced by biomaterial have been discussed in the next chapter and the methodology of the same has been elaborated subsequent section.

3.2.1 Physical parameters

Density of the as-prepared glasses is calculated using standard Archimedes' principle with xylene as a buoyant medium:

$$\rho_{sample} = \frac{w_a}{w_a - w_x} \times \rho_{xylene} \tag{3.1}$$

where, ρ_{sample} and ρ_{xylene} are the density of sample and xylene, respectively. w_a and w_x are the weight of the sample in air and xylene, respectively. Density of xylene is 0.863 g/cm^{3}at room temperature. Some other physical parameters (molar volume, excess volume, oxygen molar volume etc.) were also calculated by density data as discussed in the next chapter.

3.2.2 X-ray diffraction (XRD)

XRD is the sophisticated technique to prove the amorphousness of the present samples. Similarly the heat treated pellets of as quenched samples is also confirmed to be crystalline or amorphous by XRD. Cathode ray tube produces X-rays, which is filtered to generate monochromatic radiation, collimated to concentrate, and directed toward the sample. XRD is based on constructive interference of monochromatic X-rays which is diffracted from the crystalline sample. The interaction between sample incident rays produces constructive interference of the diffracted rays when the Bragg's low condition ($2d \sin\theta = n\lambda$) is satisfied. X-rays are having wavelength (λ) between 0.1-100 Å, which is exactly of the same order as of the inter-planar spacing (d) of the crystals. Therefore, the interaction between X-rays and crystals would cause of diffraction patterns as per Bragg's law as shown in Figure 3.1. The details of structure along with volume of crystalline phases, crystallite size and strain etc. can be calculated by XRD [1]. Glass being amorphous materials does not possess diffraction peaks. Instead of diffraction peaks, a broad halo or more are observed. The position of the centre of the broad halo depends on the composition of the glasses. More than one broad halo in the XRD patterns, which directly indicates the phase separated glasses. The phase separated glasses are the consequence of compositions containing immiscible phases in the melt [2]. The phenomenon of phase separation is governed by the overall lowering of the energy. If the separation of the mixture of two components favors the lowering of free energy, then glass becomes phase separated [3], sometimes homogeneous melt without any phase separation lead to lowering of free energy.

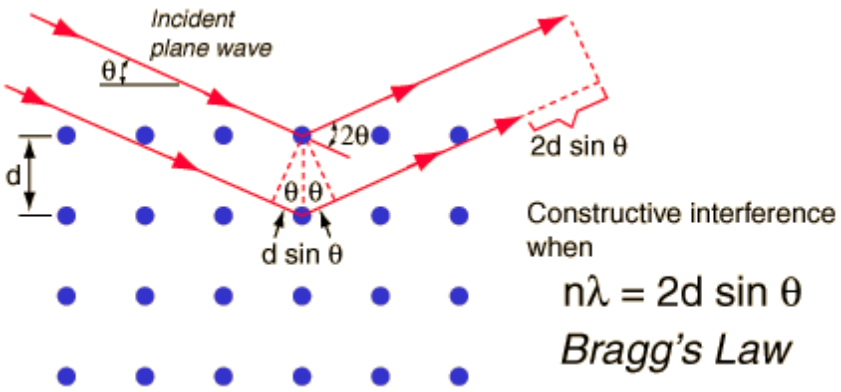

Figure 3.1 Schematic diagram of illustration of Bragg's law [4].

The XRD patterns of glass-ceramics provide adequate information about the crystalline phase (s) which got developed into the amorphous phases either by virtue of heat treatment or development of HCA after soaking in the solution in SBF. Glass-ceramics possess some crystalline peaks which are embedded in the base glass matrix. The volume fraction of different phases, crystallite size and type of strain such as compressive and tensile in the samples etc. of the crystalline phases can be obtained. In this study, the XRD patterns of the as-quenched samples before and after immersion in SBF were recorded using a PANalytical's X'Pert Pro X-ray diffractometer with CuK_{α} radiation having wavelength λ=1.54Å. Measurements were done in air between the 2θ ranges of 10-80°. The scanning speed and step size were kept ~3° min^{-1} and 0.017°, respectively. The crystalline phases and their peaks were matched by the standard ICDD card using high score software.

3.2.3 Fourier transforms infrared spectroscopy (FTIR)

This method uniquely characterizes the chemical bond present in the glass or any substance. It is worked on the interaction between IR radiations and the matter. Two covalently bonded atoms can visualized to be similar to a mass less spring which is attached with two heavy balls at both ends vibrating with some unique frequency. When the frequency of incident radiation becomes equal to the frequency of vibration of a bond it gets absorbed which produced an IR-band. Molecule can be vibrated with different modes such as stretching,

bending, rocking etc. depending on its available degrees of freedom [5]. Same bond can also be given more than one IR bands at different wave numbers. Shifting of IR-bands is very useful to know about the weakening or strengthening of the bonds of the materials. Broadness of the FTIR bands is due to close continuum vibrational frequencies which are difficult to resolve. It shows the range of bond lengths, bond strength of the functional groups available in the materials. Also, it is decent tool to examine the bioactive properties of the glasses/ glass-ceramics before and after immersion in SBF solution. Comparison between samples before and after soaking in SBF helps to understand the any structural changes, which is induced due to interaction with SBF on the surface of the samples. FTIR spectra of all the prepared samples were recorded at ambient temperature range of 450-4000 cm^{-1} on Perkin Elmer- Spectrum-RX-IFTIR spectrometer. The spectral resolution kept 0.8 cm^{-1}. 5 mg powder sample was mixed with 20 mg KBr and then pelletized using hydraulic press at a pressure (0.63 kN/mm^2).

3.2.4 Raman spectroscopy

Information regarding structural units of the glasses was calculated by using another complementary technique i.e. Raman spectroscopy. Some of the broad band silica not resolved properly in FTIR spectra could be understood by this technique. This technique is sensitive at the wave number where FTIR is insensitive. The Raman spectroscopy works on a change in polarizability of a molecule, whereas FTIR spectroscopy works on a change in the dipole moment. The spectrum of representative powdered glass was traced within 50-1200 cm^{-1} on a Renishaw in via Raman spectrometer. Ar^+ laser (514.5 nm) was used at 20 mW for the measurements. As a reference, silicon was used to calibrate the instrument at 520 cm^{-1}. Spectral resolution of the instrument was ±1 cm^{-1}.

3.2.5 Differential thermal analyzer

Differential thermal analysis (DTA) technique is basically useful to check about the thermal stability and phase transition of the substance. It is mandatory to analyze the samples using this technique to have an account of characteristics temperature of the glasses. As already discussed in the previous chapter, the basic properties of glass characteristics temperatures (T_g). Many potentially required processing like coating; enameling etc requires subjecting glass to high crystallization temperature (T_c) zone. Hence, it is worthwhile to understand the thermal stability of the glass using DTA. In this technique, the material is under study with an inert reference is made to undergo the same thermal cycles, whereas recording temperature difference between reference and sample. This temperature difference (ΔT) is then plotted with time, or temperature (DTA curve or thermogram) resulting changes in the sample with references to the inert reference can be detected in the form of either endothermic or exothermic. Therefore, DTA graph gives data on the transformations that have occurred, such as glass transitions temperature (T_g) crystallization temperature (T_c), melting temperature (Tm), sublimation temperature and phase transition etc.

DTA has a sample holder comprising thermocouples, sample containers, furnace and recording system as depicted in fig 3.2. Two thermocouples are joined in a differential arrangement and connected to differential amplifier. One thermocouple is positioned in an inert material (Al_2O_3) and other one is positioned into test sample. With increasing temperature, a deflection in voltage can be seen due to the phase transition of the samples. This happens due to the given heat is raised inert substance temperature. But be incorporated as latent heat is responsible to change the phase in materials.

Thermal analysis was carried out on Perkin Elmer (Model: Diamond Pyris) TG/DTA equipment. The (T_g) and (T_c) were obtained from the DTA curves in the temperature range 200-1000°C at different heating rates i.e. 25, 30, 35 and 40 °C/min. Approximately 10 mg of

each glass powder was taken in a Pt crucible for the measurements. Al_2O_3 (99.9% pure) was taken as a reference material. The temperature of the samples and the reference material was measured with the accuracy of ±1°C. The softening temperature of these glasses was obtained from the dilatometeric curves obtained at $5^oC\ min^{-1}$ heating rate in the air on dilatometer (DIL402PC, Netzsch).

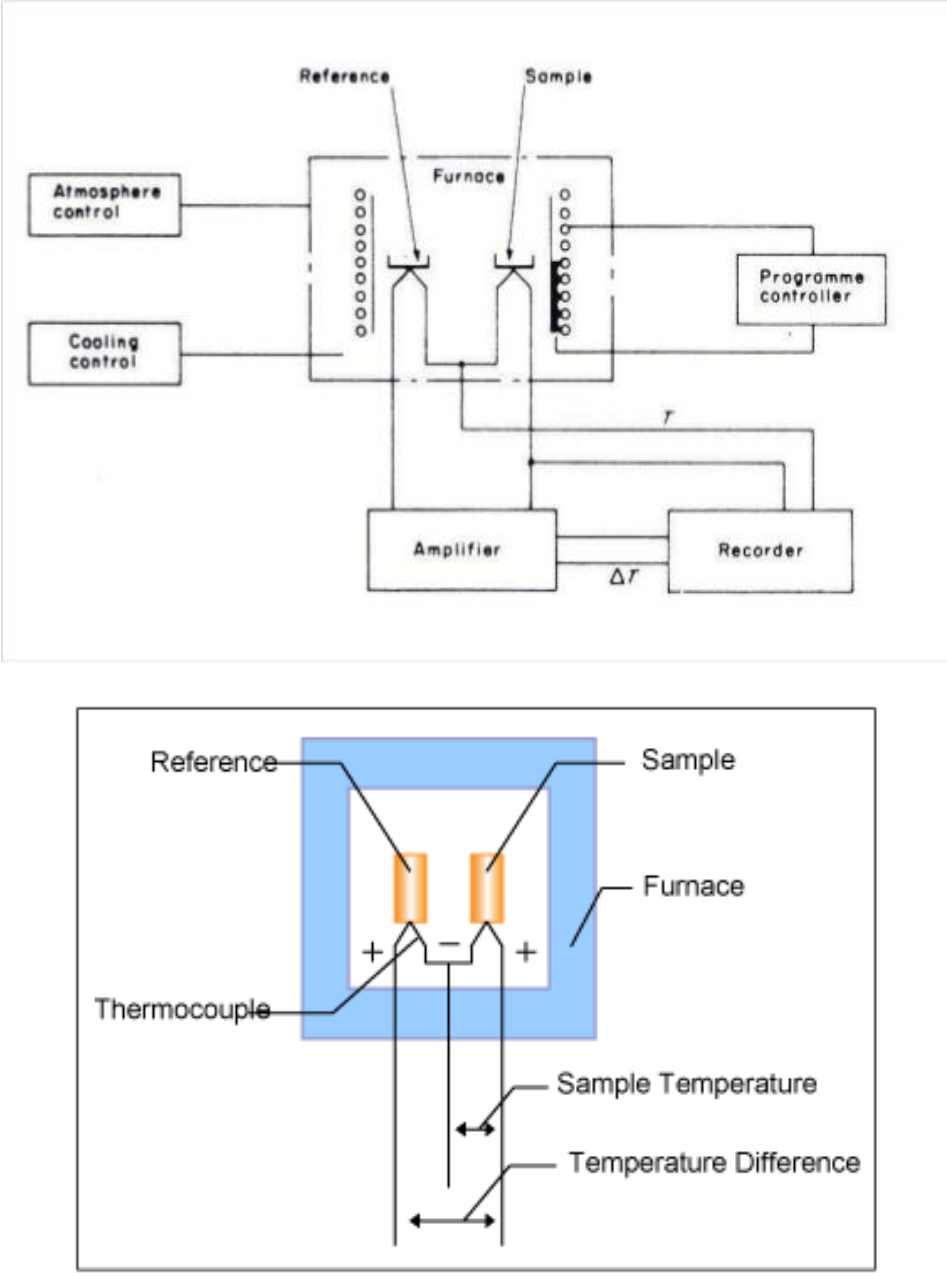

Figure 3.2 The basic assembly of differential thermal analyzer [6].

3.2.6 Impedance analyzer

Dielectric measurement was done to get an account of ion mobility and other transport phenomenon. These parameters are ultimately related to structural forming unit in the glass and glass-ceramics. So, this technique would add valuable information to understand bioactive behavior of glass which is directly linked to local structure of the glass. For this, glass ingots were cut using Buehler diamond cutter (Iso Met low speed saw) to get uniformly thick glass slices. These slices were washed ultrasonically prior to Pt coating on both sides by JEOL auto fine coater (JEC-3000FC). Operative current and time were 20mA and 160 sec, respectively. Dielectric measurements were carried out on solartron impedance analyzer (SI 1260) within temperature and frequency ranges 100-400°C and 100-1MHz, respectively. Temperature measurement error was ± 1°C.

3.2.7 UV-visible spectroscopy

When incident UV-Visible light is passed through sample dissolved in appropriated solvent the following relation between optical band gap energy (E_g) and absorption coefficient (α) for small values of absorption coefficients ($\alpha \leq 10^{-4}$) are given:

$$\alpha\, h\nu = B(h\nu - Eg)^n \tag{3.2}$$

Here, $h\nu$ denotes the energy photon. n can be have different values such as 2 for indirect allowed, 3 for indirect forbidden, ½ for direct allowed and 3/2 for direct forbidden transitions. B is constant and also known as band tailing parameter.

Optical spectra of the materials are characterized by an exponential increase of the absorbance coefficient with increase in energy of incident photons. Difference in absorption coefficient in the Urbach tail region is given as follows:

$$\alpha = \alpha_0 \exp(h\nu/E_U) \tag{3.3}$$

where , α_0 and E_U are the constant and Urbach energy, respectively [7]. Urbach energy of the glasses can be calculated taking the inverse of the slope of linear segment of the curve between *ln α* and *hv.* The optical parameters of all the samples can also be taken in powder form. For governing optical band gap and various parameters, the Kubelka-Munk function is given as follows.

$$F(R) = \frac{\alpha}{s} = \frac{(1-R)^2}{2R} \quad (3.4)$$

where, *R* and *s* are reflectance and scattering constant, respectively. UV- visible spectra of all the samples are recorded on double beam spectrophotometer (HITACHI U-3900 H) between spectral range 200-800 nm. The scattered speed 120 nmmin^{-1} and resolution 0.20 nm are used. The spectra are recorded in reflectance mode of the powder samples.

3.2.8 Vickers's micro hardness

For the measurement of microhardness, micro-indentations were done on the surfaces of the both bare and immersed pellets using a diamond Vickers indenter on a micro hardness testing machine (Mitutoyo MVK-HO, Japan). Additionally representative four glass slices cut from as quenched cuboidal block of glass sample to measure microhardness in the bulk form. The indentations using applied load 200 g for 15 sec were made at three different points on the samples. The mean of diagonal of the pyramidal shape indentations were taken. The micro hardness was calculated using the following equation:

$$H = 1.854\ F/d^2 \quad (3.5)$$

Where F is the applied load and *d* is the average length of the diagonal of pyramidal indentation.

3.3 Bioactivity tests of the bioglasses/glass-ceramics

In-vitro bioactivity of the samples was checked soaking glasses/glass-ceramics pellets in simulated body fluid (SBF). The solution was prepared by dissolving high-purity chemicals i.e. NaCl, $NaHCO_3$, KCl, $K_2HPO_4 \cdot 3H_2O$, $MgCl_2 \cdot 6H_2O$, $CaCl_2$, Na_2SO_4 in de-ionized water as given by Kokubo *et al.* [8]. The pH of the solution was adjusted to ~7.4 using 50 mM tris-hydroxymethylaminomethane ($(CH_2OH)_3CNH_2$) and 45 mMHCl. This pH value lies in the range of human blood plasma [9]. The samples were immersed in SBF solution kept in incubator containing polyethylene bottles. The temperature was maintained at 37°C. The weight (sample)/volume (SBF) ratio was maintained to be 0.02 g/ml [10]. The pH value of the SBF containing samples was measured every day. The weight loss of the samples was measured after completion of the experiment i.e. 42 days. Two of the samples i.e. G1 and G8 were soaked for 56 days to check the effect of extended immersion time. The soaked samples were taken out from SBF and were characterized using XRD, FTIR and SEM-EDS and compared with respect to pristine (unsoaked) samples. The residual SBF was characterized by microwave plasma atomic emission spectroscopy (MP-AES) to see the elemental release profile. The bioactivity of the alternate samples of the series namely G2, G4, G6 and G8 was also checked in powder form because glass finds many applications like filler materials in the powder form only [11]. 1 g powder obtained by crushing the as quenched glass samples was kept in 50 ml SBF in polyethylene bottles [12]. The observation of *in-vitro* bioactivity was undertaken using same characterizations and methodology as adopted for heat treated glasses/glass-ceramics of parent series. Additionally diffuse reflectance UV-Visible spectroscopy has also been employed to see the modifications of the powder samples. The effect of modifier on Hap layer formation and degradability of the sample could be assessed with the help of optical absorption spectroscopy [13,14]

3.4 Characterizations for bioactive properties

In addition to the above characterization techniques discussed so far, some key characterization are needed which would explicitly confirm the phenomenon of bioactivity as discussed in this section.

3.4.1 Microwave plasma-atomic emission spectroscopy (MP-AES)

MP-AES has proven its worth in many areas. It is a complimentary technique in the present bioactivity study, where the day to day pH change and overall weight change of the sample is verified by the MP-AES data. The elemental release profile up to part per billion (PPB) level of detection is given by this instrument. A magnetron and a waveguide are elementary components of the instrument. Electromagnetic energy of the range of 3.5 GHz is created by Magnetron. This energy is transferred to the waveguide assembly, which focuses this energy in radial electrical and axial magnetic fields, that field is focused on the plasma torch which gives the plasma. Nitrogen gas was purged to give plasma, resulting plasma acts as a high temperature excitation source producing high intensity emission lines. Sample is entered into the plasma through a nebulizer. It is decomposed and atomized. They emit the light of their characteristic wavelengths, when the atoms return back to the lower energy state. These emission lines are detected by the solid-state charge-coupled device detector.

In the present study, the concentration of ions leached out into the SBF solution from the sample surface was evaluated by an MP-AES system (Agilent 4100) with spectral resolution of the 25-40 pm. All the samples are prepared in 1 Normal nitric acid (HNO_3) solution. 0.1 g sample powder is added to a solution of 10 ml nitric acid and 25 ml water. Prepared solution is heated till 50% reduction of volume. The residual solution is further diluted by adding 100 ml water. All the measurements are recorded and repeated in triplicate. For the final analysis, the averaged values are used.

3.4.2 Scanning electron microscopy (SEM)

SEM is a very useful technique for the surface analysis of solid samples by taking high magnification resolution images [15] SEM uses a focused beam of electron. Magnification up to ~3,00,000 times can be achieved by advanced SEM. SEM has better resolving power as compared to optical microscope due to very small wavelength of electrons than the photons. Interaction between incident electrons and the sample surface is shown in Figure 3.3. SEM has depth of field up to 100 times greater than optical microscopes.

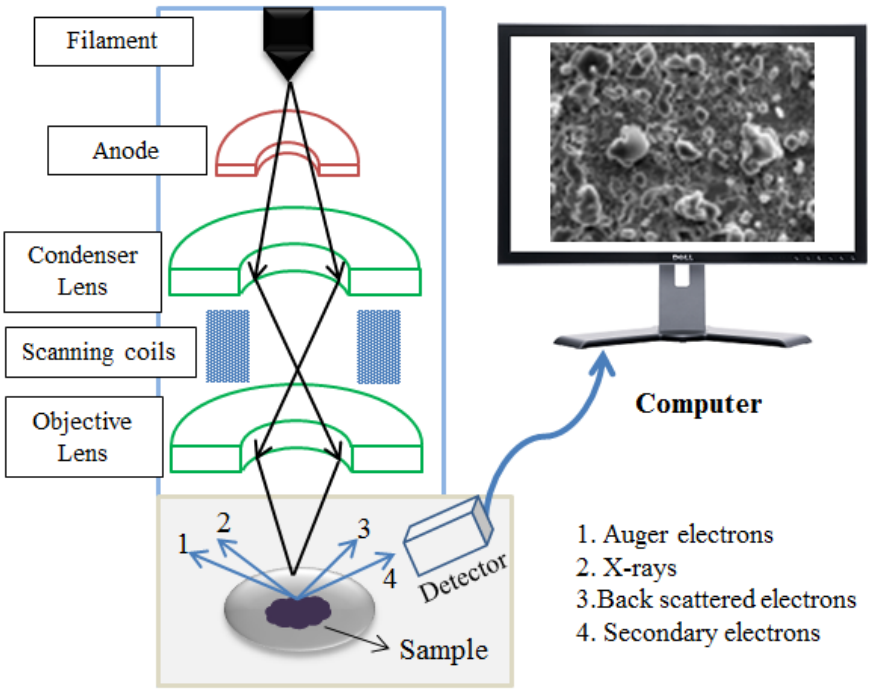

Figure 3.3 Schematic diagram of a scanning electron microscope [11].

In addition to this, SEM equipped with energy dispersive spectroscopy (EDS) gives valuable fundamental information of the selected sample surface. SEM images of the samples before and after immersion in the SBF solution produce valuable information about the changes on the surface of samples which is due to chemical reaction between glasses, glass-ceramics and SBF solution. In addition to this, SEM equipped with energy dispersive spectroscopy (EDS) enables the compositional and structural study of any formation of new entity formed on the surface of the sample.

Scanning electron micrographs of all the samples were taken using SEM JEOL/EO (version 1.0). The samples are coated with platinum, Pt on an Auto fine coater-JEOL (JEC-3000 FC) under operating current of 20 mA for 60 sec. EDS analysis is carried out using attached INCA x-act (Oxford instruments). EDS spectra of all the samples were recorded at appropriate acceleration voltages up to 10 keV.

3.5 Microbial test

Under this test susceptibility of the glass toward bacterial and fungal attack has been found. The potential of the glass as an antimicrobial agent or working of the glass in the presence of antimicrobial drug has been discussed as per the procedure discussed below [16].

3.5.1 Microbial limit test (MLT)

Under this method total aerobic bacterial count and total fungal count has been calculated. This test was employed to check susceptibility of the materials against bacterial and fungal infection. For total aerobic bacterial count experiment, 500 mg of representative fine prepared glass powder (without heat treatment) namely G2, G4. G6 and G8 which had been selected for this study was suspended in 4.5 ml of buffered sodium chloride peptone water solution (pH=7.0). Further, combination of these glass sample (375 mg) and well-known antimicrobial drug Amoxicillin 500 mg and clavulanic acid 125 mg was suspended in 9 ml of buffered sodium chloride peptone water solution to assess the antimicrobial effect of the drugs in the presence of glass. The prepared sample was incubated in the presence of molten soya bean casein digest agar (SCDA) at 30-35º (degree) for 5 days in Biochemical Oxygen Demand (BOD) incubator. The mean of colony forming unit (CFU/ml) was counted after multiplying with the dilution factor. The SCDA media without test sample served as negative control. Growth Promotion Test of the SCDA was considered as a positive control. Similar procedure had been adopted for total fungal count except the media used which was sabouraud dextrose agar (SDA). The incubation was done 20-25 º (degree) for 5 to 7 days.

3.5.2 Microbial cultivation

Pathogens are disease causing microorganism. Three classic pathogens namely *Staphylococcus aureus, Salmonella and Candida albicans,* which are genus of gram positive, gram negative bacteria and fungi, respectively. 10-100 CFU have been taken in contact with the glass sample to check microbial growth promoting or microbial growth inhibiting character of the glass sample. *Staphylococcus saureus* mainly resides on the skin hence expected to encounter at infections near implant sites. *Salmonella* generally enters our body through infected food, later infection colony could be found at anywhere in the body due to circulation of blood. *Candida albicans*is fungi associated with skin infection and other gastrointestinal tract. As mentioned above, sample was suspended in buffered sodium chloride peptone water solution in the same manner done for total microbial count test. Approximately 10-200 CFU/gm of bacterial culture of *saureus* (ATCC-6538) and *Salmonella* (NCTC-6017) were added to it. Each subculture was incubated on SCDA plates at 30-35°C for 72 h. Similarly, *Candida albicans* fungi culture taken from ATCC-10231 was incubated at SDA plate at 20-25 °C for 72 h. Confirmatory of the above test was done by carrying out positive control test simultaneously using 10-200 CFU/gm culture suspension without glass samples. This also served as reference for estimating microbial growth. Validity of the experimental condition was checked by applying negative control in which controlled suspension media without glass samples or culture media was taken.

References

[1]. B.D. Cullity, Elements of X-Ray Diffraction, Addison-Wesley Publishing Company Inc. (1956).

[2]. Y.-M. Sung, S.A. Dunn, J.A. Koutsky, J. Eur. Ceram. Soc. 14 (1994) 455.

[3]. J.E. Shelby, Introduction to Glass Science and Technology, 2nd edn, The Royal Society of Chemistry, Cambridge-UK (2005).

[4]. W. Smykatz-kioss, Differential Thermal analysis application and results in mineralogy, springer-verlag Berlin, Heidelberg (1974).

[5]. B. Schrader (ed.), Infrared and Raman Spectroscopy: Methods and applications, VCH Publishers, Inc., New York (1995).

[6]. V. Raghvan, Materials Science and Engineering (5th Edition) Prentice-Hall of India Pvt. Ltd.(2004).

[7]. F. Urbach, Phys. Rev. 92 (1953) 1324.

[8]. T. Kokubo, H. Kushitani, S. Sakka, T. Kitsugi, T. Yamamuro, J. Biomed. Mater. Res. 24 (1990) 721.

[9]. D. Zhang, M. Hupa, H.T. Aro, L. Hupa, Mater. Chem. Phys. 111 (2008) 497.

[10]. P. Siriphannon, Y. Kameshima, A. Yasumori, K. Okada, S. Hayashi, J. Biomed. Mater. Res. 60 (2002) 175.

[11]. Satwinder Singh, Structural and Bioactive Properties of Fe/Mn Oxides substituted Sodium Silicate Glasses, Ph.D Thesis (2017) Thapar University, Patiala.

[12]. P. Siriphannon, Y. Kameshima, A. Yasumori, K. Okada, S. Hayashi, J. Biomed. Mater. Res. 60 (2002) 175.

[13]. Mohini G.Jagan, Baskaran G Sahaya, Kumar V Ravi, M Piasecki, N Veeraiah, Mat. Sci & Eng C 57 (2015) 240

[14]. Ch.Vijaya Kumari, P.Sobhanachalam, C.K Jayasankar, N.Veeraih, V.Ravi Kumar, ceram.Int. 43(2017)4335

[15]. K. Shimizu, T. Mitani, New Horizons of Applied Scanning Electron Microscopy, Springer Berlin Heidelberg, Germany (2010).

[16]. Indian Pharmacopopia (IP), Vol-1, 7th edition, Indian Pharmacopopia commission, Ghaziabad (2014).

Chapter 4 Results and Discussion

As mentioned in previous chapters that all the samples are synthesized by melt quench technique. These melt-quench samples are characterized by various techniques to check their bioactivity with the structural variation due to initial constituents and their chemical nature.

4.1 Physical parameters

The quenched samples were optically transparent and bubble free. As MgO concentration increases, the color in the glass changes from whitish to light greenish. Based on density measurement, the calculated molar volume (V_m), excess volume (V_e), oxygen molar volume (V_o) of the glasses have been presented in Table 4.1. The density of the glasses was found to be decreasing on replacing CaO by MgO. It is a well reported phenomenon since density is an additive property and MgO is lighter than CaO. Molar volume (V_m) is the volume-occupied by one mole of the glass. Molar volume for the glasses was calculated using following equation:

$$V_m = M/\rho_{sample} \tag{4.1}$$

Where, M denotes the molecular weight in the sample as illustrated in Table 4.1. The molar volume also decreases with increasing MgO content in glass compositions. This is attributed to the smaller size and larger field strength of Mg^{2+} (0.45/Å^2) which makes network more compact than CaO (0.33/Å^2) containing glass [1]. In this respect, the calculation of excess volume will give a fair idea of glass compactness. Excess volume (V_e) and oxygen molar volume (V_o) values, were also calculated using the equation (4.2) and (4.3):

$$V_e = V_m - \sum_i x_i V_m(i) \tag{4.2}$$

$$V_o = \left(\sum \frac{x_i M_i}{\rho_{sample}}\right)\left(\frac{1}{\sum x_i n_i}\right) \tag{4.3}$$

Where, V_m (i) and M is the molar volume and molecular weight of i^{th} oxide, x_i is the fraction of the oxide present in composition and n_i is the number of oxygen atoms in i^{th} oxide. Excess

volume indicates the deviation from the ideal mixing volume. It can be correlated to the compactness and porosity of glasses [2]. Using the density data, the oxygen packing density (OPD) was also calculated according to equation 4.4:

$$\text{OPD} = \frac{\rho_{sample}}{M} \times \text{Number of oxygen atoms per unit formula unit} \quad (4.4)$$

The oxygen packing density (OPD) for the glasses was found to be following the opposite trend as for molar volume (V_m) as expected.

Table 4.1 Density (ρ), molar volume (V_m), excess volume (V_e), oxygen molar volume (V_o) and oxygen packing density (OPD) of the as-quenched samples.

Sample label	**G1**	**G2**	**G3**	**G4**	**G5**	**G6**	**G7**	**G8**
ρ (g/cm^3)	2.67	2.66	2.63	2.62	2.60	2.59	2.56	2.54
V_m (cm^3/mol)	23.25	23.04	23.01	22.79	22.66	22.45	22.40	22.27
V_e (cm^3/mol)	0.92	0.98	1.22	1.28	1.42	1.48	1.71	1.85
V_o (cm^3/mol)	15.00	14.86	14.84	14.71	14.62	14.48	14.46	14.36
OPD (mol/L)	66.65	67.25	67.36	67.99	68.37	69.04	69.17	69.59

This may be attributed that magnesium has a smaller ionic radius than calcium; as a result, it has higher field strength than calcium due to high charge to size ratio. Subsequently, it has a high attractive force towards non-bridging oxygen (NBO). In other words, Mg^{2+} increases the glass network connectivity by attracting anions strongly and as a result, the silicate glass network becomes more compact as compared to CaO containing glasses, which leads to decrease in the molar volume [3].

4.2 X-ray diffraction

All the eight samples show amorphous nature by the XRD. X-ray diffraction patterns of all as quenched samples are shown in Figure 4.1. The broad halos around 28º (degree) are observed in all the samples. It is a clear manifestation of the amorphous nature of the present samples. However, the halo is broader in the G8 sample as compared to other glasses.

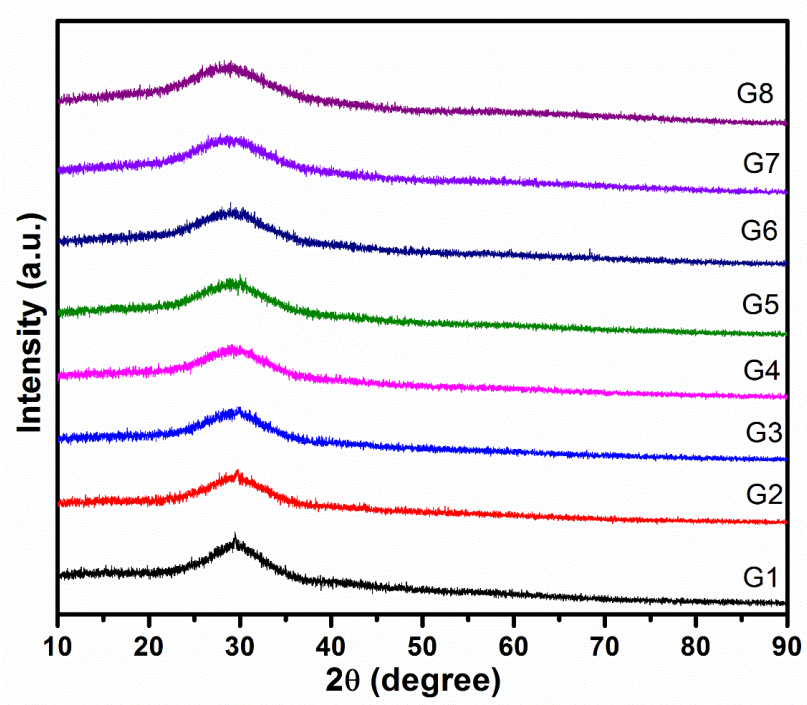

Figure 4.1 XRD patterns of the as-quenched (glasses G1 to G8) describing their amorphous nature.

It also indicates that G8 (35 % MgO) has higher disordering and a well-connected short-range order than other samples, as observed in Figure 4.1. The MgO content increases the broad hump shift towards a lower diffraction angle. In earlier study, we found, that shifting of halo to lower side is related to lower NBO, better connectivity of the network, which leads to higher characteristics temperature of the samples [4].

4.3 Characterizations of glasses

In this section, glasses namely G2, G4, G6 and G8 have been checked for complementary properties other than bioactivity. DTA not only provides the information regarding the characteristics temperature of the glass but also provides the information of the phase transformations. In addition to this, it is also very useful tool to ascertain the thermal stability of the samples.

4.3.1 Differential thermal analysis

Representative DTA thermographs of G2 glass at different heating rate are presented in Figure 4.2. The values of characteristic temperatures of the glasses i.e. T_g, T_c, and T_f are

obtained from the DTA graphs and presented in Table 4.2. Time derivative of all DTA curves yields maximum peak temperature assigned as inflection-point temperature (T_f). All the curves clearly show two close exothermic crystallization peaks i.e. T_{c1} and T_{c2}, out of which later is more pronounced. Second exothermic peaks Tc_2 are used for the thermal studies in the present work. This behavior is an indication of the phase separation in the glasses. After heat treatment, it may be crystallized differently due to different mechanisms of crystallization. Phase separation is usual in the glasses, which are having more than one network modifiers and former containing glass compositions [5].

nuclear magnetic resonance (NMR)

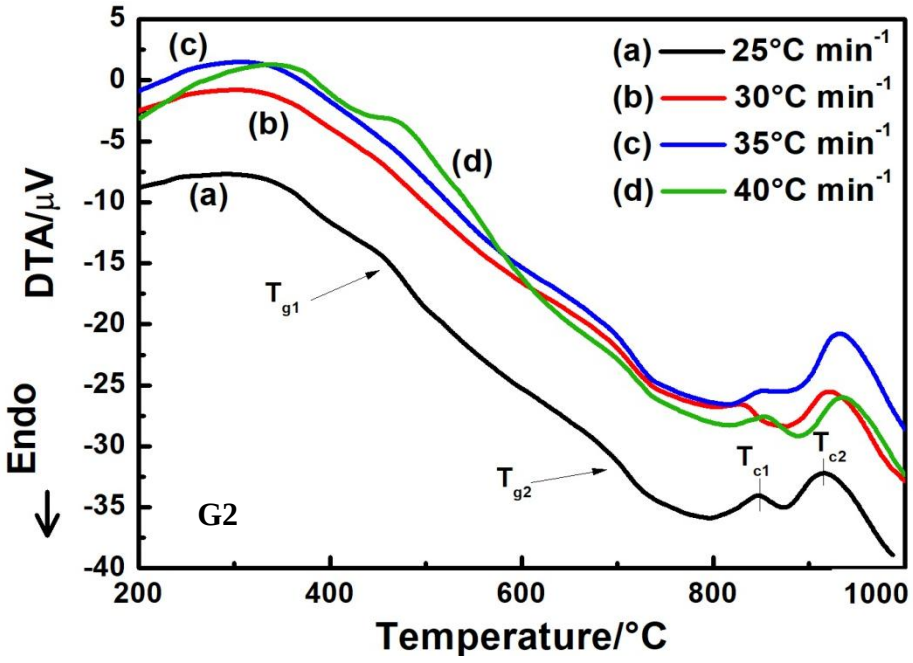

Figure 4.2 DTA thermographs of representative glass (G2) at various heating rates.

The peak crystallization temperature signifies the temperature, at which the viscous melt transforms into the crystallized entity. The major exothermic peak shows the continuous shift to higher temperatures for all the glasses along with gradual elevation in the peak height with an increase of heating rate as also observed by other reports [6]. It is expected because the higher amount of heat is available per unit time for the nuclei being crystallized. On the other

hand, T_{c1} did not show any clear trend with the heating rate. Along with this, some glasses exhibit diffused T_{c1} with low height.

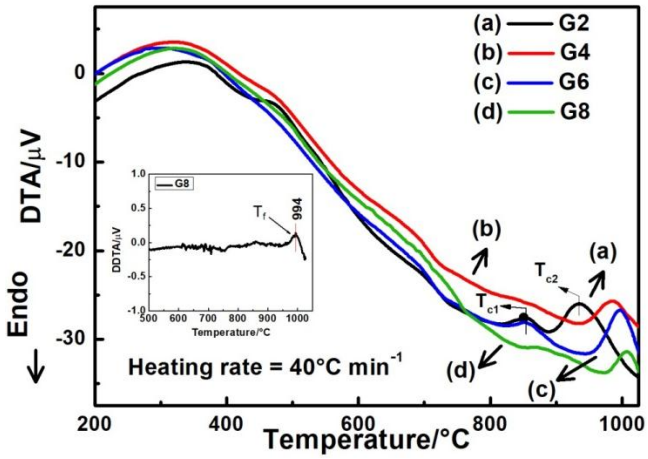

Figure 4.3 Representative DTA curves of the glasses at 40 °C/min.

These features may be indicating that instead of any single phase, some metastable phases with similar compositions are competing to grow in this temperature range. Recently, non-classical approaches of the nucleation in glasses imply the such intermediate metastable phases [7]. However, due to fluctuating dominance of the one or another phase, there is no clear trend with heating rate [8-9]. T_c is found to be higher for higher MgO containing samples. Similar shift of crystallization peaks with MgO content is also reported by Ma *et al*. [10]. DTA curves of the glasses at constant heating rate are shown in Figure 4.3. At high concentrations, MgO acts as glass former and enters into tetrahedral units $(MgO_4)^{2-}$ which restricts the majorly availability former silica based phase to grow by breaking the local symmetry of the silica rich phase. Two glass transition temperatures are observed in the same manner as that of T_c. Similar to T_{c1}, T_{g1} did not follow any particular trend; however, T_{g2} shifts to the higher temperatures at high heating rates. The shift in T_g with heating rate is well explained in literature [11-12]. At high heating rates, the relaxation time becomes smaller to become comparable to the isothermal holding time, which is the condition on the glass transition to take place. At this time, T_g varies inversely as the relaxation time. As isothermal hold time decreases with increasing heating rate, T_g shifts to higher temperatures at high

heating rate [13]. The T_g also depends upon composition, crosslink density, closeness of packing, etc. [14]. Decrease in modifier content decreases the non-bridging oxygen (NBO) atoms and hence, shifts the T_g to higher temperatures [15]. However, in present samples there is no clear trend with replacement of CaO with MgO. Mixed alkaline earth effect also plays significant role causing the anomaly in the properties of multi-component glasses both with respect to heating rate and composition.

Table 4.2 Characteristic temperatures, thermal stability parameter (ΔT), glass transition temperature range (ΔT_g) and softening temperature (T_s) of the glasses.

Sample label	α (°C min^{-1})	T_g (°C)	T_f (°C)	T_c (°C)	$\Delta T=T_c-T_g$ (°C)	ΔT_g (°C)	T_S (°C)	ΔT_{FWHM} (°C)	Avrami's constant n
G2	25	686	895	919	233	51	713	49	2.31
	30	689	901	926	237	50			
	35	691	911	934	243	49			
	40	701	913	938	237	47			
G4	25	675	946	963	288	70	709	36	3.42
	30	678	953	972	294	67			
	35	681	963	978	297	66			
	40	687	967	985	298	64			
G6	25	675	967	980	305	46	723	34	3.17
	30	687	971	986	299	45			
	35	691	975	994	303	38			
	40	693	981	998	305	39			
G8	25	709	976	995	286	58	728	26	2.97
	30	711	985	1000	289	58			
	35	718	990	1003	285	57			
	40	722	994	1009	287	57			

It is the well reported phenomenon that when one alkaline earth metal oxide is replaced with another alkaline earth metal oxide keeping the residual composition same, the non-linearity in the properties of the glasses is observed [16]. The variable size distribution of the glass powder of each sample may also affect the position of characteristic temperatures of glass, to some extent, and give rise to random trend [17]. Similar non-linearity in the properties also arises due to the concentration dependent role of MgO in glasses. In general, both CaO and MgO are supposed to be network modifiers, but at certain concentrations MgO can also form its own network**.**

This is because field strength of Mg^{2+} ($0.45/Å^2$) lies within the range, $0.4\text{-}1.3/Å^2$ i.e. for intermediate oxides as per criterion suggested by Dietzel *et al.* [18]. On the other hand, field strength of CaO ($0.35/Å^2$) is below 0.4 $Å^2$ and thus, is acts as a modifier only. $(MgO_4)^{2-}$ tetrahedron while forming its network consumes Ca^{2+} and K^+ ions for the sake of charge balancing and makes the network comparatively deficient in NBOs. In this way, the glass network symmetry is broken by the MgO at the cost of NBOs. So, the effect of MgO in disrupting the network is sometimes not appreciable, which may be responsible for the deviation in the observed trends. The concentrations, at which both the oxides act as a modifier, the difference among the properties arise due to the different ionic size and corresponding field strengths of Ca^{2+} and Mg^{2+} ions. In addition to this, the affinity of these ions towards other modifiers i.e. K_2O is obvious to be different, due to distinct Columbic interactions. All these factors collectively give rise to irregular trend in the ascertained properties. The observed fashion of T_g is also supported by the softening temperature obtained from dilatometric measurements of these glasses.

4.3.2 Effect on thermal stability

The thermal stability of the glasses at variable rate of heat flow has been measured by the following equation:

$$\Delta T = T_c - T_g \tag{4.5}$$

The calculated values are given in Table 4.2. The mean values of the ΔT were taken for the analysis. ΔT increases up to G6 and then drops down for G8 glass. The significance of this parameter lies in the fact that high value of ΔT refers to be large sintering temperature region, which could be beneficial for coating the bioinert ceramics (Ti etc.) required for biomedical applications without crystallization [19]. In this regard, G6 seems to be the most suitable sample for coating on the bioinert ceramics.

4.3.3 Kinetics and phase formations

The nucleation and growth of crystalline phases within the glass matrix depend upon a number of factors, including composition and network connectivity of the glass, interfacial energy (glass/crystal), viscosity, free energy change between glassy and crystalline phases, diffusion coefficient and thermodynamic driving force etc. [20]. Two types of activation energies are of the most importance during the transformation of amorphous to crystalline phase, namely activation energy of glass transition (E_g) and activation energy of crystallization (E_c). Various models are available to explain these thermal parameters under non-isothermal conditions. According to Kissinger's model [21], T_g of the glass depends on the heating rate (α) as follows:

$$\ln [T_g^2/\alpha] = E_g/(RT_g) + constant \tag{4.6}$$

where, R is the universal gas constant. $\ln\left(T_g^2/\alpha\right)$ is plotted against $1000/T_g$ to extract activation energies for the glasses. The data points were fitted into straight lines using least square method (Figure 4.4) and the measured slopes were put into equation (4.6) to get E_g values. On the other hand, according to Augis-Bennett model the relation between T_g and heating rates is:

$$\ln\left(T_g/\alpha\right) = E_g/\left(RT_g\right) + constant \tag{4.7}$$

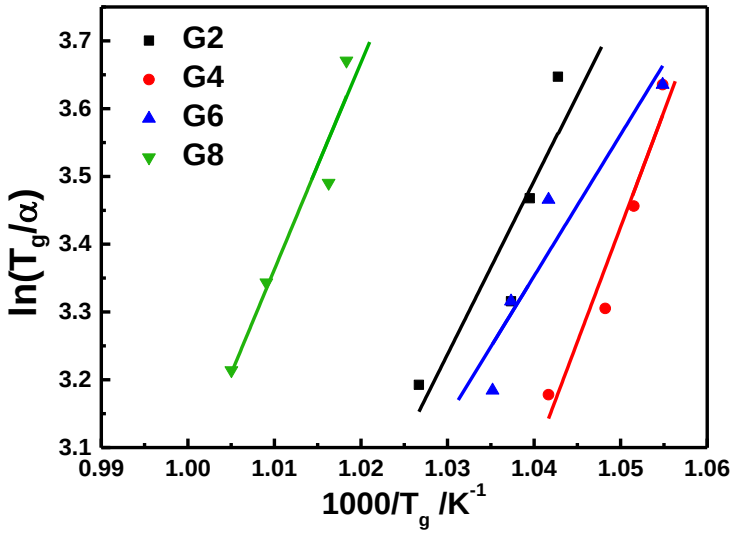

Figure 4.4 Kissinger's plots for activation energy of glass transition temperature.

To obtain activation energy, $ln\left(T_g/\alpha\right)$ was plotted versus $1000/T_g$ (Figure not shown) and the slopes of the fitted data were used in the equation 4.7. The activation energies calculated from both the models are presented in Table 4.2. The activation energy for glass transition is maximum for G4 glass and minimum for G6 glass. Both the models are in close agreement with each other as shown in Figure 4.5. Higher value of activation energy for glass transition implies greater strength of the glass as compared to one with lower activation energy of glass transition. For more insight into the glass transition phenomenon of present glasses, ΔT_g was calculated (Table 4.2). It corresponds to the temperature difference from starting the glass transition region up to the end of the endothermic peak. The maximum and minimum values of ΔT_g are obtained for G4 and G6 glasses, respectively. This parameter is related to the relaxation dynamics during transition process. In the present case, ΔT_g decreases slightly with the increase of heating rate. However, the difference is very less i.e. transition process is not practically influenced by the heating rate. However, ΔT_g has shown strong compositional dependence in the present glasses. ΔT_g is maximum for G4 and following the trend G4>G8>G2>G6. It must be noticed that CaO/MgO ratio for G4 glass is ~1.33.

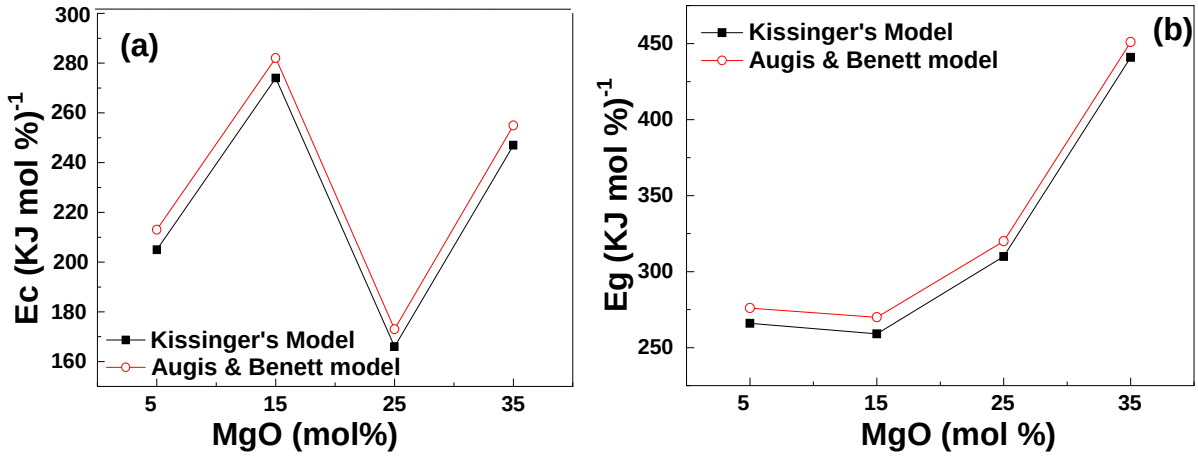

Figure 4.5 Comparison between the activation energies for glass transition temperature and crystallization temperatures calculated from Kissinger's and Augis-Bennet models.

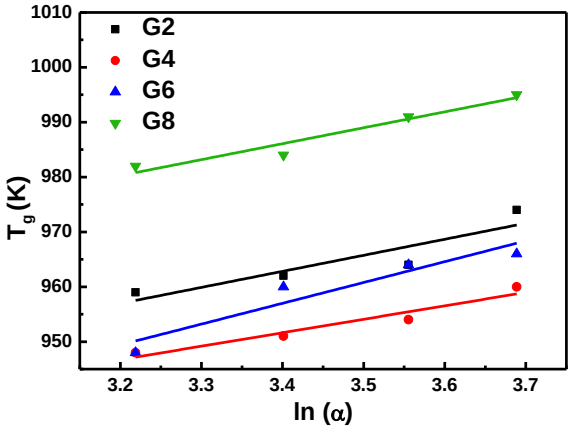

Figure 4.6 Lasocka plots for the glasses.

It seems that at nearly equal concentrations of the modifiers, the network structure becomes slightly stronger than the glass with dissimilar concentration of modifiers. ΔT_g is in agreement with the activation energy of the T_g for corresponding glasses. G4 needs more energy for glass transition than other samples, and the transition continues to wider temperature range. On the other hand, G6 with minimum activation energy relaxes sooner and the glass transition range is over in narrow temperature window (ΔT_g). This is also supported by the *B* parameter calculated from Lasocka model. According to Lasocka model [22]:

$$T_g = A + B \ln \alpha \tag{4.8}$$

Where, A is defined as T_g when heating rate is 1 ºC/min.

A plot between T_g and $ln\ \alpha$ yields a nearly straight line (Figure 4.6), which is fitted to straight line to get A and B values. B is a constant, which indicates the configurationally changes occurring near the glass transition region. Its value depends on the glass composition and the quenching rate during the preparation of the glasses. Calculated parameters are presented in Table 4.3. Low value of B corresponds to less configurational changes during the glass transformation. Figure 4.6 shows the variation in B and ΔT_g with the composition of glasses. ΔT_g and B parameters are maximum and minimum for G4 glass, respectively.

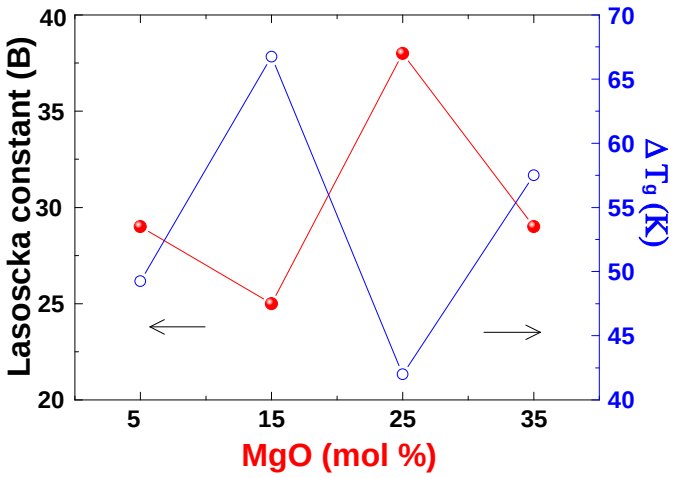

Figure 4.7 Variation in Lasocka parameter (B) and glass transition temperature range (ΔT_g) with composition.

This implies that G4 glass exhibits very less configurational changes during glass transformation and takes more time to transform in the glass. On the other hand, G6 with minimum activation energy of glass transition exhibits maximum configurational changes (B) and rapidly transforms to glassy state (low ΔT_g). This way B and ΔT_g follow the inverse trend with respect to each other. The dependence of the crystallization temperature (T_c) can also be described using the Kissinger and Augis-Bennett model. In accordance with Kissinger's model, the activation energy of crystallization (E_c) can be estimated from the following relation:

$$\ln [T_c^2/\alpha] = E_c/(RT_c) + constant \qquad (4.9)$$

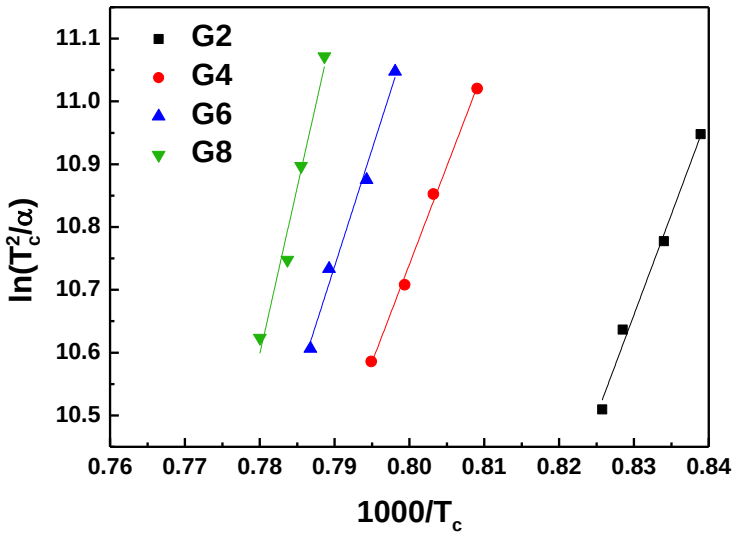

Figure 4.8 Kissinger's plots for the calculation of activation energy of crystallization for the glasses.

Here, *v* is known as the crystallization frequency factor and gives the number of attempts per sec made by the nuclei to overcome the energy barrier. Lower the value of *v*, higher is the thermal stability. E_c is higher for maximum MgO containing samples, while minimum for lower MgO containing sample as shown in figure 4.8. This indicates that MgO increases the resistance towards the crystallization of the glasses by disrupting the local silica network and consuming modifying ions in this process.

4.3.4 Avrami's constant

Sharp exothermic peak in the DTA graph of a sample indicates the bulk crystallization. On the other hand, broader peak signifies the surface crystallization. From the width of crystallization peak (ΔT_{FWHM}) and the activation energy (E_c) calculated from models discussed above, Avrami's constant (*n*) was calculated using the equation (6) as suggested by Augis and Bennett [23]:

$$n = 2.5/\Delta T_{FWHM} * RT_c^2/E_c \qquad (4.10)$$

n usually varies from 1 to 4. When *n* is nearly 1, surface crystallization dominates. On the other hand, *n* approaching 3 signifies the volume crystallization. Avrami's constant is close to 3 for a G4, G6 and G8 glasses (Table 4.3). However, *n* is ~2 for G2 glass. It can be concluded that the bulk crystallization predominates for all the samples. G2 exhibits one dimensional

crystallization growth, while other glasses show two-dimensional crystallization. *n* first increases from G2 to G4, and decreases thereafter. It may be possible that MgO at lower concentrations is not affecting crystallization of the glass significantly. However, at higher concentrations decrease of Avrami's constant indicates the decreasing tendency towards bulk crystallization.

Table 4.3 Thermal parameter of the glasses calculated from various models.

Sample label	Kissinger's Model			Augis & Benett Model			Lasoscka Constants	
	E_g (kJ mol^{-1})	E_f (kJ mol^{-1})	E_c (kJ mol^{-1})	E_g (kJ mol^{-1})	E_c (kJ mol^{-1})	Frequency (ν) (s^{-1})	A(°C)	B
G2	205	250	266	213	276	2.6×10^{10}	590	29
G4	274	244	259	282	270	5.0×10^{9}	595	25
G6	166	411	310	173	320	4.5×10^{11}	555	38
G8	247	319	441	255	451	7.8×10^{16}	614	29

In other words, MgO partly prevents the crystallization of the glasses in present compositions. The results are in agreement with previously reported effect of MgO on crystallization of phosphosilicate glasses [10].

4.3.5 Fourier transforms infrared spectroscopy (FTIR)

FTIR spectra of G1-G8 glasses are shown in Figure 4.9. The magnified spectra of samples G1, G4 and G8 are shown separately in Figure 4.10. The main bands in the glass structure due to glass forming atoms will be broad because of the very short range order present in the glass. The spectra show two major bands, i.e. at 737 cm^{-1} due to stretching vibrations of Si-O [2] and the second broad band with maxima at around 1009 cm^{-1}. It might be associated to SiO_2 structural unit formed by interaction with network modifiers like K_2O, MgO and CaO, etc. Some weak bands are also observed at 1393 cm^{-1}, 1461 cm^{-1} and 1530 cm^{-1} particularly

in the case of G1, G2 and G3 glasses. These bands become diffused as the MgO concentration increases in the glass compositions. This can be attributed to a decrease of calcium content in the glasses marked G5 to G8. These bands can be associated with a (Mg/Ca)-O-H band [24]. However, these bands are prominent in CaO containing glasses as compared to MgO containing glasses. It might be ascribed to the fact that CaO is heavier than MgO. The sharp band around 1675 cm^{-1} is due to bending vibration of H_2O molecules [3].

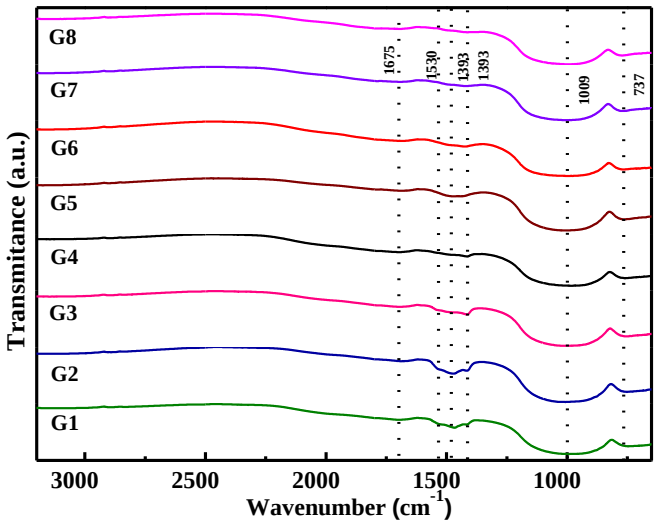

Figure 4.9 FTIR spectra of the as-quenched glasses showing different vibrational bands.

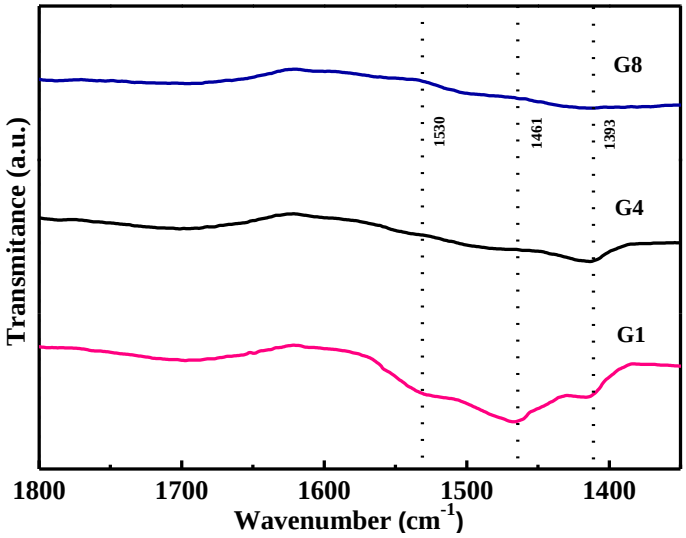

Figure 4.10 Magnified FTIR bands of the glasses G1, G4 and G8.

The XRD result also supports this observation as the halo becomes broader with the MgO content and shifted towards lower diffraction. Besides these bands, some weak bands are also

observed at 2443 cm^{-1}, 2849 cm^{-1} and 2910 cm^{-1}. These bands are related to the symmetric and asymmetric modes of interstitial water molecules [25]. Conclusively, the CaO containing glasses absorb water easier than MgO containing glasses. The FTIR bands become more diffused with increasing content of MgO in glasses.

4.3.6 Raman Spectroscopy

The Raman spectra of the present glasses are shown in Figure 4.11. G2 and G4 glasses show broad Raman bands within 500-1200 cm^{-1}, while G6 and G8 did not show any observable band throughout the measured wave number range. Broad band in the spectra arises due to the overlapping of more than one closely spaced Raman bands. It is reported that some Q_i units (majorly Q_2) contribute to the spectra with more than bands. Thus, the spectra becomes more difficult to analyze [26-27]. Raman bands over 500-1200 cm^{-1} are significant with respective to various Si-O vibrations. Therefore, the broad band observed in the spectra of G2 and G4 glasses were deconvoluted to resolve the possible occurrence of individual bands. Deconvoluted peaks of G2 and G4 glasses are shown in Figure 4.11 (a) and (b), respectively. The Raman bands ~600 cm^{-1} correspond to bending vibrations of depolymerized units [28]. Appearance of Raman bands near 700-850 cm^{-1} is due to the symmetric stretching vibrations of bridging oxygen atoms between silica tetrahedra [28]. This range includes Si-O-Si symmetric stretching vibrations, Si-O-Si bending and vibrations of orthosilicate (SiO_4^{4-}) units at 790, 807 and 850 cm^{-1}, respectively [28–31]. Metasilicate structural units give rise to Raman shift in the range 950-1000 cm^{-1}. In the present glasses, K^+, Ca^{2+} and Mg^{2+} can easily form their metasilicate units within the network, which arises due to modification action of these cations. These units are weaker than disilicate units where there is stronger sharing of oxygen between two silicate tetrahedra. Raman bands for disilicate units appear at relatively higher wave numbers near 1080 cm^{-1} [31]. Bands near 1100 cm^{-1} are due to asymmetric stretching vibrations of Si-O-Si bonds [28].

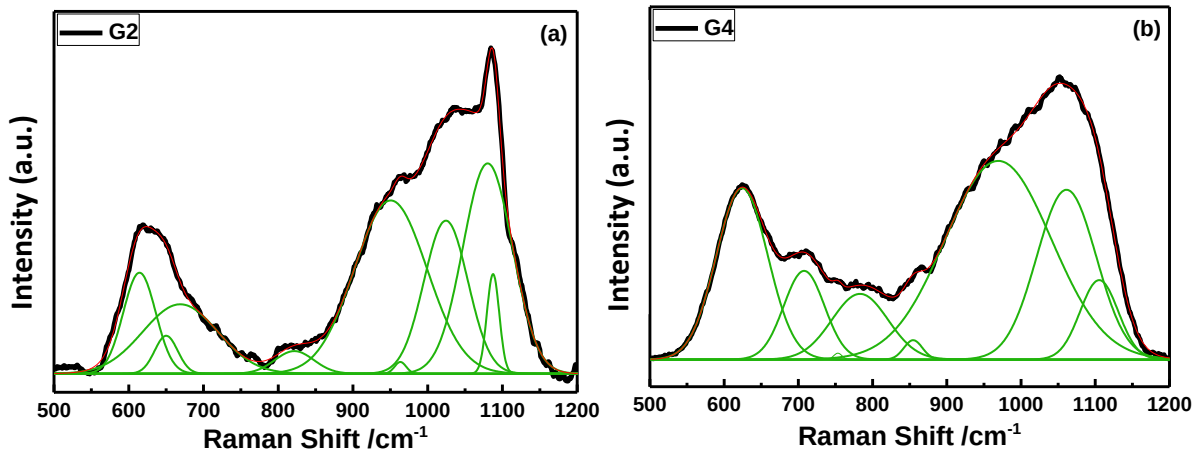

Figure 4.11 Deconvolution of selected region of the Raman spectra of (a) G2 and (b) G4 glasses.

The ratio of areas under the Raman bands within 950-1000 cm^{-1} and 1050-1100 cm^{-1}gives the approximate ratio of NBO/BO for a glass and is proportional to the degree of polymerization (Q_3/Q_2 ratio). The Q_0, Q_1, Q_2 and Q_3 are basically silicate structural units having 0, 1, 2 and 3 non bridging oxygen, respectively. Transport properties like viscosity, electrical resistivity are expected to be linear function of Q_3/Q_2 ratio [32]. The ratio is less for G2 glass (0.59) than G4 glass (0.62). It suggests that G4 glass is relatively more polymerized than G2 glass. It is also supported by the theoretical calculations. For glass compositions with higher MgO, the predominant bridged species are the dimeric $Si_2O_7^{6-}$and hence the Q_3/Q_4 ratio for G4 glass is higher as compared to G2 glass [33]. The deconvoluted bands of G4 glass are at higher wave number in comparison to the similar bands of G2 glass, which also supports the formation of more disilicate units in G4 glass and its better network connectivity.

4.3.7 UV-Visible spectroscopy

A diffuse reflectance spectrum of G1 to G8 glasses is shown in Figure 4.12 and 4.13. The variations of $\alpha h\nu^{1/2}$ with respect to the $h\nu$ are shown for glass samples G1-G8 in Figure 4.14 and 4.15. The optical band gap energies are obtained by extrapolation of the linear region of curves to $h\nu$ axis i.e. $\alpha h\nu^{1/2} = 0$ [34]. The values of the optical band gap are given in Table 4.4. The optical band gap of glass samples gradually increased from 3.42 eV to 3.65 eV with an

increase of MgO content. This is because Mg^{2+} having a smaller radius and a larger polarizability than Ca^{2+} induces more charge on NBOs which decreases the ionic character of oxygen ions and lowers the top of the valence band and leads to an increase in the optical band gap [35]. It has also been well established that replacement of a lighter element by heavier element decreases the optical band gap and vice versa [36]. The introduction of heavier metal breaks the Si-O-Si bond leads to appearance to NBO, which has more negative charge than bridging oxygen which leads to increase of ionic character.

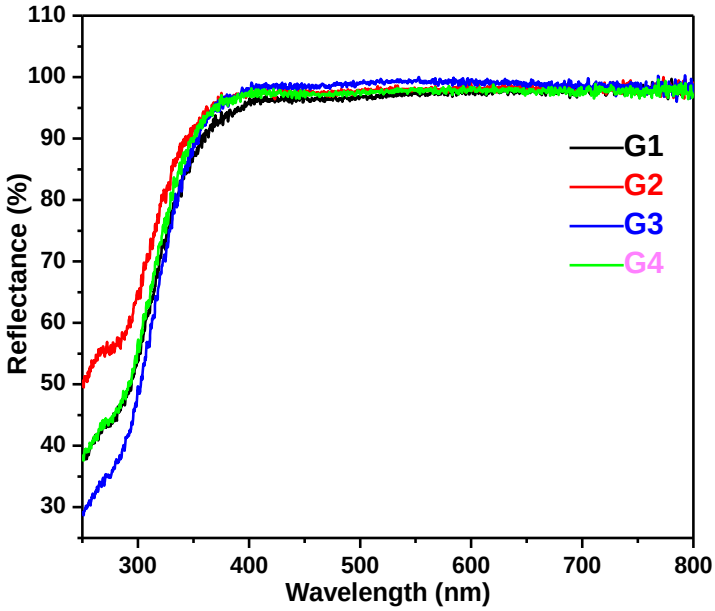

Figure 4.12 Reflectance spectra of glasses G1, G2, G3 and G4.

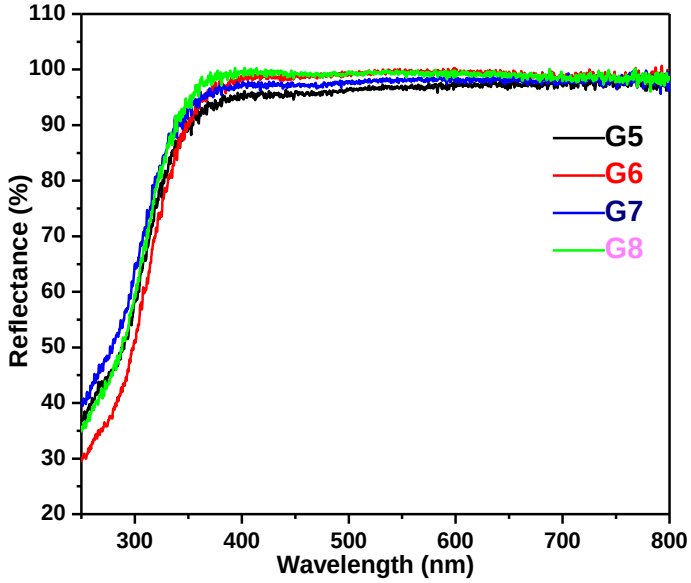

Figure 4.13 Reflectance spectra of glasses G5, G6, G7 and G8.

This results to rising of valence band and as result energy band gap is decreased. The defects in the system can be correlated to the Urbach energy. The relation between the Urbach energy *(E_u)* and the absorption coefficient *$\alpha(\upsilon)$* is given by the empirical Urbach law as [37]:

$$\text{Ln } \alpha = \frac{h\,\nu}{E_u} + \text{Constant} \tag{4.11}$$

The value of the Urbach energy is calculated from the slope of the linear portion of the curve between ln *α* and *$h\upsilon$* which is given in Table 4.4. The Urbach energy is related to the width of localized states in the optical band gap.

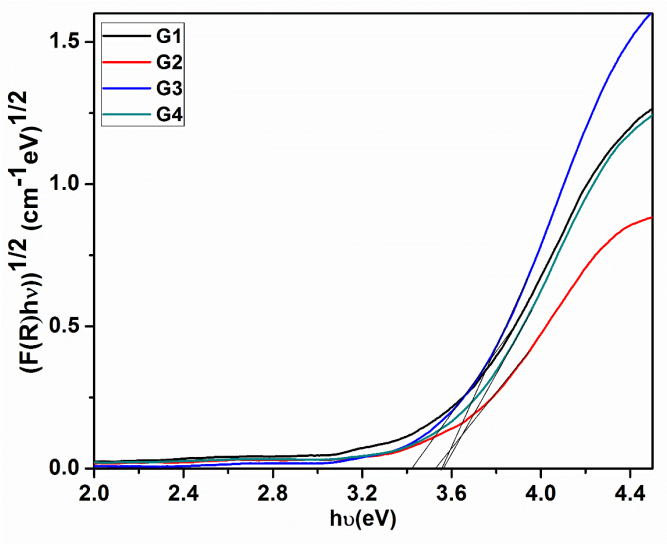

Figure 4.14 Tauc's plot for determination of optical band gap of glasses (G1-G4).

Table 4.4 Optical band gap and Urbach energy of the glasses.

Sample label	G1	G2	G3	G4	G5	G6	G7	G8
Optical band gap (eV)	3.42	3.46	3.52	3.56	3.59	3.63	3.70	3.72
Urbach energy (eV)	0.18	0.16	0.13	0.15	0.18	0.13	0.17	0.11

The origin of the exponential absorption is generally related to the random fluctuations in the potential associated with any lattice absorptions like thermal vibrations, dislocations or electric fields of defects which can further affect the energy bands and cause tailing of energy states into the forbidden gap [38]. The Urbach energy values lie between 0.18 eV to 0.11 eV for all the present glasses. The lower value accounts for lesser defects or NBO in the glasses.

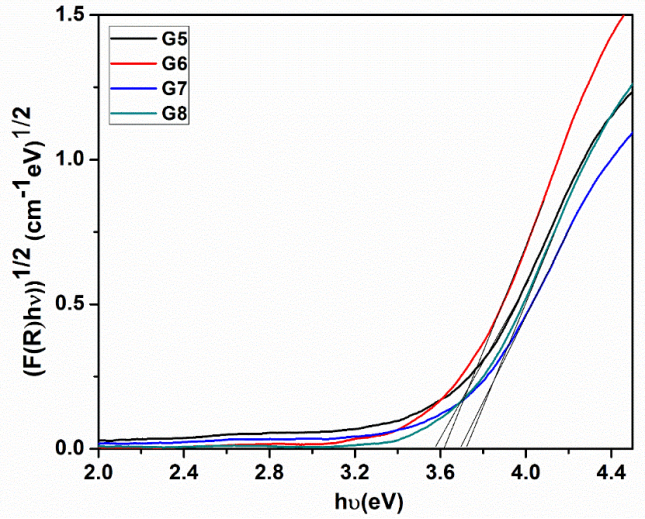

Figure 4.15 Tauc's plot for determination of optical band gap of glasses (G5-G8).

The Urbach energy values did not follow any trend on replacing CaO with MgO. The possible reason is that both the oxides are approximately of similar chemical nature. So, it indicates that the NBO is approximately same order in all the glasses except for field strength and electro-negativity difference to each other.

4.3.8 Dielectric measurement

The dielectric behavior of a material with applied alternating field is given by the following equation:

$$\epsilon_r(\omega) = \epsilon_r'(\omega) - i\,\epsilon(\omega) \tag{4.12}$$

Here, $\epsilon_r(\omega)$ is the dielectric permittivity, $\epsilon_r'(\omega)$ and $\epsilon''(\omega)$ are the real and imaginary parts of the dielectric permittivity, respectively [39]. At room temperature and 100 Hz, maximum dielectric permittivity is observed for G4 glass (~22), while G6 glass has shown minimum dielectric permittivity (~12) among the present glasses. G2 glass has second highest dielectric permittivity (~15) after G4. G8 has dielectric permittivity (~13) close to that of G6 glass. Raman spectra of these glasses revealed their more polarizable nature than G6 and G8. The dielectric measurements are also compatible with conclusions drawn from the thermal analysis in previous sections. G4 with most rigid structure prevents the movement of ions. Basically, the free NBOs may provide the path for the movement of ions. Hence, there is less

probability of loss in dielectric values due to conduction [40]. On the other hand, G6 having least rigid structure has more possibility to give way for ionic motions, which increases the ionic conductivity and eventually decreases the dielectric permittivity. At constant temperature, all the glasses showed declination in dielectric permittivity at high frequencies (Figure not shown). At low frequencies, higher dielectric permittivity is well explained by the Maxwell-Wagner theory. The observed trend in dielectric permittivity is the universal frequency dependence behavior shown by most of the materials [41-42].

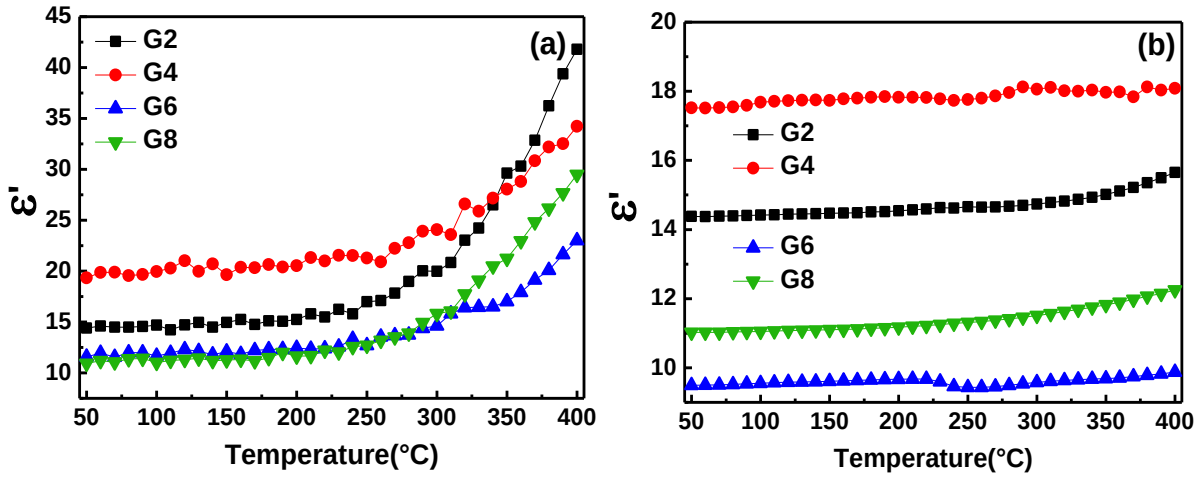

Figure 4.16 (a) Variation in dielectric permittivity of the glasses with respect to temperature at 100 Hz and (b) Variation in dielectric permittivity of the glasses with respect to temperature at 10^5 Hz.

At 100 Hz, dielectric permittivity of all the samples is independent of the temperature up to ~250 °C, which is shown in Figure 4.16 (a). Thereafter, it showed a continuous rise for all the samples. However, at high frequencies (>10^5 Hz), the dielectric permittivity of the glasses could not change significantly (despite of slight increase) throughout the measured temperature range as shown in Figure 4.16 (b). Temperature has dual and complex effect on the dielectric properties of glasses. Thermal vibrations due to increasing temperature can randomize the aligned electric dipoles of the dielectric material and decrease the dielectric permittivity. But, at the same time, it facilitates the ions to move a little, which are trapped in the various sites, defects, phase boundaries etc. to increase the dielectric permittivity [39-43]. The governance of the particular effect over the other at certain temperature decides the final

value of the dielectric permittivity. Orientational polarization prevails at lower frequencies, while diminishes at higher frequencies. Similarly, contribution of ionic polarization to the total dielectric permittivity ceases with rapidly switching electric field [44]. Both these polarizations are temperature dependent mechanisms. Hence, at higher frequencies, in the deficiency of these polarizations, the permittivity remains almost constant with respect to temperature. Minor increase with frequency at high temperatures may be due to electrode polarization effect [45], which is resolved more clearly in modulus formulation as discussed in next section.

4.3.8.1 Dielectric modulus

For ionic conductors, such as glasses, it becomes necessary to make use of modulus formulation for better understanding of relaxation dynamics [46]. This formulation is usually used to suppress the electrode effects. When relaxation peak is not clear in ϵ'', the relaxation processes due to simple dc conduction effects appear as clear peaks in M''[47]. The electric modulus ($M^\star$) is a function of the complex permittivity ($\epsilon^\star$) of glass as follows:

$$M^\star = {}^1/_{\epsilon^\star} = M'(\omega) + M''(\omega) = M_\infty \left[1 - \int_0^\infty e^{-i\omega\tau} \frac{d\phi(t)}{dt}\right] \quad (4.13)$$

In this equation, $d\phi\ (t)/dt$ symbolizes the time development of the electric field within the material. The real and imaginary parts of complex $M^\star$ can be solved as:

$$M'(\omega) = \frac{\epsilon^{'}(\omega)}{\left(\epsilon'(\omega)^2 + \epsilon''(\omega)^2\right)}; \quad M''(\omega) = \frac{\epsilon^{''}(\omega)}{\left(\epsilon'(\omega)^2 + \epsilon''(\omega)^2\right)} \quad (4.14)$$

$M'(\omega)$ and $M''(\omega)$ as a function of frequency of the glasses at selected temperatures are presented in Figure 4.17 and 4.18, respectively. $M'(\omega)$ curves of all the glasses show a dip towards zero at low frequencies and this behavior becomes clearer at high temperatures. It can be concluded that electrode effects are predominant at high temperatures [48]. Relaxation phenomenon in the glasses occurs mainly due to motion of modifying ions [49-50]. G6 shows relaxation peaks at all the selected temperatures.

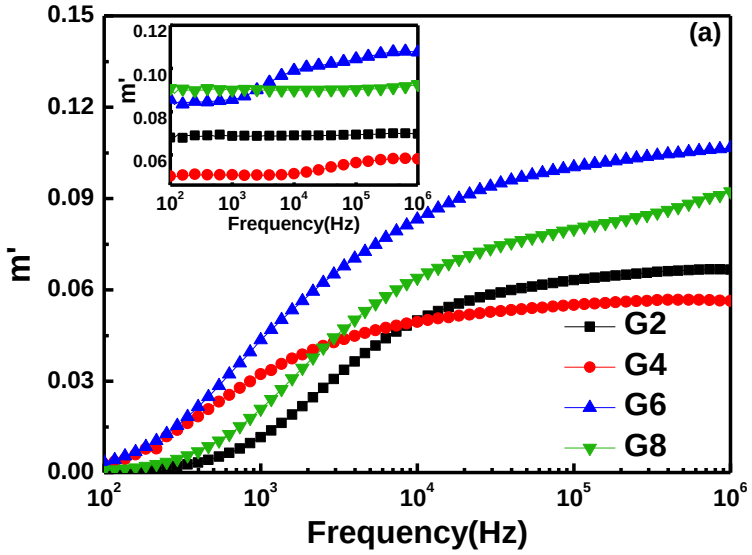

Figure 4.17 Variation in real part of dielectric modulus with frequency at 400°C. Inset-At 100°C.

It implies that within G6 glass the ion can move more freely than that in other glasses. However, other glasses exhibited the relaxation peak at high temperatures only. At 400°C, G2 and G4 glasses have relaxation peaks at similar positions and have comparable peak width. G4 and G6 glasses have relaxation peaks at relatively lower frequencies with G6 exhibiting the broadest peak. Broad relaxation peak denotes that large number of relaxation processes taking place within the material [43]. The most peaks are observed in G6 glass indicated more relaxation processes are involved in this glass.

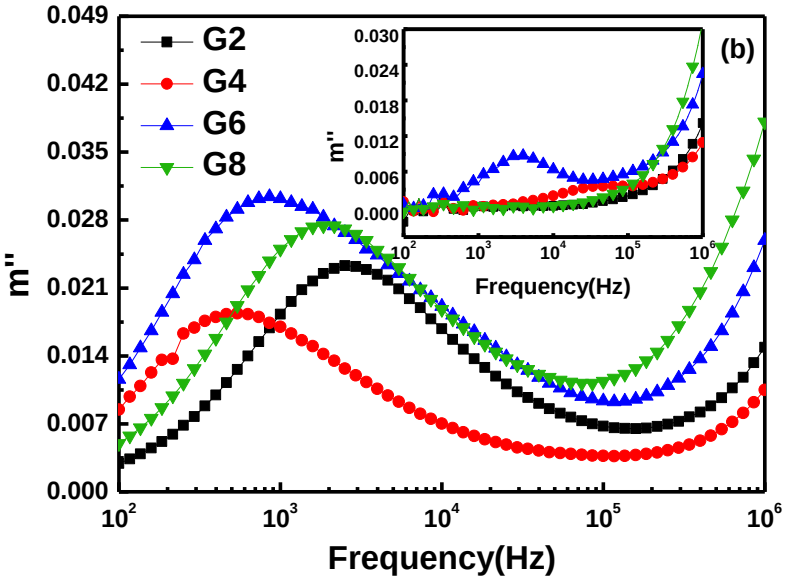

Figure 4.18 Variation in imaginary part of dielectric modulus with frequency at 400°C. Inset-At 100°C.

4.3.9 Microhardness of the bulk glasses

The micro hardness values are depicted in Table 4.5. The hardness is in the range of 464-502 *Hv*. The micohardness depends upon porosity and bond strength of the glass component. In other words, the higher polymerized of glass exhibit higher hardness. The replacement of CaO by MgO increases the hardness of the glasses. It can be correlated with the bond length and bond strength of MgO in comparison to CaO.

Table 4.5 Microhardness of the as-quenched bulk glasses.

Sample label	**G2**	**G4**	**G6**	**G8**
Microhardness (Hv)	464	471	502	498

The field strength of Mg^{2+} (0.45/Å^2) is higher than Ca^{2+} (0.33/ Å^2) which increases the polymerization in the glass. It is supported that the replacement of CaO by MgO leads to increase in the compactness of glass network with better and strong bonding. These results also support that in the present glasses MgO might act as glass network former. The hardness of the present samples is in the required range as the bone hardness is in same range [51].

4.4 Effect of heat treatment

4.4.1 X-ray diffraction

Effect of heat-treatment on the glasses is depicted in Figure 4.19 (a) and Figure 4.19 (b). Glasses G1, G2, G3 and G4 formed some crystalline phases. Minor amount of diopside i.e. $CaMgSi_2O_6$ (ICDD No. 01-075-1092) phase was formed in G2, G3 and G4. However, the diffraction peaks of G1 did not match with any single crystalline phase. Filled circles denote $CaMgSi_2O_6$, open circles denote SiO_2 and triangle denotes $CaSiO_3$. These peaks could be indexed with SiO_2 (ICDD No. 01-081-1665 and 00-04601242) and $CaSiO_3$ (ICDD No.00-042-0550). It is possible that both the crystalline phases are not grown fully in the glass matrix. The degree of crystallinity of the glass-ceramics is observed to be <5%. Formation of small amount of these silicate based crystalline phases indicates the surface crystallization.

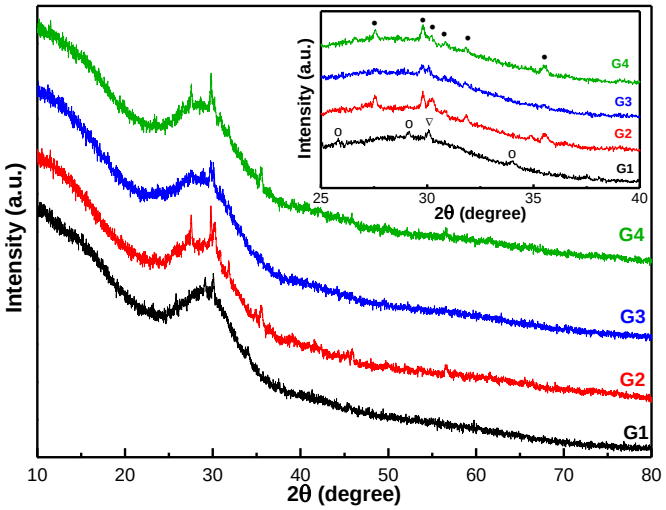

Figure 4.19 (a) XRD patterns of heat-treated glass-ceramics G1-G4. Inset shows the zoomed view in 25-40° range. Filled circles denote $CaMgSi_2O_6$, open circles denote SiO_2 and triangle denotes $CaSiO_3$.

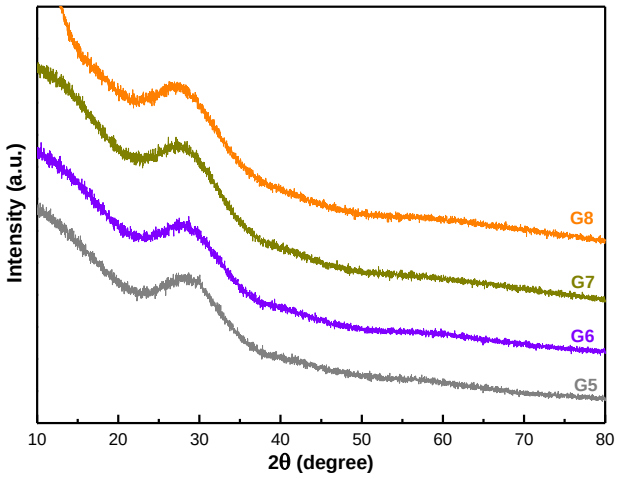

Figure 4.19 (b) XRD patterns of heat-treated glasses G5-G8.

It is reported that crystallization of silicate glasses occurs through the initial nucleation of silica rich phase and later incorporation of other ions [52]. Absence of any crystalline peak signifies the amorphous nature of the glasses even after heat-treatment. Interestingly, glasses with higher MgO content i.e. G5-G8 did not exhibit any crystalline peak. It indicates that higher CaO content is favorable for crystallization of the glasses, while MgO hinders the vitrification of the glasses. Glasses with higher MgO exhibited higher values of crystallization temperatures (T_c). Thus, at given heat-treatment temperature, the nucleation in higher MgO containing glasses could not start.

4.4.2 Fourier transforms infrared spectroscopy (FTIR)

FTIR is very sensitive technique to check local level changes in the glass structure. The FTIR spectra of pellets as given in the Figure 4.20 (a) and 4.20 (b) give some change with respect to the FTIR spectra of as quenched powder glass.

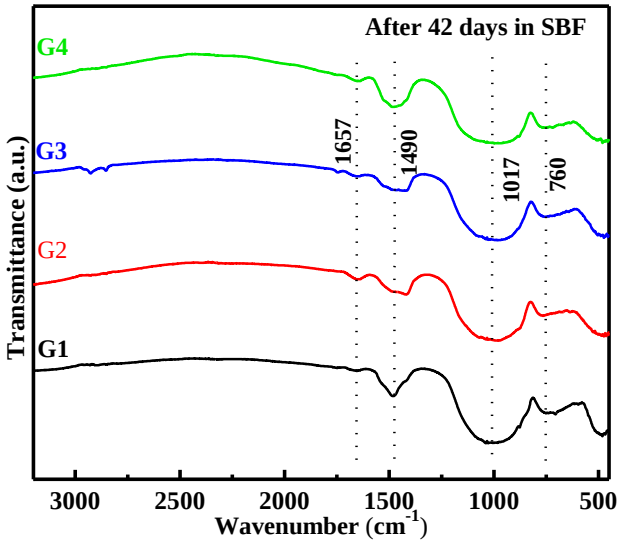

Figure 4.20 (a) FTIR spectra of glass-ceramics G1 to G4.

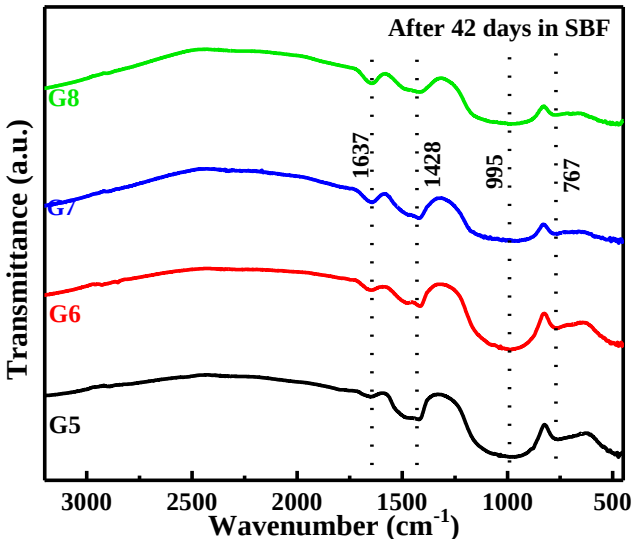

Figure 4.20 (b) FTIR spectra of glass-ceramics G5 to G8.

The band shoulder positioned near 1416 cm^{-1} and 1524 cm^{-1} becomes diffused in glass-ceramics i.e. G1, G2, G3 and G4 glass sample as a result main band centered near 1465 cm^{-1} also becomes broader. This is the loss of Ca/Mg-O-H bands due to heating. The hydroxyl band near 2856 cm^{-1} and 2928 cm^{-1} becomes exactly out of phase in pellets sample compared

to the powder sample i.e. at place of transmittance crest there is trough at the corresponding position in the powder samples due to shifting of bands. The other weaker signature of the bands at 2956 cm^{-1} and 3000 cm^{-1} is almost absent in powder sample. This is due to loss of interstitial hydroxyl vibrations. The hydroxyl loss phenomenon is very prominent in G1 glasses unlike other glasses. The other weaker bands at 1700 cm^{-1} and 1793 cm^{-1} shift to lower wave number side after pelletizing the powder glasses due to crystallization of glass [53]. The G5, G6, G7 and G8 glasses having more than 20 wt% MgO ceased to have shoulder near 1416 and 1524 cm^{-1}, so the pellet and powder sample have similar spectrum. The band position at 1427, 1659 and 1758 cm^{-1} becomes sharper particularly in G8 glasses i.e. highest MgO containing glass.

4.4.3 Microhardness of the heat-treated glasses

The microhardness of the glasses/glass-ceramics lies in the range of 208-290 Hv (Table 4.6). In general, the microhardness of glasses depends upon the porosity and bond strengths of the glass components [54]. Furthermore, hardness of the glass-ceramics depends on the relative growth of the crystalline phase(s) within the glassy matrix and their volume fractions. Irregular trend of microhardness with respect to the compositions may be due to the position of indentations occurring at glassy part or crystalline part. The heterogeneous growth of the crystalline phases adds further complexity to the observation of microhardness [55].

Table 4.6 Microhardness of glasses/glass-ceramic pellets.

Sample Label	**G1**	**G2**	**G3**	**G4**	**G5**	**G6**	**G7**	**G8**
Microhardness (Hv)	278	272	245	266	279	290	208	217

When indenter load is applied, the glass may deform either by shear flow process or by pressure-dominated densification process. The former process involves the breaking and formation of bonds with neighboring atoms; while in the later process, the atoms are forced to

move into glass network. The modifiers such as CaO and MgO assist the deformation by facilitating the easy slip ways through the glass network [56].

4.5 *In-Vitro* bioactivity: glass/glass-ceramic pellets

4.5.1 X-ray diffraction

Figure 4.21 (a) and (b) shows the comparison of XRD patterns of glass-ceramic sample G1-G8 and after evaluation of bioactivity. After soaking in SBF, the crystalline peaks of the glass-ceramics became more prominent due to preferential loss of amorphous phase over the crystalline phase [57].

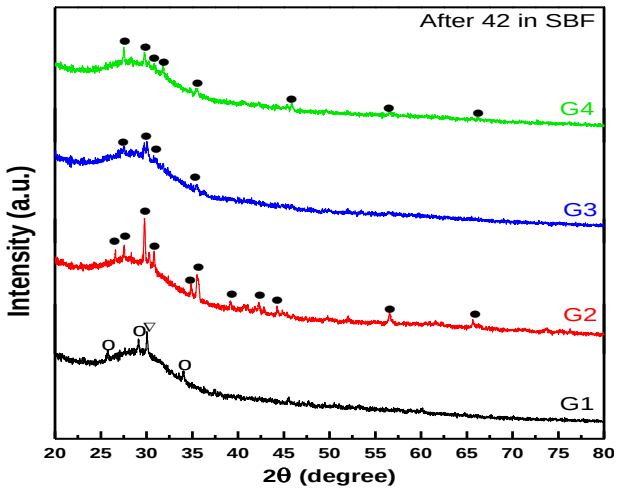

Figure 4.21 (a) XRD pattern of soaked glass-ceramic pellets (G1-G4).

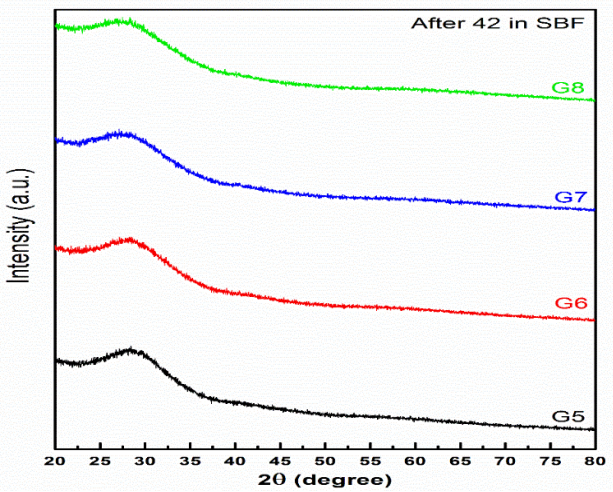

Figure 4.21 (b) XRD patterns of soaked glass-ceramic pellets (G5-G8).

Glasses G5-G8 did not exhibit any significant change in their XRD patterns after soaking in SBF. Increasing soaking time to 56 days could not show any remarkable change in the position and broadening of the crystalline peaks of the glass-ceramics as illustrated in Figure 4.22. No XRD peak of crystalline HAp layer was found in the XRD pattern of any glass/glass-ceramic after soaking in the SBF. It indicates that there might be the formation of amorphous HAp which could not be crystallized during the course of experimental time [58].

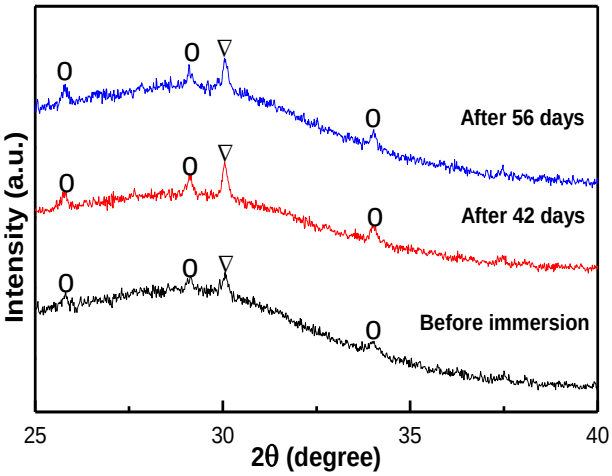

Figure 4.22 Representative comparisons of the XRD patterns of G1 glass-ceramic before soaking, after 42 days and 56 days of soaking in SBF.

4.5.2 Fourier transforms infrared spectroscopy (FTIR)

Minimum spectroscopic changes have been occurred on increasing the soaking time from 42 to 56 days. However the shoulder near 1468 cm^{-1} in the glass-ceramics pellets at the same position changes into sharp band after soaking the glass sample in the SBF. However differential violet shift were observed after soaking the glasses with respect to pristine glasses. An interesting changes has been observed in the IR spectrum of G2 soaked and unsoaked glasses. The soaked glass spectrum viz-a-viz the band positions at 1413, 1478 and 1652 at resembles more like powder sample than the G2 glass pellets. This may be due to the fact that on pelletization structural modifications taking place which again returns towards like powdered structure in terms of sharpness and positions on soaking the glass pellets in the SBF. But certain frequency which are indicative of stages of bioactivity (discussed in section

4.6.2) at ~876,940, 1040, 1227 were found to be less formed suggesting sluggish formation of any layer as compared to powder samples

4.5.3 SEM-EDS

The SEM micrographs (Figure 4.23-4.24) depict appreciable surface modification of the glasses/glass-ceramics upon their soaking in SBF. The formation of heterogeneous calcium phosphate based phase was identified in the glasses/glass-ceramics with little variation in the morphology. As clear from the Table 4.7, the elemental compositions of the new layer formed on the soaked glasses had chemisorption of calcium, phosphorous, potassium and other ions to it [59]. As a result of interaction with SBF, some faceted crystals are formed such as shown in for G4 glass-ceramic. Such crystals were found in few zones of other glasses/glass-ceramics too (not shown here). EDS analysis carried out on these crystals indicates that they belong to chlorides of alkali and metals such as KCl and NaCl. Morphology of G3 and G6 is different from other samples. EDS data revealed that G3 did not show phosphorus content on its surface after 42 days of soaking in SBF.

Table 4.7 Elemental compositions (wt%) of the soaked glasses/glass-ceramics.

Sample label	O	Na	Mg	Si	P	Cl	K	Ca
G1	37.58	7.06	0.71	5.05	4.59	17.37	1.12	12.88
G2	49.77	2.32	5.54	12.78	6.10	3.01	4.57	10.35
G3	57.61	0	5.65	24.88	0	0.47	3.0	10.89
G4	36.42	10.51	3.77	6.63	4.35	17.47	0.92	9.01
G5	44.09	6.89	3.52	5.94	9.31	11.39	1.62	13.40
G6	56.34	4.77	3.71	21.0	0.49	4.63	1.98	2.41
G7	43.25	7.20	3.98	7.27	5.57	8.98	1.27	6.76
G8	48.87	3.46	4.18	21.37	1.53	5.70	2.69	2.36

However, other samples showed substantial amount of phosphorus. On the other hand, G6 is unique among other samples exhibiting high amount of Si and O that signifies that it possesses silica gel on its surface after 42 of soaking in SBF.

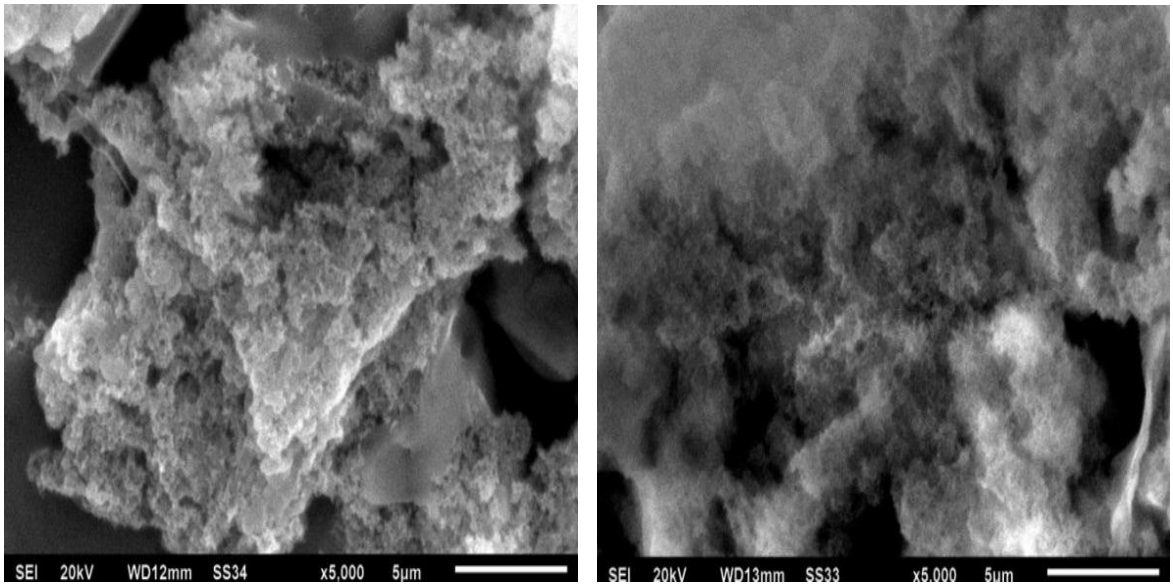

Figure 4.23 SEM images of (a) G1 (b) G8 glass-ceramic after 42 days of soaking in SBF.

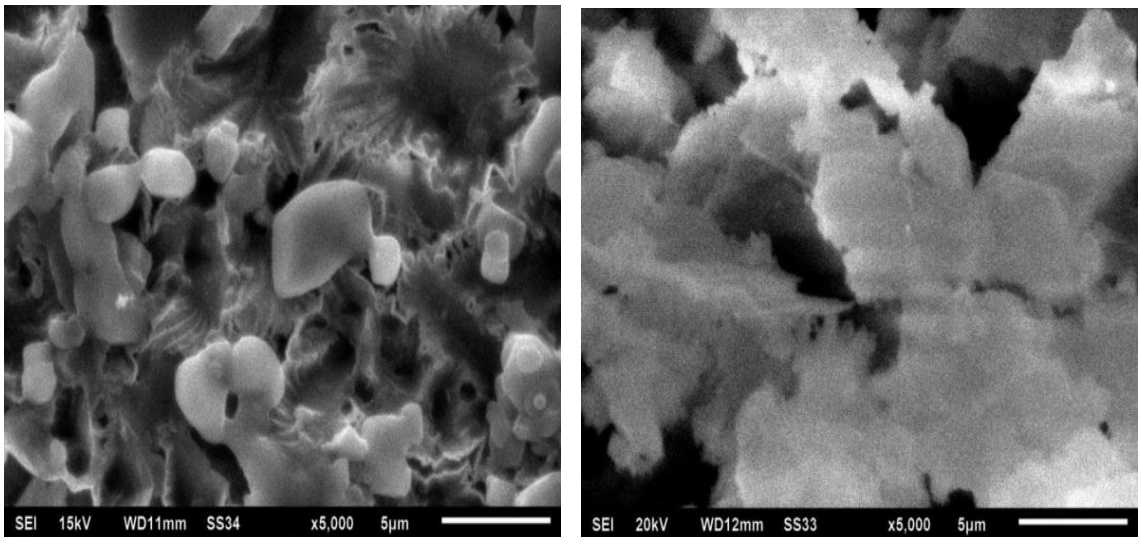

Figure 4.24 SEM images of (a) G3 (b) G6 after 42 days of soaking in SBF.

The potential bioactive glass among all is explored by weight change data (Section 4.5.5). G6 leached out maximum and has possibility to form higher silica gel. It is also in accordance with the MP-AES data (next section), which reveals that G6 exhibited maximum loss of silica in the SBF. It indicates that the process of release of silanol groups from glass surface keeps

on occurring for long time that may have slightly delayed the other steps of bioactivity mechanism. Similarly, signatures of silica gel seem to appear on the surface of G8 (Figure 4.24) that might indicate the possible dissolution of HAp into SBF [60].

4.5.4 MP-AES analysis

MP-AES gives quantitative supports to the change in the pH occurring in the glasses on soaking in SBF. Importantly, it is seen in the compositional release profile of glasses/glass-ceramics. The network modifiers i.e. $Ca^{2+}$and K^{+} cations have variable percentage of ion release. On the other hand, network former cations i.e. Si^{4+} and intermediate Mg^{2+} were released in similar fashion with respect to composition. Mg can act as modifier as well as glass former [61]. Because of this, Mg^{2+} act as glass former in the present samples. Secondly, both these ions have been released more from glasses (G5-G8) than that of glass-ceramics (G1-G4) as shown in Figure 4.25 and 4.26. However, G5-G8 glasses are more prone to bioactive reactions as compared to G1-G4 glass-ceramics in which crystalline phases are embedded in the glass matrix. Ca^{2+} ions in glass-ceramics G1-G4, with exception of G2, have higher concentration level than the pristine SBF. It indicates that not significant amount of Ca ions go back to the surface of parent sample after being dissolve in SBF. On the other hand, higher MgO containing glasses i.e. G5-G8 exhibit the lower Ca concentration level than the pristine SBF. It indicates that the SBF is deficient in the original amount of Ca^{2+} ions. These Ca^{2+} ions have migrated to the glass surface to form the calcium phosphate layer which converts into HAp layer in later stage reactions [62]. These results indicate that the glass-ceramics due to higher durability in SBF have lower tendency to form HAp layer as compared to less durable glasses. It supports the results of previous reports observing lower bioactivity of the glass-ceramics as compared to glasses [63-64]. Figure 4.26 shows that most of the samples, except G3, exhibit lower concentration of potassium than originally present in pristine SBF.

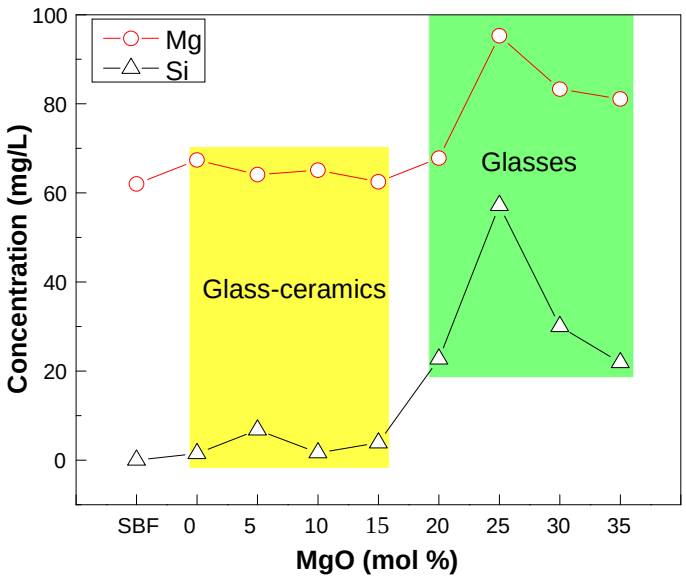

Figure 4.25 Ions release profile of traditional and conditional glass former cations i.e. Si and Mg ions after 42 days of soaking of the samples in SBF.

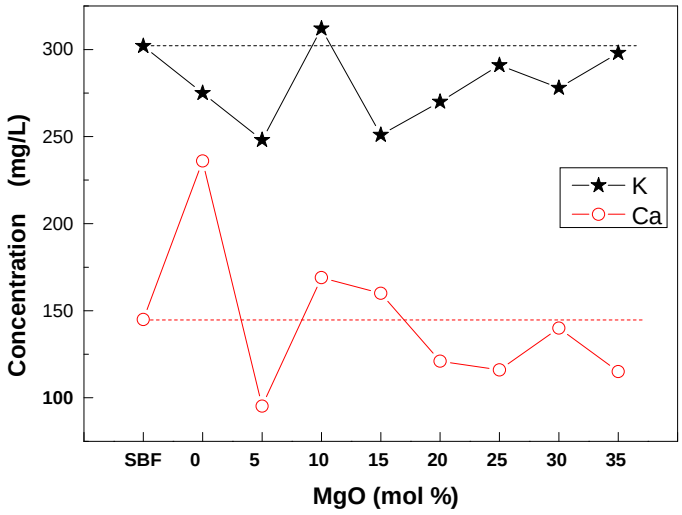

Figure 4.26 Concentration of potassium and calcium ions in the SBF after 42 days of soaking of the glasses/glass-ceramics.

It seems that affinity of glass/glass-ceramic surface toward potassium ions plays important role to attract phosphate groups, which is essential for HAp layer formation. On the other hand, G3 with lesser affinity for potassium did not form HAp after 42 days of soaking in SBF. The potassium ions in case of G1, G2 and G4-G8 specimens partially took part in modified HAp formation [65] and partially formed KCl crystals on the surfaces as discussed in the section 4.5.3.

4.5.5 pH Variation and weight change

The pH rise is related to exchange of ions between glass and SBF. The change in pH is desirable for glass to be a bioactive material. All the samples degrade in the SBF; maximum degradation corresponds to maximum pH change. The pH of the SBF after soaking of samples increased initially from 7.4 to 7.7 and almost saturated for the rest of the soaking time. Initial rise in the pH corresponds to the release of basic ions like K^{+}, Ca^{2+} and Mg^{2+} in SBF. It is in accordance with the initial steps of the mechanism of formation of HAp as proposed by Kokubo *et al.* [66]. Later on, the pH changes due to neutralization caused by release of acidic radicals like Si^{4+} in the form of silanol groups (Si-OH). Figure 4.27 show the percentage weight changes of the glasses/glass-ceramics due to physiological reaction with SBF. Higher weight loss of G5-G8 glasses than that of glasses G1-G4 glass-ceramics is ascribed to the less durable structure of the glasses than glass-ceramics [67]. After 42 days of soaking in SBF, the weight of the all samples, except G3, declined in the SBF possibly because of more loss of ions than gain on the surface. G3 exhibited slight weight gain after 42 days of soaking in SBF. It seems to be negligible weight change; however, it played significant role in determining its bioactivity as discussed in previous sections.

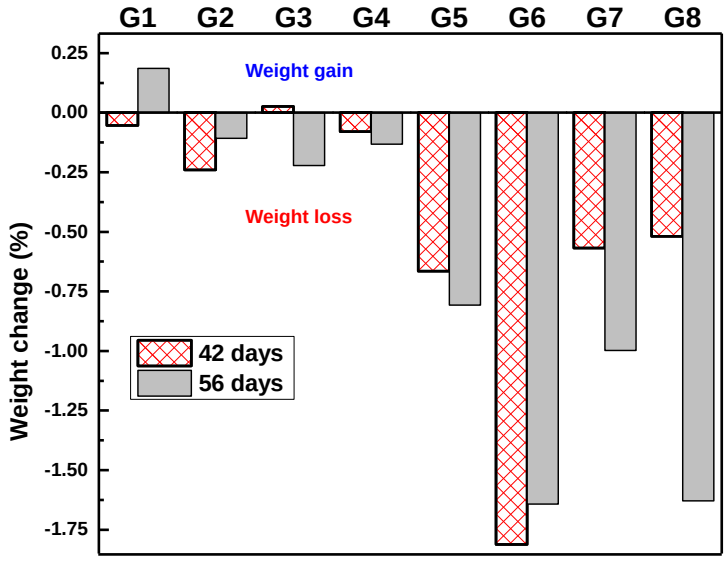

Figure 4.27 Weight changes of the glass/glass-ceramic pellets after 42 and 56 days of soaking in SBF. Error bars are not visible as uncertainty in measurements was below 10^{-5}.

4.5.6 Microhardness of the soaked samples

Microhardness of the samples after soaking in SBF originates primarily from the deposited HAp layer, which is clearly indicated by the fairly lower values of the microhardness as given in table 4.8. The observed microhardness of the immersed samples is comparable to that of human tissues/bone [68]. Mechanical parameters of the implant must be in close proximity with the host body part; the absence of which may cause undesirable effects. The HAp layer formed on the surface of the samples acts as an intermediate adhesive at implant-bone interface and also serves to bring mechanical compatibility between the both. Thus, mechanical properties of present samples reveal their promising potential as implant materials.

Table 4.8 Microhardness value of glass/glass-ceramic pellets after soaking in SBF.

Sample label	**G1**	**G2**	**G3**	**G4**	**G5**	**G6**	**G7**	**G8**
Microhardness (Hv)	65	59	59	36	43	82	73	77

4.6 *In-Vitro* bioactivity of glass powder

4.6.1 X-ray diffraction

The XRD patterns of the soaked and unsoaked glasses are given in Figure.4.28. The XRD pattern of soaked and unsoaked glasses does not show any appreciable change. The XRD pattern of soaked glasses show broader halo than pristine glasses. It is related to leaching of ions from the glasses. In other words, more disordering might be created in glasses after soaking in SBF. In addition to this, some amorphous layer might form on the surface of the glasses. It is well reported in the literature that in earlier stage of soaking an amorphous layer of apatite is formed on the surface of the glasses [59].

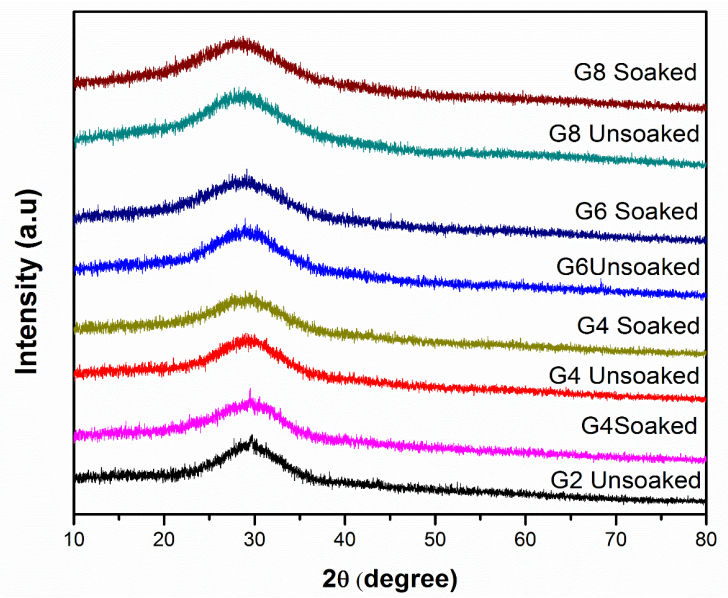

Figure 4.28 XRD patterns of soaked and unsoaked glasses powder.

4.6.2 Fourier transforms infrared spectroscopy (FTIR)

The FTIR spectra of soaked glass powder reveals more information to that of glass/glass ceramic pellets. The FTIR spectra of soaked and unsoaked glasses powder are given in Figure 4.29.

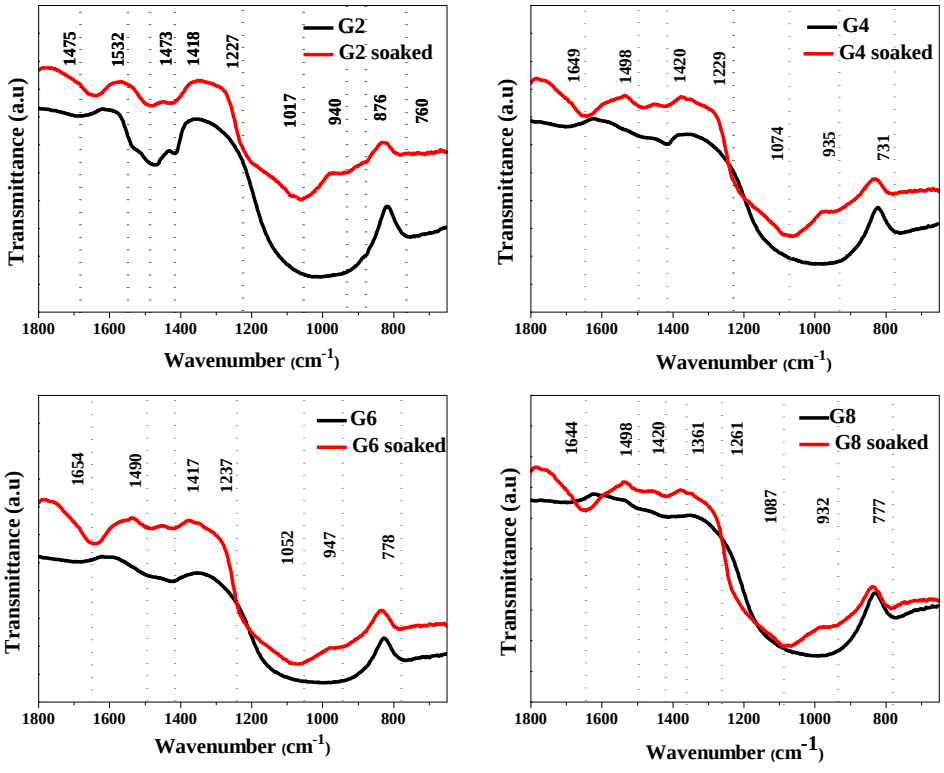

Figure 4.29 Comparison of FTIR spectra of selected glasses before and after soaking in SBF.

The band at ~760cm^{-1} is associated with Si-O-Si bending vibration. This band shifts slightly to higher wave number side after soaking in SBF for all the glasses. The cause in the shift is consequence of leaching of the alkali and alkaline earth metal ions which makes the surface comparatively free of NBO. It is based on the fact that frequency of absorption of Si-O bonds increases with the decreases in amount of NBO [69]. It is a clear manifestation of degradation of the glass. A broad band is observed at~1017 cm^{-1}. It is attributed to the asymmetric stretching vibrations of Si-O-Si tetrahedral consisting of Q_0, Q_1, Q_2 and Q_3 silicate group visible at ~860, ~900, ~950, ~1070 cm^{-1} [70-71]. After soaking the glasses in SBF many weak band/shoulder appeared in the FTIR spectra. One extra band at ~876 cm^{-1} in G2 glass is also seen. This may be ascribed to v2 frequency of CO bond originating from carbonate ions formed on the glass [72]. This band could not be seen clearly in other glasses. This could be related to the better bioactivity of this particular glass. This fact is also supported by pH and ion release behavior of G2 glass. The reason of the same is more disordered network compared to other glasses. Also, high field strength of Mg^{2+} is responsible for low release of Mg^{2+}. Moreover, one extra weak shoulder was also formed at ~1227 cm^{-1}. It is associated to Si-O-Si vibration of the newly formed silica gel on the surface [72].

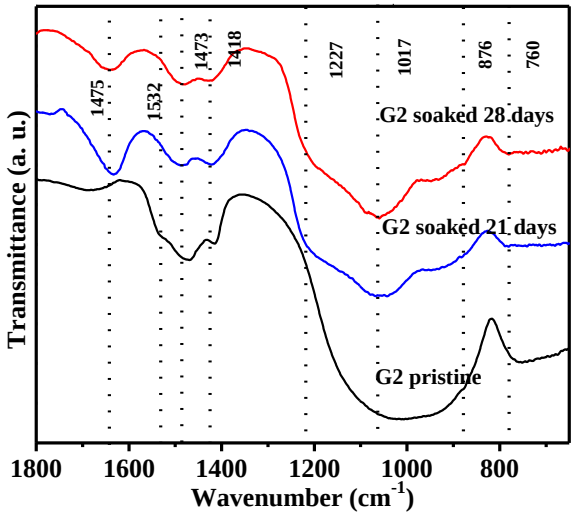

Figure 4.30 Evolution of FTIR spectra of G2 glass with respect to soaking time.

A new band at above 940 cm^{-1} is also formed due P-O bending vibration of apatite like layer [73]. The vibration spectra of Si and P in the spectral range 940-1100 cm^{-1} would be difficult to distinguish as both the groups are sensitive to absorption in this region. However this effect could be better observed through FTIR-Raman, which show characteristics band corresponding to P-O bending vibration at ~952-960 cm^{-1} [73]. The bands due to phosphorous (P) have been masked by the broad band of silica at the same frequency range. Other bands are seen in Figure 4.30 originates due to Si-OH (silanol group) which is formed near ~1040 cm^{-1} [74]. This band manifests that some modification on the glass surface has been taken place. This can be associated with bioactivity of the glasses. The band due to Si-OH and Si-O-Na are very difficult to resolve as their positions are very much close to each other [74-75]. The formation of silica gel takes place at some minimum threshold pH value i.e., above pH 8. At this pH, only sufficient exchange of cation takes place to form Si-OH (Silanol group). Therefore, the band at ~1040 and ~1227 cm^{-1} becomes more prominent with increase in soaking time from 21 days to 28 days. Other bands also grow with increase in soaking time as it is clear from Figure 4.31. The Si-OH (Silanol group) would further consolidate to form silica gel followed by incorporation of carbonate and phosphate groups. The main band formed around ~1017 cm^{-1} shifted to higher wave number which is due to contribution from phosphate species since bands of P also lie in this region. The other bands particularly around 1418-1473 cm^{-1} and a weak shoulder near 1532 cm^{-1} formed in pristine glass due to interaction of Mg/Ca with OH^{-1} ion exhibits blue shift and become more diffused with soaking in SBF [4]. This is due to loss of $Mg^{2+}$and Ca^{2+} ion from the glass into the SBF. Finally, the band at 1675 cm^{-1} related to bending vibration of H_2O molecule became sharper and more intense after soaking in SBF due to ample dehydration of the glasses. Similarly, weaker bands at 2857 and 2922 cm^{-1} owing to symmetric and asymmetric modes of interstitials water also becomes intensified after soaking in the SBF. Commonly, all the bands

of G2 are sharper than other glasses following a decreasing trend from G2 to G8; this is because order of polymerization and compactness increase from G2 to G8 as explained in the previous section.

4.6.3 Variation in pH

The variation of pH measured everyday has been given in Figure. 4. 31. Commonly the pH rises very fast initially followed by marginal change in pH with respect to time. In the present case, rise or fall in pH is governed by sum total of concentration of acidic ions like Si^{4+} and basic ions namely K^{+}, $Ca^{2+}$and Mg^{2+}in SBF. The pH rises very fast due to fast release of basic ions followed by release of acidic ions Si^{4+} in later stage of soaking. This stabilized the pH value as the equilibrium is established in the reaction taking place between glass and SBF. Chemically, it can be explained as follows:

$$Si\text{-}O^{-}K^{+} + H^{+} \rightarrow Si\text{-}O^{-}OH + K^{+} \qquad (4.16)$$

The pH value increases by approximately 0.7-0.8 units after 3 days, whereas, the value just increased further 0.4-0.7 units after next 25 days soaking the glass in SBF. Individually, G2 glass exhibits maximum change in pH value followed by G4, G6 and G8.Hench *et al.* reported that the initial stage of apatite layer formation is due to leaching out of cations from the glasses.

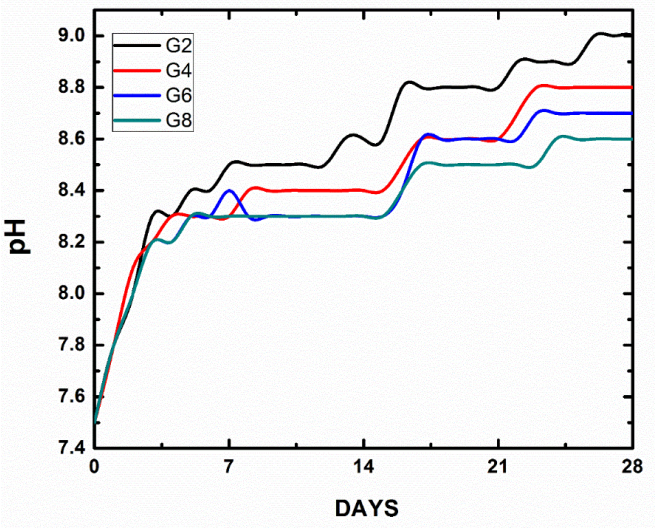

Figure 4.31 Variation of pH with soaking 28 days for glasses G2, G4, G6 and G8.

According to them the glass exchanges ions (K^+, Mg^+, Ca^+ etc.) with the hydronium ion (H_3O^+) in the first step of apatite formation followed by other process. So, the increase in alkaline nature of SBF after glass powder soaking supports the above phenomenon. In other way, the pH will also govern the direction of the reaction. At lower pH, the reaction proceeds to right side of the chemical reaction and extensive exchange of ions takes place, however, as the alkaline nature of the solution increases little exchange takes place and pH of the SBF stabilizes. Although calcium and magnesium both are glass modifiers, however, magnesium is also believed to participate in forming network [76-77]. So, decrease in calcium at the cost of magnesium will effectively change the dissolution rate and hence pH of the SBF. However, the changes are insignificant because of the comparable electro negativity and field strength of Ca^{2+} and Mg^{2+}, the calcium takes the edge in modifying the silicate network. Magnesium may make the glass somewhat chemically durable as the $[MgO_4]^{2-}$ network consumes other cation Ca^+, K^+ from the network for charge balancing [18]. This also facilitates for less release of cations and consequently, lesser rise in pH in G8 glass than other glasses. The overall stagnation of pH for the entire sample is explained on the basis of precipitation of carbonate/phosphate ions which shifts the equilibrium towards right hand side of the equation as given below.

$$HCO^-_3 \rightarrow CO^{2-}_3 + H^+ \quad (4.17)$$

$$HPO^{2-}_4 \rightarrow PO^{3-}_4 + H^+ \quad (4.18)$$

4.6.4 MP-AES analysis

The change in the ionic concentration of soaked SBF w.r.t. original SBF has been represented by bar graph in Figure 4.32. Maximum leaching of ions have been observed in G2 glass owing to less polymerised glass network as compared to other glasses. Potassium which is present in equal ratio in all the samples shows unequal release of ions in SBF for each glass, which might be associated with the dual role of MgO in glasses. Maximum K^+ ion is released

from the G2 glass followed by G4, G6, and G8 glasses owing to the fact that Mg makes the network compact with increasing content of MgO, hence, release of K^+ will be hindered. G4, G6 and G8 glasses have approximately released same K^+ ion in the solution. It expected to follow decreasing trend for K^+ as the ions will be consumed by $[MgO_4]^{2-}$tetrahedral in the glass network for balance the charge, however, the value is almost same or slightly increase in G8 glass. This is supported by the fact that maximum 14% MgO can participate in network formation irrespective of the amount present in the glass [78]. Silica is another element whose amount is same in all the glass concentration. Dissolution of this ion is almost same for the G2, G4, G6 and G8 glasses. It clearly indicates that MgO has feeble effect in release of Si^{4+}as this ion has to release from well-connected glass network in the form of silanol group Si-OH. However, leaching of Si^{4+} ion from glass network is possible in the later stage of apatite formation ions after sufficient degradation of the network takes place. The dependence of dissolution of Ca^{2+} and Mg^{2+} content in SBF is different. The rate of dissolution of Mg^{2+} and Ca^{2+} ions is 5.33 and 10.98 units per mol (%), respectively.

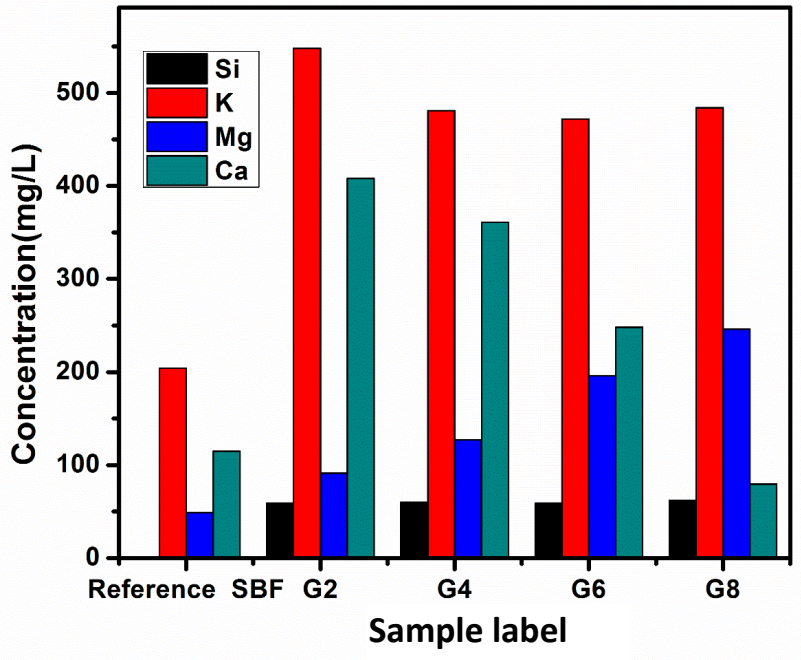

Figure 4.32 Concentration of different ions released into SBF from the different glass.

Interestingly, the final content of the calcium in the solution soaked with G8 glass is lesser than initially present in SBF. Pristine G8 glass does not contain any calcium content. On the other hand, other glasses contain calcium oxide, so the decrease of calcium marginally below the amount originally present in SBF. It is noticeable in case of G8 glasses only. It clearly gives an impression that calcium may have come out of the solution and incorporated to the glass surface to form calcium rich layer. This accounts for decrease of calcium from the SBF. This is in agreement with saturation of pH values as explained above in section 4.6.3 in precipitation reaction of carbonate and phosphate ions.

4.6.5 SEM-EDS

The typical SEM micrographs of G4 and G8 glass after soaking in SBF are shown in Figure 4.33 (a) and (b). Heterogeneous distribution of white colored flakes has adherered to the glass surface. These flakes are seen throughout the glass surfaces. The overall composition of soaked glass calculated from EDS data are tabulated in Table 4.9. The EDS analysis also supports the phenomenon of leaching as explained in section 4.6.4.

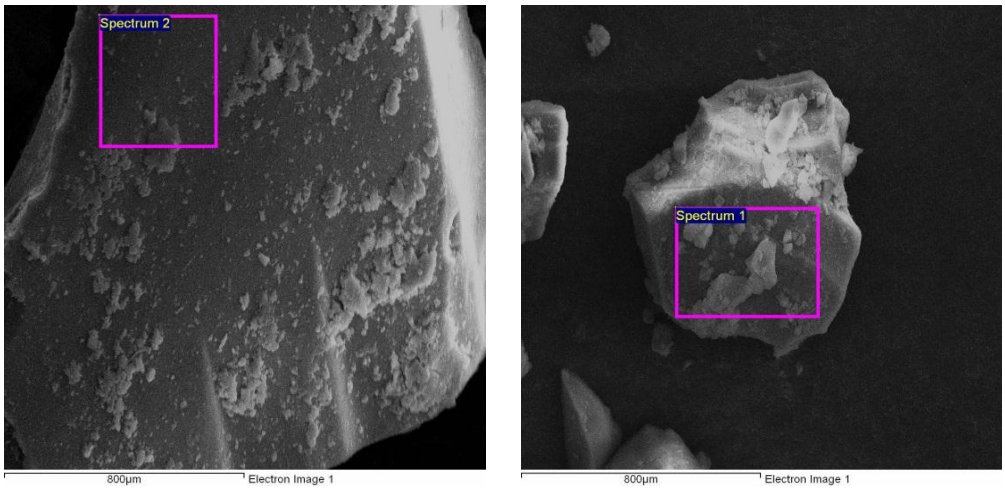

Figure 4.33 Representative SEM images of soaked glasses (a) G4 (b) G8.

The amount of silicon remains almost same as the virgin glasses. But the calcium, magnesium and potassium significantly reduced after soaking in the SBF. The MP-AES data also supported the EDS data since the percentage of these elements increased in SBF after glass soaking.

Table 4.9 Elemental composition of the soaked glass powders.

Sample label	Amount (wt. %)				
	Si	K	Ca	Mg	O
G2	25.33	6.27	8.32	1.40	58.68
G4	24.48	11.05	8.55	4.58	51.35
G6	20.32	6.04	3.04	8.90	61.69
G8	24.00	6.54	0	7.75	52.33

4.6.6 UV-Visible Spectroscopy

The study of fundamental transitions in UV region may help to know some modifications in glasses due to soaking in SBF. In other words the formation of any layer on the glass surface or leaching of ions from the glass may change the optical band gap of the materials due to change in absorption of the UV-Visible light. By plotting the graph between $\alpha h\nu^{1/2}$ and $h\nu$ extrapolating the linear region of curves to $h\nu$ axis for soaked glasses G2, G4, G6 and G8 as shown in Figure 4.34, one can find the optical band gap of the materials. In present case we have used Kubelka-Munk function $F(R)$ in place of absorbance α in the calculation of band energy from the F(R) $h\nu^{1/2}$ versus $h\nu$ plot.

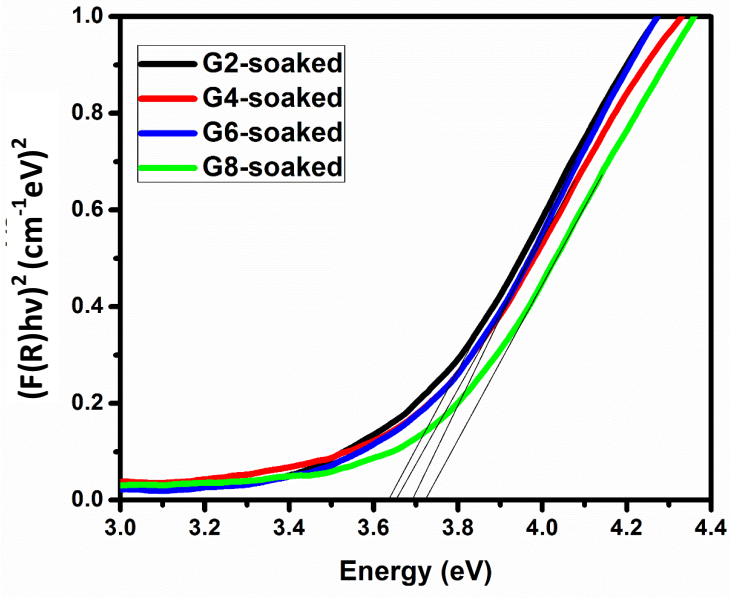

Figure 4.34 Tauc's plot for calculations of band gap of glasses G2, G4, G6 and G8.

The obtained values are given in Table 4.10 along with optical band gap of pristine glasses. The band gap of the material is expected to change due to various physio-chemical reactions

taking place at the surface. This would bring about remarkable change in compositions and physical parameter like porosity. Hence, the band gap of the materials will change. The band gap of glasses (G2 to G8) gradually increased from 3.46 eV to 3.65 eV with an increase of MgO. The Mg is responsible for creation of lesser number of NBO as compared to Ca^{2+} due to network forming ability of MgO. Similarly, after soaking the band gap has increased from 3.64 eV to 3.72 eV from G2 to G8 glasses. This clearly indicates the reduction in NBO caused by leaching of alkali and alkaline earth metal ions from glass to the surface without formation of any significant crystalline layer on the glass surface. The top of the valence band gets lowered leading to increase in the band gap with the decrease in NBO. However, the band gap values of the soaked and unsoaked glasses exhibit lesser difference with higher MgO containing glasses. This is indicative of the fact that higher MgO (G8) containing glasses are more polymerized glass network and have lesser NBO content as compared to other glasses which contain lesser amount of MgO. Therefore, the reduction in NBO due to leaching will not take place significantly as a result the optical band gap remains approximately same for this particular glass. The calculated value of Urbach energy is summarized in Table 4.10. The width of the tails of the localized states within the optical band gap is given by Urbach energy. The cause of the Urbach energy is random electric field associated with structure disorder. The Urbach energy values lie between 0.16 eV to 0.11 eV for unsoaked glasses and between 0.11 to 0.15 eV for soaked glasses. The Urbach energy value decreased significantly in case of G2 glasses after soaking in SBF whereas, it remain almost constant in case of G4, G6 and G8 glasses. Alkali and alkaline earth metal cations while leaving their sites induces charge at the vacant sites. In order to maintain the charge neutrality of the sample other ions with different sizes may occupy these vacant sites, which create the defects leading to higher Urbach energy in unsoaked glasses. The soaked glasses

which are comparatively deficient in alkali and alkaline earth metal ions due to leaching exhibit lesser band gap. The Urbach energy decreased to maximum content in case of G2.

Table 4.10 Optical band gap and Urbach energy of the glasses.

Sample label	Band gap (eV)		Urbach energy (eV)	
	Unsoaked	Soaked	Unsoaked	Soaked
G2	3.46	3.64	0.16	0.11
G4	3.56	3.67	0.15	0.15
G6	3.63	3.69	0.13	0.12
G8	3.72	3.72	0.11	0.12

4.7 Microbial study

4.7.1 Microbial limit test

The outcome of this section is giving the probability of formation of microbial colony on the glass surface when exposed to media facilitating the growth of microorganisms. All the glasses developed negligible growth for bacterial pathogens. This suggests inertness of all the glasses with respect to bacterial contamination. Practically no growth of microbial colony could be found in pure antimicrobial drug as well as glass sample in combination with the drug. Consequently it may be remarked here that the glass sample do not affect the working of antimicrobial drug when used in combination with the glass sample. This illustrates future potential application of glass as carrier of antimicrobial drug also.

4.7.2 Microbial inhibition

We know that optimum pH for growth of bacteria is close to neutral; any growth in pH should inhibit the growth of bacteria [79]. The high pH and high osmotic pressure caused by non-physiological concentration of the ions kills the bacteria by damaging their cell wall [79]. Therefore the high pH environment was maintained to validate the maximum bactericidal potential of the sample in most favorable condition. The numbers of viable micro organism counts along with their pH values are summarized in table 4.11. None of the samples promoted growth of microorganism in the culture media. Bacteriostatic behavior meaning almost same number of viable bacteria as in positive control was observed for G2 and G8.

The glass composition having 15 mol% MgO /20 mol% CaO (G4) and 25 mol % MgO/10 mol% CaO (G6) had better bactericidal property. The pH value of media is measure of the amount of glass sample dissolved in buffered sodium chloride peptone water solution. pH remained almost constant for the entire incubation period i.e. 72. It is reported that magnesium invariably inhibits the growth of bacteria [80].

Table 4.11 Growth/inhibition of microbial species caused by glasses.

Sample label	pH	Growth *S.aureus* (cfu/gm)	Growth *S.aureus* (cfu/gm) Positive control	Growth *salmonella* (cfu/gm)	Growth *salmonella* (cfu/gm) Positive control	Growth *C. albicans* (cfu/gm)	Growth *C. albicans* (cfu/gm) Positive control
G2	10.06	115	104	117	78	40	65
G4	9.40	24	--	34	--	37	--
G6	10.11	36	--	38	--	12	--
G8	10.26	113	--	89	--	0	--

Here in present case certain ratio of MgO/CaO inhibits bacteria more effectively than others. The release of ions may not be fast in the culture medium as indicated by less change in pH. So the killing action would take place effectively if more ions of same type of are released from the glass. This possibly happens easier in G4 glass which most effective in suppressing the bacterial growth. Viable cells of *C.albicans* fungi are lesser than positive control counterpart. Hence all the glasses are effective in inhibiting the growth of fungi. However there is one to one relationship between the fungal suppression and MgO content of the glass.

Overall, the variation of MgO content with respect to CaO has been synthesized by melt quench method. Based on the DTA results, these samples were heat treated at 850°C for 0.5 hours. The glasses and glass-ceramics were immersed in standard SBF solutions to study their bioactive properties. The bioactive properties have been checked on the glass pellets and powder of the glasses. The pH value and weight change occurring in the samples were

monitored systematically. The glasses samples exhibited better bioactive properties than the glass-ceramics. The XRD of immersed samples could not show any peaks which indicates the formation of amorphous Hap layer as observed in SEM observations. The hardness of the glasses and glass-ceramics after dipping changed drastically in related to the amorphous layer formation of Hap.

References

[1] S. Singh, K. Singh, Non-Cryst. Solids 386 (2014) 100.

[2] J.M. Stevels, The electrical properties of glass, Vol. 20, Springer, Berlin (1957).

[3] P. Courtial, D.B. Dingwell, Am. Mineral 84 (1999) 465.

[4] A.M. Hofmeister, J.E. Bowey, Mon. Not .R. Astron. Soc 367 (2006) 577.

[5] P.K. Jha, O.P. Pandey, K. Singh, J. Non-Cryst. Solids 379 (2013) 89.

[6] A. Arora, A. Goel, E.R. Shaaban, K. Singh, O.P. Pandey, J.M.F. Ferreira, Physica B Condens. Matter 403 (2008) 1738.

[7] L. Cormier, Procedia Mater. Sci. 7 (2014) 60.

[8] Y. Sun, F. Zhang, Z. Yue, Y. Zhang, X. Fang, Z. Ding, Sci. Rep. 6 (2016) 23734.

[9] D. Chandler, J.P. Garrahan, Annu. Rev. Phys. Chem. 61 (2010) 191.

[10] J. Ma, C.Z. Chen, D.G. Wang, X. Shao, C.Z. Wang, H.M. Zhang, Ceram. Int. 38 (2012) 6677.

[11] C.T. Moynihan, A.J. Easteal, J. Wilder, J. Tucker, J. Phys. Chem. 78 (1974) 2673.

[12] S.R. Joshi, A. Pratap, N.S. Saxena, M.P. Saksena, A. Kumar., J. Mater. Sci. Let. 13 (1994) 77.

[13] I. Avramov, T. Vassilev, I. Penkov, J. Non-Cryst. Solids 351 (2005) 472.

[14] L. Abbas, L. Bih, A. Nadiri, Y. E. Amraoui, H. Khemakhem, D. Mezzane, J. Therm. Anal. Calorim. 90 (2007) 453.

[15] J. Kjeldsen, M.M. Smedskjaer, J.C. Mauro, R.E. Youngman, L. Huang, Y. Yue, J. Non-Cryst. Solids 369 (2013) 61.

[16] V.C. Reynoso, K. Yukimitu, T. Nagami, C. Carvalho, J.C. Moraes, E. Araújo, Phys. Chem. Solids 64 (2003) 27.

[17] A. Al-Noaman, S.C.F. Rawlinson, R.G. Hill. J. Non-Cryst. Solids 358 (2012) 3019.

[18] J.E. Shelby, Introduction to Glass Science and Technology, Royal Society of Chemistry, UK (2005).

[19] K. Thieme, I. Avramov, C. Rüssel, Sci. Rep. 6 (2016) 25451.

[20] S. Huang, P. Cao, Y. Li, Z. Huang, W. Gao, Cryst. Growth. Des. 13 (2013) 4031.

[21] H.E. Kissinger, J. Res. Natl. Bur. Stand. 57 (1956) 217.

[22] M. Lasocka, J. Therm. Anal. Calorim. 16 (1979) 197.

[23] J.A. Augis, J.E. Bennett, J. Therm. Anal. Calorim. 13 (1978) 283.

[24] K. Mageshwari, R. Sathyamoorthy, Conference Proceedings National Conference on Developing Scenario in Applied Science and Communicative English, Coimbatore,

Tamilnadu, India (2012).

[25] J. Stelling, H. Behrens, M. Wilke, J. Gottlicher, E.C. Aljanabi, Geochim. Cosmochim. Acta 75 (2011) 3542.

[26] N. Zotov, E. Ebbsjo, D. Timpel, H. Keppler, Phys. Rev. B 60 (1999) 6383.

[27] V.P. Zakaznova-Herzog, W.J. Malfait, F. Herzog, W.E. Halter, J. Non-Cryst. Solids 353 (2007) 4015.

[28] M. Wang, J. Cheng, M. Li, F. He, Physica B: Condens. Matter 406 (2011) 3865.

[29] A.G. Kalampounias, Bull. Mater. Sci. 34 (2011) 299.

[30] B.O. Mysen, L.W. Finger, D. Virgo, F.A. Seifert, Am. Mineral 67 (1982) 686.

[31] P. Mcmillan, Am. Mineral 69 (1984) 622.

[32] J.H. Park., ISIJ Int. 52 (2012) 1627.

[33] A.G. Kalampounias, N.K. Nasikas, G.N. Papatheodorou., J. Chem. Phys. 131 (2010) 114513.

[34] J. Tauc, Mater. Res. Bull. 5 (1970) 721.

[35] C. Rajyasree, D.K. Rao, J. Non-Cryst. Solids 357 (2011) 836.

[36] G. Kaur, O.P. Pandey, K. Singh, J. Non-Cryst. Solids 358 (2012) 2589.

[37] F. Urbach, Phys. Rev. 92 (1953) 1324.

[38] E. Mansour, E.-Egili K, G. Damrawi, Physica B: Condens. Matter 389 (2007) 355.

[39] S.S. Danewalia, G. Sharma, S. Thakur, K. Singh, Sci. Rep. 6 (2016) 24617.

[40] X. Zhang, Z. Du, H. Wu, Y. Yue, Surf. Rev. Lett. 20 (2013) 1350030.

[41] A.K. Jonscher, Nature 267 (1977) 673.

[42] A.K. Jonscher, J. Phys. D: Appl. Phys. 32 (1999) 57.

[43] S.K. Arya, S.S. Danewalia, K. Singh, J. Mater. Chem. C 4 (2016) 3328.

[44] C. Kittel, Introduction to solid state physics, John Wiley & Sons, Inc. (2007).

[45] P. B. Ishai, M.S. Talary, A. Caduff, E. Levy, Y. Feldman, Meas. Sci. Technology 24 (2013) 102001.

[46] R. Richert, Solid State Ion. 105 (1998) 167.

[47] P.B. Macedo, C.T. Moynihan, R. Bose, Phys. Chem. Glasses 13 (1972) 171.

[48] R. Vaish, K.B.R. Verma, J. Appl. Phys. 106 (2009) 064106.

[49] Z. Wang, Y. Hu, H. Lu, F. Yu, J. Non-Cryst. Solids 354 (2008) 1128.

[50] V. Sundar, R. Yimnirun, B.G. Aitken, R.E. Newnham, Mater. Res. Bull. 33 (1998) 1307.

[51] G. Boivin, Y. Bala, A. Doublier, D. Farlay, L.G. Ste-Marie, P.G. Meunier, P.D. Delmas, Bone 43 (2008) 532.

[52] N. Lahl, D. Bahadur, K. Singh, L. Singheiser, K. Hilpert, J. Electrochem. Soc. 149 (5) (2002) A607.

[53] A. K. Yadav, C.R. Gautam, A. Gautam, V. K. Mishra, Phase Trans. 10 (2013) 86.

[54] M. U. Hashmi, Saqlain A. Shah, M. J. Zaidi, S. Alam , Ceram. Silikáty 56 (4) (2012) 347.

[55] A.I. Berezhnoi, S.A. Mersol, A.G. Pincus, Glass-Ceramics and Photo-Sitalls, Plenum Press, New York, London (1970).

[56] T. Kavetskyy, J. Borc, K. Sangwal, V. Tsmots, J. Optoelectron. Adv. M. 12 (2010) 2082.

[57] A.R. Boccaccini, Q. Chen, L. Lefebvre, L. Gremillard, J. Chevalier, Faraday Discuss. 36 (2007) 27.

[58] R.A. Martin, H. Twyman, D. Qiu, J.C. Knowles, R.J. Newport, J. Mater. Sci. Mater. Med. 20 (2009) 883.

[59] L.L. Hench, R.J. Splinter, W.C. Allen, T.K. Green-lee Jr, J. Biomed. Mater. Res. 2 (1971) 117.

[60] K. Singh, I. Bala, V. Kumar, Ceram. Int. 35 (2009) 3401.

[61] G. S. Lázaro, S. C. Santos, C. X. Resende, E. A. d. Santos, J. Non-Cryst. Solids 386 (2014) 19

[62] L.L. Hench, O.H Andersson, Bioactive Glasses. In: An Introduction to Bioceramics, Wilson, World Sci. Pub. Co., London-Singapore, (1993).

[63] O. Peit, E.D. Zanotto, L.L. Hench, J. Non-Cryst. Solids 292 (2001) 115.

[64] H. Arstila, L. Hupa, K.H. Karlsson, M. Hupa, Glass Technol. 48 (2007) 196.

[65] H. Pan, X. Zhao, B.W. Darvell, W.W. Lu, Acta Biomater. 6 (2010) 4181.

[66] T. Kokubo, Biomaterials 12 (1991) 155.

[67] P. Pisciella, S. Crisucci, A. Karamanov, M. Pelino, Waste Manag. 21 (2001) 1.

[68] G. P. Evans, J. C. Behiri, J. D. Currey, W. Bonfield, J. Mat. Sci. Mat. Med. 1 (1990) 38.

[69] S. Singh, K. Singh, J. Mol. Struct. 1081 (2015) 211.

[70] H.C. Li, D.G. Wang, X.G. Meng, C.Z. Chen, Colloids Surf. B Biointerfaces 118 (2014) 226.

[71] A.G. Kalampounias, Bull. Mater. Sci, 34 (2011) 299.

[72] M. Cerruti, D. Greenspan, K. Powers, Biomaterials 26 (2005) 1665.

[73] K. Koutsopoulos, J. Biomed. Mater. Res, 62 (2002) 600.

[74] K. Glock, O. Hirsch, P. Rehak, B. Thomas, C. Jager, J. Non-Cryst. Solids 232 (1998) 113.

[75] S.A. MacDonald, C.R. Schardt, D.J. Masiello, J.H. Simmons, J. Non-Cryst. Solids 275 (2000) 72.

[76] A. Pedone, G. Malavasi, M.C. Menziani, J. Phys. Chem. C 113 (2009) 15723.

[77] P.W. McMillan, Glass Ceramic, 2nd edition, Academic Press, London (1979).

[78] S.J. Watts, R.G. Hill, M.D. O'Donnell, R.V. Law, J. Non-Cryst. Solids 356 (2010) 517.

[79] E. Munukka, O.L. Ranta, M. K. Ki, M. Vaahtio ,T. Peltola, D. Zhang, L. Hupa, H. Ylanen, J. I. Salonen, M. K. Viljanen, E. Eerola, J. Mater. Sci. Mater. Med. 19 (2008) 27.

[80] J. Sawai, J. Microbiol. Methods 54 (2003) 177.

Chapter 5 Conclusions and future scope

5.1 Conclusions

In the present work, glasses and glass-ceramics with composition $55SiO_2$-$10K_2O$-35CaO-(35-*x*) MgO are prepared by conventional melt and quench technique. The constituents of the present compositions are selected on the basis of their biocompatibility with the human body parts as well as desired thermo-mechanical properties. These types of glasses/glass-ceramics are suitable for the use inside the human body as bioactive implant materials. The physical, structural, optical, thermal and dielectric properties of the glasses and glass-ceramics are investigated using various techniques. Bioactivity of the glasses/glass-ceramics in powder as well as pellet form was checked *in-vitro* using simulated body fluids (SBF). Selected samples were further investigated for the effect of heat-treatment of MgO content on various properties. Following conclusions are drawn from the present work:

The present glasses/samples are amorphous in nature and phase separated. The phase separation leads to dual T_g and T_c. The additive properties such as density directly depend upon the molar mass of the glasses. MgO shows concentration dependent role in the present glasses which leads to the non-linear trends in various properties. Glasses having certain ratio of MgO/CaO were found to be more polymerized than others. CaO acts as better network modifier and reduces the optical band gap of the glasses. Higher MgO content (>20 mol%) hinders the crystallization due to breakage of SiO_4network and formation of $(MgO_4)^{2-}$ structural units. Heat-treatment leads to form nanocrystalline phase (<5%) that helps to control dissolution rate of the samples in SBF without adverse effect on *in-vitro* bioactivity. Glass-ceramics interacted with SBF to lower extent as compared to the glasses. Consequently, the formation of HCA layer on glass-ceramics surfaces was delayed slightly. pH value do not change significantly during soaking of glass pellets in SBF whereas

appreciable pH change was observed in case of powder samples owing to more surface area/volume ratio. The reduced values of microhardness of soaked glass pellet also indicated the formation of non-crystalline layer on the glass. The formation of new interfacial layer upon soaking in SBF brought the microhardness values close to human bone. The most thermally stable glass is G4, where the ratio of both the alkaline earth metals is ~1. Highest dielectric permittivity is observed for G4 glass, while it is lowest for G6 glass. Electrode polarization dominates the dielectric permittivity at lower frequencies. The network forming role of MgO at higher concentrations is indicated by the gradual increase in the optical band gap of glasses with MgO content. The microhardness of the bulk glass specimen lie is in the range of 464-502 HV. The change in pH of the SBF and leaching of ions as measured through MP-AES were in consistent to the sequential series of mechanism of changes occurring on the surface of glasses/glass-ceramics as well reported in the literature. After soaking, the optical band gap of the glass powder has increased. The crystalline peaks of the glass-ceramics become more prominent after soaking in SBF solution due to preferential dissolution of glassy phase over glass-ceramics. All the samples exhibited heterogeneous distribution flakes of different morphology to the glass surface. The EDS results confirmed the deposition of ions from the SBF onto the glass surface confirming the elemental release profile of MP-AES. Apatite layer formation has been better visualized in pellets as compared to glass powder. The glasses were found least prone to microbial infections.

5.2 Scope for future study

The compositions similar to present glasses containing lesser amount of SiO_2 may be studied to explore the conditions for glass formation and other properties. Variation of SiO_2 content of the glass may lead to better bioactive properties than present glass which will be tried in future. These glasses synthesized by sol-gel technique may have even better bioactive properties. Many other mechanical parameters like fracture toughness, Young's modulus,

elastic constant etc. of these glasses/glass-ceramics can be tested. The *in-vivo* studies must be conducted on the present glasses and glass-ceramics to check their performance in the real physiological environments. Additional characterizations such as nuclear magnetic resonance (NMR), neutron diffraction and X-ray photoelectron spectroscopy (XPS) can be employed to identify the local structure of these glass/glass-ceramics in terms of various silicate structural units namely Q_0, Q_1, Q_2 and Q_3. The use of solid state nuclear magnetic resonance (NMR) shall be utilized in future to understand the local structure of the glass and effect of each constituent on glass structure. The effect of long term immersion in SBF on the stability of the formed HAp must be studied. The bioactivity may also be checked in other soaking media such as phosphate alkaline bufferred solution, tris-solution, saline water and deionized water. The *in-vitro* cytotoxicity of theses glasses/ glass-ceramics must be checked in suitable assay or media. The *in-situ* antimicrobial effect of glass in combination with some other drugs may be studied further to explore the compatibility of these glasses with drugs in curing the affected body parts. These glasses may be used as bioactive coatings onto suitable and mechanically stronger substrates for advanced bone tissue engineering applications.